

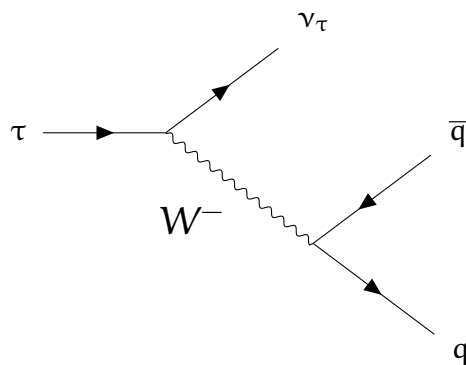
A PhD Thesis in Physics

---

# The QCD Strong Coupling from Hadronic $\tau$ Decays

---

Dirk Hornung



June 2019

---

SUPERVISOR: Matthias Jamin



# The QCD Strong Coupling from Hadronic $\tau$ Decays

---



I, **Matthias Rudolf Jamin** hereby certify that the dissertation with title *The QCD Strong Coupling from Hadronic  $\tau$  Decays* was written by **Dirk Hornung** under my supervision in partial fulfilment of the doctoral degree in physics.

Bellaterra, 18. June 2019

Supervisor and tutor  
**Dr Matthias Rudolf Jamin**

Author  
**Dirk Hornung**



# Abstract

In this work, we perform a *quantum chromodynamics* (QCD) analysis on hadronic  $\tau$  decays. We make use of the ALEPH data to fit the strong coupling and higher order *operator product expansion* (OPE) contributions. Our approach is based on the QCD *sum rules* (QCDSR), especially the framework of *fixed-order perturbation theory* (FOPT), which we apply for the *vector + axial-vector* (V+A) channel of the inclusive Cabibbo-allowed hadronic  $\tau$  decay data. We perform fits using a new set of analytic weight functions to shed light on the discussion of the importance of *duality violation* (DV). Since the inclusion of a model to parametrise contributions of DV by Boito et al. [12] there has been an ongoing discussion, especially with the group around Pich [68], which disfavours the usage of the DV model. Within this work, we want to give a third opinion arguing that DV are not present in double pinched weights. Even for single pinched weights, we find that DV are sufficiently suppressed for high precision measurements of the strong coupling. Another unsolved topic is the discussion of FOPT vs *contour-improved perturbation theory* (CIPT). Beneke et al. [8] have found that CIPT cannot reproduce the *Borel summation* (BS), while the creators of CIPT [70, 58] are in favour of the framework. To investigate the validity of FOPT we apply the BS. The parameters we obtain from both frameworks are in high agreement. Performing fits in the framework of CIPT lead to different results. Consequently, in the discussion of FOPT vs CIPT we argue for FOPT being the favoured framework. For our final result of the strong coupling we perform fits for ten different weights. For each weight, we further fit 20 different moments by varying the energy limit  $s_0$ . We select the best fit of each weight in a

final comparison. The fits are in high agreement and the average of the parameters we obtain yields a value of  $\alpha_s(m_\tau^2) = 0.3261(51)$  for the strong coupling,  $\rho^{(6)} = -0.68(20)$  for the dimension six OPE contribution and  $\rho^{(8)} = -0.80(38)$  for the dimension eight OPE contribution.

# Acknowledgements

I would like to express my sincere gratitude to my advisor Dr Matthias Jamin for his continuous support, for his motivation and for his enormous knowledge. I especially thank him for not giving up on me even in complicated times.

I want to thank my university UAB and the Institute IFAE for guiding me through every obstacle and offering plentiful events to widen my research from various perspectives. I am especially grateful for the opportunity to grow as a teacher of many gifted students.

Having spent four months at the CPT/CNRS in Marseille I also want to thank the Université d'Aix-Marseille for offering me this opportunity. I particularly thank Dr Marc Knecht who perfectly organised my two stays. Additionally I want to thank Dr Laurent Lellouch and Dr Aoife Bharucha, who were more than welcoming.

I want to thank Ramon Miravtillas Mas and Xabier Lobregat for guiding me throughout this thesis. Especially, Ramon helped me out with his tremendous mathematical knowledge.

Last but not least, I would like to thank the persons closest to me. My parents for being as supportive as ever, my sister for her motivational speeches and Beata for just being there, when needed.





# Contents

## Notation and Conventions

<b>1. Introduction</b>	<b>1</b>
<b>2. QCD Sum Rules</b>	<b>9</b>
2.1. Quantum Chromodynamics . . . . .	10
2.2. Two-Point Function . . . . .	20
2.3. Operator Product Expansion . . . . .	26
2.4. Sum Rules . . . . .	31
<b>3. Tau Decays into Hadrons</b>	<b>37</b>
3.1. The Inclusive $\tau$ Decay Ratio . . . . .	38
3.2. Theoretical Computation of $R_\tau$ . . . . .	41
3.3. Duality Violations . . . . .	49
3.4. Borel Summation . . . . .	51
3.5. Experiment . . . . .	54
3.6. The Method of Least Squares . . . . .	58
<b>4. Measuring the Strong Coupling</b>	<b>61</b>
4.1. Fit Strategy . . . . .	62
4.2. Fits . . . . .	64
4.3. Comparison . . . . .	75
4.4. Final Results . . . . .	78
<b>5. Conclusions</b>	<b>81</b>

## CONTENTS

<b>A. Constants</b>	<b>83</b>
<b>B. Coefficients</b>	<b>85</b>
B.1. $\beta$ function . . . . .	85
B.2. Anomalous mass dimension . . . . .	86
B.3. Adler function . . . . .	86
<b>Bibliography</b>	<b>91</b>

# Notation and Conventions

Citations are hyperlinked to the bibliography at the end of this work. They are numerated in squared brackets.

Abbreviations are given in small caps. E.g sm instead of SM.

New terminology will be written cursive in its first appearance.

Every abbreviation is indexed at the end of this thesis.

Important formulas are emphasised by a grey background.

We make use of the abbreviations *eq.* and *fig.* for referencing equations and figures.

The four dimensional metric we use is defined as  $g_{\mu\nu} = \text{diag}(1, -1, -1, -1)$ .

Closed contour integrals are denoted by  $\oint$  and executed counter clockwise.

$\log x$  represents the natural logarithm of  $x$ .



# Introduction

In particle physics, we are concerned about small objects and their interactions. The smallest of these objects are referred to as *elemental particles*. Their dynamics are governed by the laws of nature. These laws are organised through symmetries, which are currently best described by the *Standard Model* (SM).

The SM classifies all known elementary particles and describes three of the four fundamental forces: the electromagnetic, the weak and the strong force. The particles representing matter are contained in two groups of fermionic, spin-1/2 particles. The former group, the leptons consist of: the electron (e), the muon ( $\mu$ ), the tau ( $\tau$ ) and their corresponding neutrinos  $\nu_e$ ,  $\nu_\mu$  and  $\nu_\tau$ . The latter group, the quarks contain u, d (up and down, the so-called light quarks), s (strange), c (charm), b (bottom or beauty) and t (top or truth). The three fundamental forces, the SM differentiates, are described through their carrier particles, the so-called bosons: the photon ( $\gamma$ ) for the electromagnetic, the Z or W boson for the weak and the gluon (g) for the strong interaction. The Leptons solely interact through the electromagnetic and the weak force (also referred to as electroweak interaction), whereas the quarks additionally interact through the strong force. A short summary of the taxonomy of the SM can be seen in [fig. 1.1](#)

From a more mathematical point of view, the SM is a gauge *quantum field theory* (QFT), which is a combination of *classical field theory*, *special relativity* and *quantum mechanics*. Its fundamental objects are ruled through its gauge group

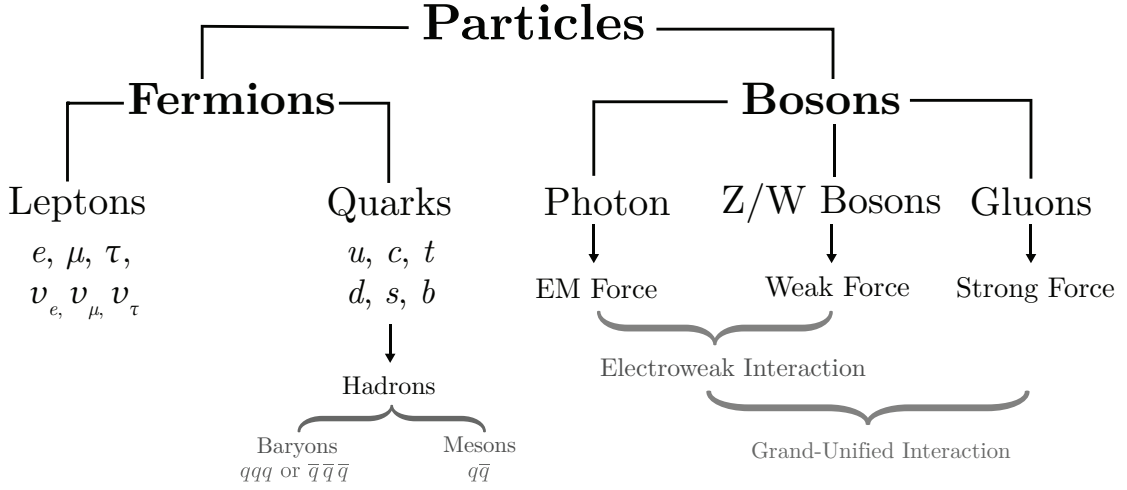


Figure 1.1.: Taxonomy of the Standard Model.

$SU(3) \times SU(2) \times U(1)$ . Each of its subgroups introduces a global and a local gauge symmetry. The global symmetry introduces the charges, which the fields are carrying. The local symmetry introduces the gauge fields, which represent the previously mentioned force carriers. Naively every subgroup<sup>1</sup> of the gauge group of the standard model is responsible for one of the three forces:

**U(1)** the *abelian* gauge group governs the representation of *quantum electrodynamics* (QED), which is commonly known as the electric force. Its global and local symmetry introduces the electric charge and the photon field.

**SU(2)** Is the *non-abelian* symmetry group responsible for the weak interaction. It introduces the  $W^+, W^-$  and  $Z$  bosons and the weak charge. The gauge group  $U(1)$  has been merged with  $SU(2)$  to form the *electroweak interaction*.

**SU(3)** The  $SU(3)$  group is also non-abelian and governs the strong interactions, which are summarised in the theory of QCD. The group yields the three colour charges and due to its eight-dimensional adjoint represen-

<sup>1</sup>Actually  $U(1)$  and  $SU(2)$  have to be regarded as a combined group to be mapped to the electromagnetic-and weak-force in form of the electroweak interaction.

tation, eight different gluons.

Unfortunately, we are still not able to include gravity, the last of the four forces, into the SM. There have been attempts to describe gravity through QFT with the graviton, a spin-2 boson mediator, but there are unsolved problems with the renormalisation of *general relativity* (GR). Until now GR and quantum mechanics (QM) remain incompatible.

Apart from gravity not being included, the SM has a variety of flaws. One of them is being dependent on many parameters, which have to be measured accurately to perform high-precision physics. In total, the Lagrangian of the SM contains 19 parameters. These parameters are represented by ten masses, four CKM-matrix parameters, the QCD-vacuum angle, the Higgs-vacuum expectation value and three gauge coupling constants. Highly accurate values with low errors are crucial for theoretical calculated predictions. One of the major error inputs of every theoretical output are uncertainties in these parameters. In this work, we will focus on one of the parameters, namely the strong coupling  $\alpha_s$ .

The strong coupling is currently measured in six different ways: through  $\tau$  decays, QCD lattice computations, deep inelastic collider results and electroweak precision fits [82]. We have displayed the values of each of the methods in fig. 1.2. In this work we will focus on the subfield of  $\tau$  decays to measure the value of the strong coupling  $\alpha_s(m_\tau^2)$  at the  $m_\tau^2$  scale. We will see that in QCD the value of the coupling “constant” depends upon the scale. The  $\tau$  is an elementary particle with negative electric charge and a spin of  $1/2$ . Together with the lighter electron and muon it forms the group of charged leptons<sup>2</sup>. Even though it is an elementary particle it decays via the weak interaction with a lifetime of  $\tau_\tau = 2.9 \times 10^{-13} \text{ s}$  and has a mass of

<sup>2</sup>Leptons do not interact via the strong force.

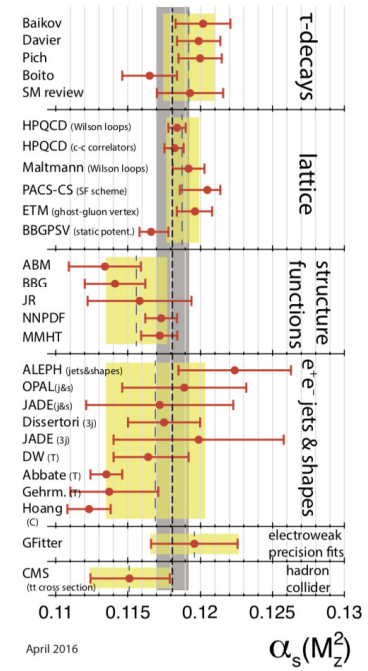


Figure 1.2.: The six different subfields and their results for measuring the strong coupling  $\alpha_s$  [82].

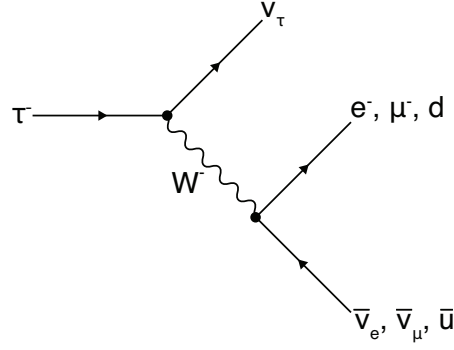


Figure 1.3.: Feynman diagram of common decay of a  $\tau$  lepton into pairs of lepton-antineutrino or quark-antiquark by the emission of a  $W$  boson.

1776.86(12) MeV[82]. It is furthermore the only lepton massive enough to decay into hadrons, thus of interest for our QCD analysis. The final states of a decay are limited by conservation laws. In case of the  $\tau$  decay, they must conserve the electric charge ( $q_e = -1$ ) and invariant mass of the system. Thus, we can see from the corresponding Feynman diagram [fig. 1.3](#)<sup>3</sup>, that the  $\tau$  decays by the emission of a  $W$  boson and a tau-neutrino  $\nu_\tau$  into pairs of  $(e^-, \bar{\nu}_e)$ ,  $(\mu^-, \bar{\nu}_\mu)$  or  $(q, \bar{q})$ . We are foremost interested in the hadronic decay channels, meaning  $\tau$  decays that have quarks in their final states. Quarks have never been measured isolated. Due to the  $\tau$  mass of  $m_\tau \approx 1.8 \text{ GeV}$  the  $\tau$  particle decays into light mesons (pions ( $\pi$ ), kaons ( $K$ ), and eta ( $\eta$ ), see [table 1.1](#)), which can be experimentally detected. The hadronic  $\tau$  decay provides one of the most precise ways to determine the strong coupling [68] and is theoretically accessible to high precision within the framework of QCD.

The theory describing strong interactions is QCD. As the name suggest<sup>4</sup> QCD is characterised by the colour charge and is a non-abelian gauge theory with symmetry group  $SU(3)$ . Consequently, every quark has next to its type one of the three colours blue, red or green. The colour force is mediated through eight gluons, which each being bi-coloured<sup>5</sup>, interact with quarks and each

<sup>3</sup>The  $\tau$  particle can also decay into strange quarks or charm quarks, but these decays are rather uncommon due to the heavy masses of  $s$  and  $c$ .

<sup>4</sup>Chromo is the Greek word for colour.

<sup>5</sup>Each gluon carries colour and anti-colour.



Name	Symbol	Quark content	Rest mass (MeV)
Pion	$\pi^-$	$\bar{u}d$	139.570 61(24) MeV
Pion	$\pi^0$	$(u\bar{u} - d\bar{d})/\sqrt{2}$	134.9770(5) MeV
Kaon	$K^-$	$\bar{u}s$	493.677(16) MeV
Kaon	$K^0$	$d\bar{s}$	497.611(13) MeV
Eta	$\eta$	$(u\bar{u} + d\bar{d} - 2s\bar{s})/\sqrt{6}$	547.862(17) MeV

Table 1.1.: List of mesons produced by a  $\tau$  decay. Rare final states with branching ratios smaller than 0.1 have been omitted. The list is taken from [34] with corresponding rest masses taken from [82].

other. The strength of the strong force is given by the coupling constant  $\alpha_s$ , which depends on the renormalisation scale  $\mu$ . We often choose the renormalisation scale in a way that the coupling constant  $\alpha_s(q^2)$  depends on the energy  $q^2$ . Thus the coupling varies with energy. It increases for low and decreases for high energies<sup>6</sup>. This behaviour has two main implications. The first one states, that for low energies the coupling is too strong for isolated quarks to exist. Until now we have not been able to observe an isolated quark and all experiments can only measure quark compositions. These bound states are called *hadrons* and consist of two or three quarks<sup>7</sup>, which are referred to as mesons<sup>8</sup> or baryons<sup>9</sup> respectively. This phenomenon, of quarks sticking together as hadrons, is referred to as *confinement*. As the fundamental degrees of freedom of QCD are given by quarks and gluons, but the observed particles are hadrons we need to introduce the assumption of *quark-hadron duality* to match the theory to the experiment. This means that a physical quantity should be similarly describable in the hadronic or quark-gluon picture and that both descriptions are equivalent. Quark-hadron duality is in general violated. These so-called DV have an impact on our strong coupling determinations and can be dealt with either suppression or the inclusion of a model [25]. Throughout this work, we will favour the former approach. The second implication, of the

<sup>6</sup>In contrast to the electromagnetic force, where  $\alpha(q^2)$  decreases!

<sup>7</sup>There exist also so-called *exotic hadrons*, which have more than three valence quarks.

<sup>8</sup>Composite of a quark and an antiquark.

<sup>9</sup>Composite of three quarks or three antiquarks.

running of  $\alpha_s$ , concerns *perturbation theory* (PT). The lower the energies we deal with, the higher the value of the strong coupling and the contributions of *non-perturbative* (NP) effects. Currently, there are three solutions to deal with NP effects:

- **Chiral Perturbation Theory** (CHPT): Introduced by Weinberg [86] in the late seventies. CHPT is an effective field theory constructed with a Lagrangian symmetric under a chiral transformation in the limit of massless quarks. Its limitations are based on chiral symmetry, which is only a good approximation for the light quarks  $u$ ,  $d$  and in some cases  $s$ .
- **Lattice QCD** (LQCD): Is the numerical approach to the strong force. Based on the Wilson Loops [88] we treat QCD on a finite lattice instead of working with continuous fields. LQCD has already many applications but is limited due to its computational expensive calculations.
- **QCD Sum Rules** (QCDSR): Were also introduced in the late seventies by Shifman, Vainshtein and Zakharov [78, 77]. They relate the observed hadronic picture to quark-gluon parameters through a dispersion relation and the use of the OPE, which treats NP effect through the definition of vacuum expectation values, the so-called QCD *condensates*. They are a precise method for extracting the strong coupling  $\alpha_s$  at low energies, although limited to the unknown higher order contributions of the OPE.

In this work, we focus on the determination of the strong coupling  $\alpha_s$  within the framework of QCDSR for  $\tau$  decays which has been exploited at the beginning of the nineties by Braaten, Narison and Pich [19]. Within this setup, we can measure  $\alpha_s(m_\tau^2)$  at the  $m_\tau^2$  scale. As the strong coupling gets smaller at higher energies, so do the errors. Thus if we obtain the strong coupling at a low scale we will obtain high precision values at the scale of the Z boson mass  $m_Z$ , which is the standard scale to compare  $\alpha_s$  values.

The QCDSR for the determination of  $\alpha_s$ , from low energies, contains three major issues.

1. There are two different approaches to treat perturbative and non-perturbative contributions. In particular, there is a significant difference between results obtained using FOPT or CIPT, such that analyses based

on CIPT generally arrive at about 7% larger values of  $\alpha_s(m_{\tau^2})$  than those based on FOPT [82]. There have been a variety of analyses on the topic been performed [66, 23, 48] and we will favour the FOPT approach.

2. There are several prescriptions to deal with the NP contributions of higher order OPE condensates. Typically terms of higher dimension have been neglected, even if they knowingly contribute. In this work, we will include every necessary OPE term.
3. Finally, there are known DV leading to an ongoing discussion of the importance of contributions from DV. Currently, there are two main approaches: Either we neglect DV, arguing that they are sufficiently suppressed due to *pinched weights* [68] or model DV with a sinusoidal exponentially suppressed function [25, 12, 16] introducing extra fitting parameters. We will argue for the former method, implementing pinched weights that sufficiently suppress DV contributions such that DV have only a negligible effect on our analysis.

In the following chapter, we want to summarise the necessary theoretical background for working with the QCDSR. Starting with the basics of QCD we want to motivate the *renormalisation group equation* (RGE), which is responsible for the running of the strong coupling. We then continue with the two-point function and its usage in the dispersion relation, which connects the hadronic picture with the quark-gluon picture. Then we introduce the OPE to treat the NP part of QCD before we combine everything to formulate the QCDSR. In the third chapter, we will apply the theory, gathered in the second chapter to  $\tau$  decays. In the fourth chapter, we will state and interpret our fitting results before concluding in the last chapter.



## QCD Sum Rules

The theory of QCD was formulated to find one single framework that describes the many hadrons that exist. Unfortunately making use of *perturbative* QCD (PQCD) is limited. QCD predicts a large coupling constant for low energies. As a consequence, we can only ever observe hadrons, but our theoretical foundation is ruled by the DOF of quarks and gluons. To extract QCD parameters (the six quark masses and the strong coupling) from hadrons we need to connect the quark-gluon picture with the hadron picture. To do so we will introduce the framework of QCDSR.

We will start by setting up the foundations of strong interactions with introducing the QCD Lagrangian. The QCD Lagrangian is ruled by the abelian gauge group  $SU(3)$ . The group implies an energy dependence of the coupling and thus limits the applicability of PT for low energies, where the coupling is large. Next, we will focus on the two-point function, which plays a major role in the framework of QCDSR. The two-point function is defined as vacuum-expectation values of the time ordered product of two local fields

$$\Pi_{\mu\nu}(q^2) = \int \frac{d^4 q}{(2\pi)^4} e^{iqx} \langle \Omega | T \{ J_\mu(x) J_\nu(0) \} | \Omega \rangle, \quad (2.0.1)$$

where  $J_\mu$  is the Noether current. We can use it to theoretically describe processes, as  $\tau$  decays into hadrons, by matching the quantum numbers of the fields, we choose in specifying the two-point function, to the outgoing hadrons. We will see, that the two-point function  $\Pi(q^2)$  is related to hadronic states, by poles for  $q^2 > 0$ . Here NP effects become important and we need to introduce

the OPE, which handles NP parts through the QCD condensates. The condensates form part of the full physical vacuum and would not exist regarding the perturbative vacuum solely. Consequently, the condensates are not accessible through PT methods and have to be fitted from experiment or calculated with the help of NP tools, like LQCD. Finally, we will combine a dispersion relation and Cauchy's theorem to finalise the discussion on the QCDSR with developing the *finite energy sum rules* (FESR), which we will apply to extract the strong coupling from  $\tau$  decays into hadrons.

## 2.1. Quantum Chromodynamics

Since the formulation of QED at the end of the forties, it had been attempted to construct a QFT of the strong nuclear force, which has been achieved in the seventies as QCD [41, 40, 43, 71, 85]. The fundamental fields of QCD are given by Dirac spinors of spin 1/2, the so-called quarks, with a fractional electric charge of  $\pm 1/3$  or  $\pm 2/3$ . The theory furthermore contains gauge fields of spin 1. These gauge fields are called gluons, do not carry an electric charge and are massless. They are the force mediators, which interact with quarks and themselves, because they carry colour charge, in contrast to photons of QED, which interact only with fermions.

The corresponding gauge group of QCD is the non-abelian group  $SU(3)$ . Each of the quark flavours  $u, d, c, s, t$  and  $b$  belongs to the fundamental representation of  $SU(3)$  and contains a triplet of fields  $\Psi$ .

$$\Psi = \begin{pmatrix} \Psi_1 \\ \Psi_2 \\ \Psi_3 \end{pmatrix} \quad (2.1.1)$$

The labels of the triplet are the colours red, green and blue, which play the role of *colour charge*, similar to the electric charge of QED. The gluons belong to the adjoint representation of  $SU(3)$ , contain an octet of fields and can be expressed using the Gell-Mann matrices  $\lambda_a$

$$B_\mu = B_\mu^a \lambda_a \quad a = 1, 2, \dots, 8 \quad (2.1.2)$$

Flavour	Mass
u	2.50(17) MeV
d	4.88(20) MeV
s	93.44(68) MeV
c	1.280(13) GeV
b	4.198(12) GeV
t	173.0(40) GeV

Table 2.1.: List of quarks and their masses. The masses of the up, down and strange quark are quoted in the four-flavour theory ( $N_f = 2 + 1 + 1$ ) at the scale  $\mu = 2 \text{ GeV}$  in the  $\overline{\text{MS}}$  scheme. The charm and bottom quark are also taken in the four-flavour theory and in the  $\overline{\text{MS}}$  scheme, but at the scales  $\mu = m_c$  and  $\mu = m_b$  correspondingly. All quarks except for the top quark are taken from the *Flavour Lattice Averaging Group* (FLAG) [4]. The mass of the top quark is not discussed in [4] and has been taken from direct observations of top events [82].

The classical *Lagrange density* of QCD is given by [90, 63]:

$$\mathcal{L}_{\text{QCD}}(x) = -\frac{1}{4}G_{\mu\nu}^a(x)G^{\mu\nu a}(x) + \sum_A \left[ \frac{i}{2}\bar{q}^A(x)\gamma^\mu \overleftrightarrow{D}_\mu q^A(x) - m_A \bar{q}^A(x)q^A(x) \right], \quad (2.1.3)$$

with  $q^A(x)$  representing the quark fields and  $G_{\mu\nu}^a$  being the *gluon field strength tensor* given by:

$$G_{\mu\nu}^a(x) \equiv \partial_\mu B_\nu^a(x) - \partial_\nu B_\mu^a(x) + gf^{abc}B_\mu^b(x)B_\nu^c(x), \quad (2.1.4)$$

with  $f^{abc}$  as *structure constants* of the gauge group  $\text{SU}(3)$  and  $\overleftrightarrow{D}_\mu$  as covariant derivative acting to the left and to the right. Furthermore we have used  $A, B, \dots = 0, \dots, 5$  as flavour indices,  $a, b, \dots = 0, \dots, 8$  as colour indices and

$\mu, \nu, \dots = 0, \dots, 3$  as Lorentz indices. Explicitly the Lagrangian writes:

$$\begin{aligned}
 \mathcal{L}_0(x) = & -\frac{1}{4} \left[ \partial_\mu G_\nu^a(x) - \partial_\nu G_\mu^a(x) \right] \left[ \partial^\mu G_a^\nu(x) - \partial^\nu G_a^\mu(x) \right] \\
 & + \frac{i}{2} \bar{q}_\alpha^A(x) \gamma^\mu \partial_\mu q_\alpha^A(x) - \frac{i}{2} \left[ \partial_\mu \bar{q}_\alpha^A(x) \right] \gamma^\mu q_\alpha^A(x) - m_A \bar{q}_\alpha^A(x) q_\alpha^A(x) \\
 & + \frac{g_s}{2} \bar{q}_\alpha^A(x) \lambda_{\alpha\beta}^a \gamma_\mu q_\beta^A(x) G_a^\mu(x) \\
 & - \frac{g_s}{2} f_{abc} \left[ \partial_\mu G_\nu^a(x) - \partial_\nu G_\mu^a(x) \right] G_b^\mu(x) G_c^\nu(x) \\
 & - \frac{g_s^2}{4} f_{abc} f_{ade} G_\mu^b(x) G_\nu^c(x) G_d^a(x) G_e^\nu(x)
 \end{aligned} \tag{2.1.5}$$

The first term is the kinetic term for the massless gluons. The next three terms are the kinetic terms for the quark field with different masses for each flavour. The rest of the terms are the interaction terms. The fifth term represents the interaction between quarks and gluons and the last two terms the self-interactions of gluon fields.

The corresponding Feynman rules have been displayed in [fig. 2.1](#). The rules are based on PT, but can be enhanced with the QCD condensates, as we will see in the discussion of the OPE in [section 2.3](#)

Having derived the Lagrangian leaves us with its quantisation. The Dirac-spinors can be quantised as in QED without any problems. The  $\Psi(x)$  quantum field can be written as:

$$\Psi(x) = \int \frac{d^3 p}{(2\pi)^3 2E(\vec{p})} \sum_\lambda \left[ u(\vec{p}, \lambda) a(\vec{p}, \lambda) e^{-ipx} + v(\vec{p}, \lambda) b^\dagger(\vec{p}, \lambda) e^{ipx} \right], \tag{2.1.6}$$

where the integration ranges over the positive sheet of the mass hyperboloid  $\Omega_+(m) = \{p | p^2 = m^2, p^0 > 0\}$ . The four spinors  $u(\vec{p}, \lambda)$  and  $v(\vec{p}, \lambda)$  are solutions to the Dirac equations in momentum space

$$\begin{aligned}
 [\not{p} - m]u(\vec{p}, \lambda) &= 0 \\
 [\not{p} + m]v(\vec{p}, \lambda) &= 0,
 \end{aligned} \tag{2.1.7}$$

with  $\lambda$  representing the helicity state of the spinors.

The quantisation of the gauge fields is more cumbersome. One is forced to introduce supplementary non-physical fields, the so-called Faddeev-Popov ghosts  $c^a(x)$  [\[39\]](#), to cancel unphysical helicity degrees of freedom of the gluon fields.



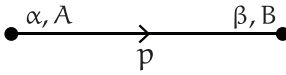
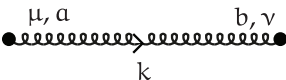
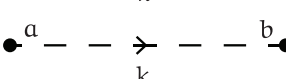
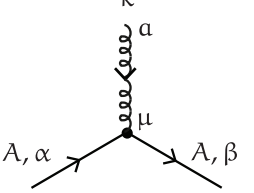
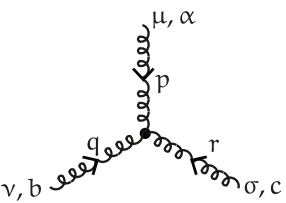
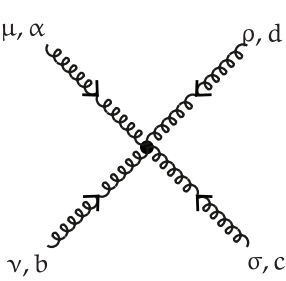
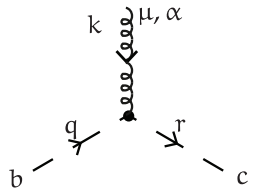
Quark propagator		$= \frac{i\delta_{\alpha\beta}\delta_{AB}}{\not{p} - m_A + i\epsilon}$
Gluon propagator		$= \frac{-i\delta_{ab}}{k^2 + i\epsilon} \left[ g^{\mu\nu} - (1 - a) \frac{k_\mu k_\nu}{k^2 + i\epsilon} \right]$
Ghost propagator		$= \frac{-\delta_{ab}}{k^2 + i\epsilon}$
Fermionic vertex		$= g \left( \frac{\lambda_a}{2} \right)_{\beta\alpha} \gamma^\mu$
Triple gluon vertex		$= -igf_{abc} [g_{\mu\nu}(p - q)_\sigma + g_{\nu\sigma}(q - r)_\mu + g_{\sigma\mu}(r - p)_\nu]$
Quartic gluon vertex		$= -g^2 [f_{abe}f_{cde}(g_{\mu\sigma}g_{\nu\rho} - g_{\mu\rho}g_{\nu\sigma}) + f_{ace}f_{bde}(g_{\mu\nu}g_{\sigma\rho} - g_{\mu\rho}g_{\nu\sigma}) + f_{ade}f_{cbe}(g_{\mu\sigma}g_{\nu\rho} - g_{\mu\nu}g_{\sigma\rho})]$
Ghost vertex		$= -igf_{abc}r^\mu$

Figure 2.1.: QCD Feynman rules.

The free propagators for the quark, the gluon and the ghost fields are then given by

$$\begin{aligned}
 iS_{\alpha\beta}^{(0)AB}(x-y) &\equiv \overline{q_\alpha^A(x)} q_\beta^B(y) \equiv \langle 0 | T \{ q_\alpha^A(x) \overline{q}_\beta^B(y) \} | 0 \rangle = \delta_{AB} \delta_{\alpha\beta} iS^{(0)}(x-y) \\
 &= i\delta_{AB} \delta_{\alpha\beta} \int \frac{d^4 p}{(2\pi)^4} \frac{\not{p} + m}{(p^2 - m^2 + i\epsilon)} \\
 iD_{ab}^{(0)\mu\nu}(x-y) &\equiv \overline{B_a^\mu(x)} B_b^\nu(y) \equiv \langle 0 | T \{ B_a^\mu(x) B_b^\nu(y) \} | 0 \rangle \equiv \delta_{ab} i \int \frac{d^4 k}{(2\pi)^4} D^{(0)\mu\nu}(k) e^{-ik(x-y)} \\
 &= i\delta_{ab} \int \frac{d^4 k}{(2\pi)^4} \frac{1}{k^2 + i\epsilon} \left[ -g_{\mu\nu} + (1-a) \frac{k_\mu k_\nu}{k^2 + i\epsilon} \right] e^{-ik(x-y)} \\
 i\tilde{D}_{ab}^{(0)}(x-y) &\equiv \overline{\phi_a(x)} \phi_b(y) \equiv \langle 0 | T \{ \phi_a(x) \overline{\phi}_b(y) \} | 0 \rangle = i\delta_{ab} \int \frac{d^4 q}{(2\pi)^4} \frac{-1}{q^2 + i\epsilon} e^{-iq(x-y)} \\
 &\equiv i\delta_{ab} \int \frac{d^4 q}{(2\pi)^4} \tilde{D}^{(0)}(q) e^{-iq(x-y)},
 \end{aligned} \tag{2.1.8}$$

The previously introduced Feynman rules and propagators all make use of the perturbative vacuum  $|0\rangle$  and thus count as tools of PT. Consequently, they need a small coupling to approximate excitations of full QCD vacuum. We will see in the following section, that the strong coupling runs with energy and is large for small energy scales.

### 2.1.1. Renormalisation Group

Computing observables with the QCD Lagrangian (eq. 2.1.3) lead to divergencies, which have to be *renormalised*. To render these divergent quantities finite we have to introduce a suitable parameter such that the “original divergent theory” corresponds to a certain value of that parameter. This procedure is referred to as *regularisation* and there are various approaches:

- **Cut-off regularisation:** In cut-off regularisation, we limit the divergent momentum integrals by a cut-off  $|\vec{p}| < \Lambda$ . Here  $\Lambda$  has the dimension of mass. The cut-off regularisation breaks translational invariance, which can be guarded by making use of other regularisation methods.
- **Pauli-Villars (P-V) regularisation:** [64] In P-V regularisation the propagator is forced to decrease faster than the divergence to appear. It re-

places the nominator by

$$(\vec{p}^2 + m^2)^{-1} \rightarrow (\vec{p}^2 + m^2)^{-1} - (\vec{p}^2 + M^2)^{-1}, \quad (2.1.9)$$

where  $M$  acts similar to the previously presented cut-off, but conserves translational invariance.

- **Dimensional regularisation:** [17, 2, 1] Dimensional regularisation has been introduced at the beginning of the seventies to regularise non-abelian gauge theories (like QCD), where  $\Lambda$ - and  $P$ -V-regularisation failed. In dimensional regularisation we expand the four space-time dimensions to arbitrary  $D$  dimensions. To compensate for the additional dimensions we introduce an additional scale  $\mu^{D-4}$ . A typical Feynman integral then has the following appearance:

$$\int \frac{d^4 p}{(2\pi)^4} \frac{1}{\vec{p}^2 + m^2} \rightarrow \mu^{2\epsilon} \int \frac{d^D p}{(2\pi)^D} \frac{1}{\vec{p}^2 + m^2}. \quad (2.1.10)$$

Dimensional regularisation preserves all symmetries and allows easy identification of divergences and naturally leads to the *minimal subtraction scheme* (MS) [1, 84].

In all of the three regularisation schemes, we introduced an arbitrary parameter to regularise the divergence. This parameter causes scale dependence of the strong coupling and the quark masses. As we are mainly concerned with the non-abelian gauge theory QCD we will focus on dimensional regularisation, which introduced the parameter  $\mu$ .

Measurable observables (*physical quantities*) cannot depend on the renormalisation scale  $\mu$ . Therefore the derivative by  $\mu$  of a general physical quantity has to yield zero. A physical quantity  $R(q, a_s, m)$ , that depends on the external momentum  $q$ , the renormalised coupling  $a_s \equiv \alpha_s/\pi$  and the renormalised quark mass  $m$  can then be expressed as

$$\mu \frac{d}{d\mu} R(q, a_s, m) = \left[ \mu \frac{\partial}{\partial \mu} + \mu \frac{da_s}{d\mu} \frac{\partial}{\partial a_s} + \mu \frac{dm}{d\mu} \frac{\partial}{\partial m} \right] R(q, a_s, m) = 0. \quad (2.1.11)$$

Equation 2.1.11 is referred to as a *renormalisation group equation* (RGE) and is the basis for defining the two *renormalisation group functions*:

$$\beta(a_s) \equiv -\mu \frac{da_s}{d\mu} = \beta_1 a_s^2 + \beta_2 a_s^3 + \dots \quad \beta\text{-function} \quad (2.1.12)$$

$$\gamma(a_s) \equiv -\frac{\mu}{m} \frac{dm}{d\mu} = \gamma_1 a_s + \gamma_2 a_s^2 + \dots \quad \text{anomalous mass dimension.} \quad (2.1.13)$$

The  $\beta$ -function dictates the running of the strong coupling, whereas the anomalous mass dimension describes the running of the quark masses. We have a special interest in the running of the strong coupling, but will also shortly sum up the running of the quark masses.

### Running Gauge Coupling

Regarding the  $\beta$ -function, we notice, that  $a_s(\mu)$  is not a constant, but that it *runs* by varying its scale  $\mu$ . To better understand the running of the strong coupling we integrate the  $\beta$ -function

$$\int_{a_s(\mu_1)}^{a_s(\mu_2)} \frac{da_s}{\beta(a_s)} = - \int_{\mu_1}^{\mu_2} \frac{d\mu}{\mu} = \log \frac{\mu_1}{\mu_2}. \quad (2.1.14)$$

We analytically evaluate the above integral by approximating the  $\beta$ -function to first order, with the known coefficient

$$\beta_1 = \frac{1}{6}(11N_c - 2N_f), \quad (2.1.15)$$

which yields

$$a_s(\mu_2) = \frac{a_s(\mu_1)}{\left(1 - a_s(\mu_1)\beta_1 \log \frac{\mu_1}{\mu_2}\right)}. \quad (2.1.16)$$

Equation 2.1.16 has some important implications for the strong coupling:

- The coupling at a scale  $\mu_2$  depends on  $a_s(\mu_1)$ . Thus we have to take care of the scale  $\mu$  while comparing different values of  $\alpha_s$ . In the literature (e.g. [82])  $\alpha_s$  is commonly compared at the Z boson scale of around 91 GeV. As we are extracting the strong coupling at the mass of the  $\tau$  lepton, around 1.776 GeV we need to run the strong coupling up to the desired scale. While running the coupling, we have to take care of the quark thresholds. Each quark gets active at a certain energy scale, which leads to running of  $\alpha_s$  as shown in fig. 2.2. Typically one runs the coupling with the aid of software packages like *RunDec* [29, 44], which has also been ported to support C (*CRunDec*, [74]) and Python [80].
- As we have three colours ( $N_c = 3$ ) and six flavours ( $N_f = 6$ ) the  $\beta_1$  coefficient 2.1.12 is positive. Thus for the two scales  $\mu_2 < \mu_1$  the strong

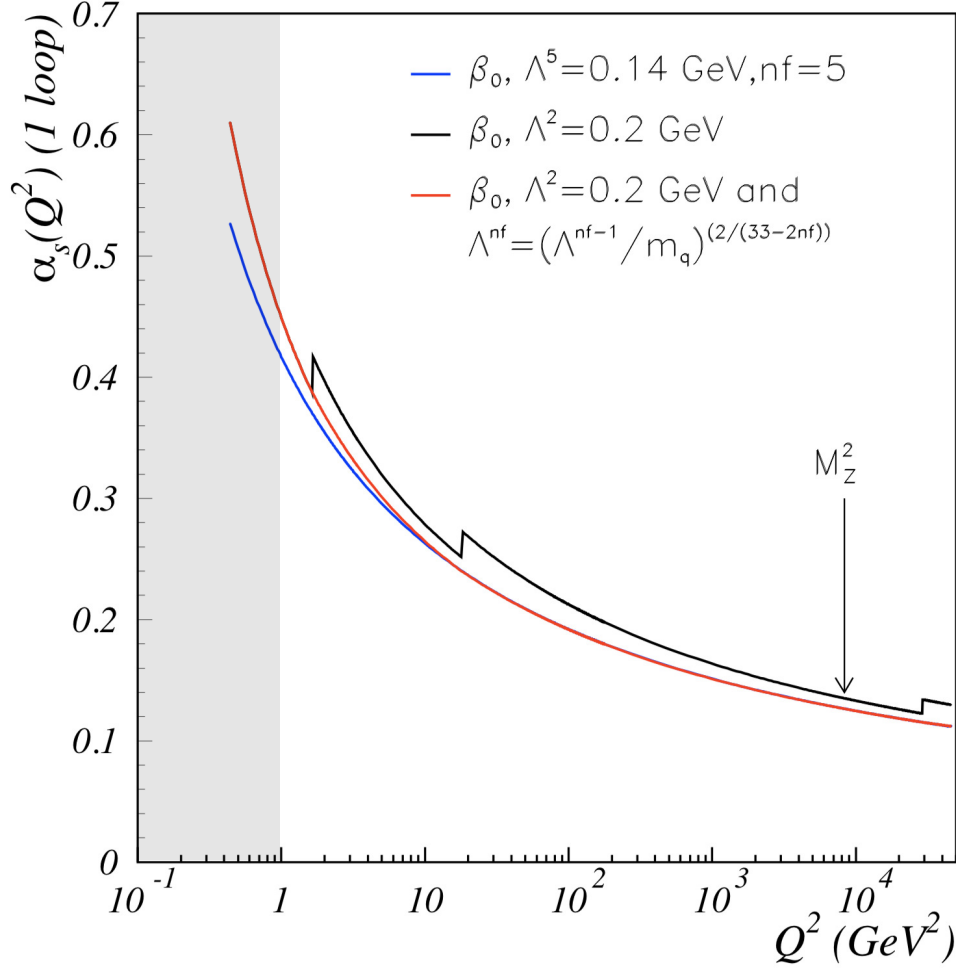


Figure 2.2.: Running of the strong coupling  $\alpha_s(Q^2)$  at first order. The blue line represents the uncorrected coupling constant, with an  $\Lambda^{n_f=5}$  chosen to match an experimental value of the coupling at  $Q^2 = M_Z^2$ . The quark-thresholds are shown by the black line and the corrected running is given by the red line. We additionally marked the breakdown of PT with a grey background for  $Q^2 < 1$ . The image is taken from a recent review of the strong coupling [36].

coupling  $\alpha_s(\mu_2)$  increases logarithmically and at a scale of  $\mu_2 = 1 \text{ GeV}$  reaches a value of

$$\alpha_s(1 \text{ GeV}) \approx 0.5, \quad (2.1.17)$$

which questions the applicability of PT for energies lower than 1 GeV (as seen from the grey zone in [fig. 2.2](#)).

- A large coupling for small scales implies confinement. We are not able to separate quarks in a meson or baryon. No quark has been detected as single particle yet. This is qualitatively explained with the gluon field carrying colour charge. These gluons form so-called *flux-tubes* between quarks, which cause a constant strong force between particles regardless of their separation. Consequently, the energy needed to separate quarks is proportional to the distance between them and at some point, there is enough energy to favour the creation of a new quark pair. Thus before separating two quarks, we create a quark-antiquark pair. We will probably never be able to observe an isolated quark. This phenomenon is referred to as colour confinement or simply confinement.
- With the first  $\beta$  coefficient being positive we notice that for increasing scales ( $\mu_2 > \mu_1$ ) the coupling decreases logarithmically. This leads to asymptotic freedom, which states, that for high energies (small distances), the strong coupling becomes diminishing small and quarks and gluons do not interact. Thus in isolated baryons and mesons, the quarks are separated by small distances, move freely and do not interact.

From the RGE, we have seen, that not only the coupling but also the masses carry an energy dependency.

### Running Quark Mass

The mass dependence on energy is governed by the *anomalous mass dimension*  $\gamma(a_s)$ . Its properties of the running quark mass can be derived similarly to the gauge coupling. Starting from integrating the *anomalous mass dimension* [eq. 2.1.13](#)

$$\log \frac{m(\mu_2)}{m(\mu_1)} = \int_{a_s(\mu_1)}^{a_s(\mu_2)} da_s \frac{\gamma(a_s)}{\beta(a_s)} \quad (2.1.18)$$

we can solve the integral analytically by approximating the *anomalous mass dimension* to first order

$$m(\mu_2) = m(\mu_1) \left( \frac{a(\mu_2)}{a(\mu_1)} \right)^{\frac{\gamma_1}{\beta_1}} (1 + \mathcal{O}(\beta_2, \gamma_2)). \quad (2.1.19)$$

As  $\beta_1$  and  $\gamma_1$  (see B.2) are positive the quark mass decreases with increasing  $\mu$ . The general relation between different scales is given by

$$m(\mu_2) = m(\mu_1) \exp \left( \int_{a_s(\mu_1)}^{a_s(\mu_2)} da_s \frac{\gamma(a_s)}{\beta(a_s)} \right) \quad (2.1.20)$$

and can be solved numerically to run the quark mass to the needed scale  $\mu_2$ . Both, the  $\beta$ -function and the anomalous mass dimension are currently known up to the 5<sup>th</sup> order and listed in the appendix B.1.

We will make use of the anomalous dimension while running the quark masses for NP contributions, which include the quark masses at different energy scales.

QCD, in general, has a precision problem caused by uncertainties and largeness of the strong coupling constant  $\alpha_s$ . The fine-structure constant (the coupling of QED) is known to eleven digits, whereas the strong coupling is only known to about four. Furthermore, for low energies, the strong coupling constant is much larger than the fine-structure constant. E.g. at the Z mass, the standard mass to compare the strong coupling, we have an  $\alpha_s$  of 0.11, whereas the fine structure constant would be around 0.007. Consequently to use PT we have to calculate our results to higher orders, including tens of thousands of Feynman diagrams, in QCD to achieve a precision equal to QED. For even lower energies, around 1 GeV, the strong coupling reaches a critical value of around 0.5 leading to a break down of PT.

In this work, we try to achieve higher precision in the value of  $\alpha_s$ . The framework we use to measure the strong coupling constant is the QCDSR. A central object needed to describe hadronic states with the help of QCD is the *two-point function* for which we will devote the following section.

## 2.2. Two-Point Function

In analogy to the Green's function for elemental fields we can define a propagator for composite currents referred to as *two-point function*

$$\Pi(x) = \langle \Omega | T \{ J(x) J(y) \} | \Omega \rangle, \quad (2.2.1)$$

where  $T\{\dots\}$  is the time-ordered product and  $|\Omega\rangle$  is the ground state/vacuum of the interacting theory. Note that the fields are in general given in the Heisenberg picture, which implies translational invariance.

$$\begin{aligned} \langle \Omega | \phi(x) \phi(y) | \Omega \rangle &= \langle \Omega | \phi(x) e^{i\hat{p}y} e^{-i\hat{p}y} \phi(y) e^{i\hat{p}y} e^{-i\hat{p}y} | \Omega \rangle \\ &= \langle \Omega | \phi(x-y) \phi(0) | \Omega \rangle, \end{aligned} \quad (2.2.2)$$

where we made use of the translation operator  $\hat{T}(x) = e^{-i\hat{p}x}$ .

In this work, we are especially concerned about the vacuum expectation value of the Fourier transform of two time-ordered QCD quark Noether currents

$$\Pi_\Gamma(p^2) \equiv \int \frac{d^4x}{(2\pi)^4} e^{ipx} \langle \Omega | T \{ J_\Gamma(x) J_\Gamma(0) \} | \Omega \rangle, \quad (2.2.3)$$

where the Noether current is given by

$$J_\Gamma(x) = \bar{q}(x) \Gamma q(x). \quad (2.2.4)$$

Here,  $\Gamma$  can be any of the following Dirac matrices  $\Gamma \in \{1, i\gamma_5, \gamma_\mu, \gamma_\mu \gamma_5\}$ , specifying the quantum number of the current (*scalar* (s), *pseudo-scalar* (p), *vector* (v) and *axial-vector* (A), respectively). By choosing the right quantum numbers we can theoretically represent the processes we want to study, which will be important when we want to describe the hadrons produced in  $\tau$  decays.

From a Feynman diagram point of view, we can illustrate the two-point function as quark-antiquark pair, which is produced by an external source, e.g. the virtual  $W$  boson of  $\tau\bar{\tau}$  annihilation as seen in fig. 2.3. Here the quarks are propagating at *short distances*, which implies that we can make use of PT, thus avoiding *long-*

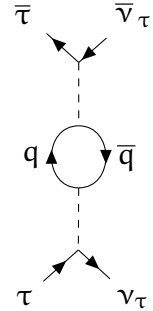


Figure 2.3.:  $\tau\bar{\tau}$ -annihilation with a quark-antiquark pair.



*distance/NPT* effects, that would appear if the initial and final states were given by hadrons [30]. It is interesting to note, that the same process with the help of the *optical theorem* can be used to derive the total decay width of hadronic tau decays.

### 2.2.1. Short Distances vs. Long Distances

If we want to calculate the two-point function in QCD we have to differentiate short and long distances (large or small momenta). In general when we talk about small distances we refer to large momenta. Large momenta imply a small strong coupling. Consequently, we can use PT for short distances without problems. On the contrary, long distances involve small momenta, which implies a large coupling constant. Thus for long distances, the NP effects become important and have to be dealt with. To apply PT to the case of the  $\tau\bar{\tau}$  annihilation we need the quark-antiquark pair of fig. 2.3 to be highly virtual<sup>1</sup>. To roughly separate long distances from short distances using a length scale, we can say that the length scale should be smaller than the radius of a hadron.

### 2.2.2. Relating the Two-Point Function to Hadrons

The two-point function can be interpreted physically as the amplitude of propagating single- or multi-particle states and their excitations. The possible states, in our case, the hadrons we describe through the correlator, are fixed by the quantum numbers of the current, we define for the vacuum expectation value. For example, the neutral  $\rho$  meson is a spin-1 vector meson with a quark content of  $(u\bar{u} - d\bar{d})/\sqrt{2}$ . Consequently by choosing a current

$$J_\mu(x) = \frac{1}{2}(\bar{u}(x)\gamma_\mu u(x) - \bar{d}(x)\gamma_\mu d(x)) \quad (2.2.5)$$

the two-point function contains the same quantum numbers as the  $\rho$  meson and is said to materialise to it. A list of some ground-state mesons for combinations of the light quarks  $u, d$  and  $s$  is given in table 2.2.

---

<sup>1</sup>Which is the same as saying, that the quark-antiquark pair needs a high external momentum  $q$ .

Symbol	Quark content	Isospin	J	Current
$\pi^+$	$u\bar{d}$	1	0	$: \bar{u} \gamma_\mu \gamma_5 d :$
$\pi^0$	$\frac{u\bar{u} - d\bar{d}}{2}$	1	0	$: \bar{u} \gamma_\mu \gamma_5 u + \bar{d} \gamma_\mu \gamma_5 d :$
$\eta$	$\frac{u\bar{u} + d\bar{d} - 2s\bar{s}}{\sqrt{6}}$	0	0	$: \bar{u} \gamma_\mu \gamma_5 u + \bar{d} \gamma_\mu \gamma_5 d - 2\bar{s} \gamma_\mu \gamma_5 s :$
$\eta'$	$\frac{u\bar{u} + d\bar{d} + s\bar{s}}{\sqrt{3}}$	0	0	$: \bar{u} \gamma_\mu \gamma_5 u + \bar{d} \gamma_\mu \gamma_5 d + \bar{s} \gamma_\mu \gamma_5 s :$
$\rho^0$	$\frac{u\bar{u} - d\bar{d}}{\sqrt{2}}$	1	1	$: \bar{u} \gamma_\mu u - \bar{d} \gamma_\mu d :$
$\omega$	$\frac{u\bar{u} + d\bar{d}}{\sqrt{2}}$	0	1	$: \bar{u} \gamma_\mu u + \bar{d} \gamma_\mu d :$
$\phi$	$s\bar{s}$	0	1	$: \bar{s} \gamma_\mu \gamma_5 s :$
$K^+$	$u\bar{s}$	$\frac{1}{2}$	0	$: \bar{u} \gamma_\mu \gamma_5 s :$
$K^0$	$d\bar{s}$	$\frac{1}{2}$	0	$: \bar{d} \gamma_\mu \gamma_5 s :$

Table 2.2.: Ground-state vector and pseudoscalar mesons for the light quarks  $u, d$  and  $s$  with their corresponding currents in the two-point function. Note that we use  $\gamma_\mu$  for vector and  $\gamma_\mu \gamma_5$  for the pseudoscalar mesons.

The correlator is materialising into a spectrum of hadrons. Thus if we insert a complete set of states of hadrons we can make use of the unitary relation

$$\langle \Omega | J_\mu(x) J_\nu(0) | \Omega \rangle = \sum_X \langle \Omega | J_\mu(x) | X \rangle \langle X | J_\nu(0) | \Omega \rangle \quad (2.2.6)$$

to represent the two-point correlator via a spectral function  $\rho(t)$

$$\Pi(p^2) = \int_0^\infty ds \frac{\rho(s)}{s - p^2 - i\epsilon}. \quad (2.2.7)$$

The above relation is referred to as *Källén-Lehmann spectral representation* [53, 59] or *dispersion relation*. It relates the two-point function to the spectral function  $\rho$ , which can be represented as a sum over all possible hadronic states

$$\rho(s) = (2\pi)^3 \sum_X \int d\Pi_X |\langle \Omega | J_\mu(0) | X \rangle|^2 \delta^4(s - p_X). \quad (2.2.8)$$

Note that the analytic properties of the two-point function are in one-to-one correspondence with the newly introduced spectral function and thus determined by the possible hadrons states, which only form on the positive real axis. A full derivation of the *Källén-Lehmann spectral representation* can be found in

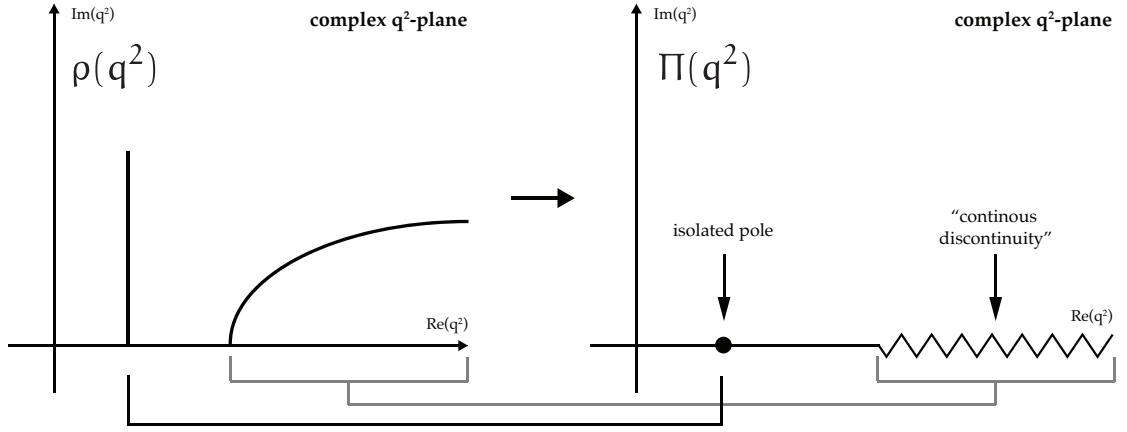


Figure 2.4.: Analytic structure in the complex  $q^2$ -plane of the Fourier transform of the two-point function. The hadronic final states are responsible for poles appearing on the real-axis. The single-particle states contribute as an isolated pole and the multi-particle states contribute as bound states poles or a continuous “discontinuity cut” [65, 92].

[72]. The spectral function is interesting to us for two reasons. First, it is experimentally measurable and second it carries a “branch cut”, which we want to discuss now.

### 2.2.3. Analytic Structure of the Two-Point Function

The general two-point function  $\rho(s)$  has some interesting analytic properties. It has poles for single-particle states and a continuous branch cut for multi-particle states. The single- and multi-particle states, for a general correlator, can mathematically be separated by

$$\rho(s) = Z\delta(s - m^2) + \theta(s - s_0)\sigma(s), \quad (2.2.9)$$

where the second term is the contribution from multi-particle states.  $\sigma(s)$  is zero until we reach the threshold, where we have sufficient energy to form multi-particle states. The analytic structure is depicted by fig. 2.4 and we can see that the spectral function has  $\delta$  spikes for single-particle states and a continuous contribution for  $s \geq 4m$  resulting from multi-particle states. These lead to poles and a continuous branch cut of the two-point function.

### 2.2.4. Decompositions

Apart from the spectral decomposition we can also Lorentz decompose the two-point function or write it in terms of  $v$ ,  $A$ ,  $s$  and  $p$  contributions.

#### Lorentz decomposition

Due to the Lorentz invariance of the two-point function, and by assuming the conservation of the Noether current, we can apply the Ward identity to decompose the correlator  $\Pi_{\mu\nu}$  into its scalar contribution  $\Pi$ .

There exist only two possible terms that can guard the structure of the second order tensor:  $q_\mu q_\nu$  and  $q^2 g_{\mu\nu}$ . The sum of both multiplied with two arbitrary functions  $A(q^2)$  and  $B(q^2)$  yields

$$\Pi_{\mu\nu}(q^2) = q_\mu q_\nu A(q^2) + q^2 g_{\mu\nu} B(q^2). \quad (2.2.10)$$

By assuming that we deal with equal quark flavours and that the vector current is conserved, i.e.  $\partial^\mu j_\mu(x) = 0$ , we can make use of the *Ward identity*

$$q^\mu \Pi_{\mu\nu} = 0 \quad (2.2.11)$$

to demonstrate, that the two arbitrary functions are related

$$\begin{aligned} q^\mu q^\nu \Pi_{\mu\nu} &= q^4 A(q^2) + q^4 B(q^2) = 0 \\ \implies A(q^2) &= -B(q^2). \end{aligned} \quad (2.2.12)$$

Thus redefining  $A(q^2) \equiv \Pi(q^2)$  we expressed the correlator as a scalar function of spin 1

$$\Pi_{\mu\nu}(q^2) = (q_\mu q_\nu - q^2 g_{\mu\nu}) \Pi^{(1)}(q^2). \quad (2.2.13)$$

In case of a current of different quark flavours, the current will not be conserved and we cannot apply the Ward identity. Consequently, the standard Lorentz decomposition into transversal and longitudinal components reads

$$\Pi^{\mu\nu}(q^2) = (q^\mu q^\nu - g^{\mu\nu} q^2) \Pi^{(1)}(q^2) + q^\mu q^\nu \Pi^{(0)}(q^2). \quad (2.2.14)$$

### Transversal and Longitudinal Relations

By comparing the standard Lorentz decomposition (eq. 2.2.14) with the decomposition into v/A and s/P parts we can identify the longitudinal components of the correlator as being purely scalar. The latter decomposition can be written as [20, 52]

$$q^2 \Pi^{\mu\nu}(q^2) = (q^\mu q^\nu - q^2 g^{\mu\nu}) \Pi^{V,A}(q^2) + g^{\mu\nu} (m_i \mp m_j) \Pi^{S,P}(q^2) + g^{\mu\nu} (m_i \mp m_j) [\langle \Omega | \bar{q}_i q_i | \Omega \rangle \mp \langle \Omega | \bar{q}_j q_j | \Omega \rangle], \quad (2.2.15)$$

where the third term is a correction arising due to the physical vacuum  $|\Omega\rangle$ . By multiplying eq. 2.2.15 by two four-momenta and making use of the Ward identity eq. 2.2.11 we can write

$$q_\mu q_\nu \Pi^{\mu\nu}(q^2) = (m_i \mp m_j)^2 \Pi^{S,P}(q^2) + (m_i \mp m_j) [\langle \bar{q}_i q_i \rangle \mp \langle \bar{q}_j q_j \rangle], \quad (2.2.16)$$

which then can be related to the longitudinal component of eq. 2.2.14 by comparison with

$$q_\mu q_\nu \Pi^{\mu\nu}(q^2) = q^4 \Pi^{(0)}(q^2) = s^2 \Pi^{(0)}(s) \quad \text{with} \quad s \equiv q^2, \quad (2.2.17)$$

leading to

$$s^2 \Pi^{(0)}(s) = (m_i \mp m_j)^2 \Pi^{(S,P)}(s) + (m_i \mp m_j) [\langle \bar{q}_i q_i \rangle \mp \langle \bar{q}_j q_j \rangle]. \quad (2.2.18)$$

Note that all appearing mass terms are related to the longitudinal component. As the  $\tau$  decays, with the limiting factor of the tau mass, can only decay into light quarks we will often neglect the quark masses and work in the so-called *chiral limit* ( $m_q \rightarrow 0$ ), in which the longitudinal component is going to vanish.

By defining a combination of the transversal and longitudinal correlator

$$\Pi^{(1+0)}(s) \equiv \Pi^{(1)}(s) + \Pi^{(0)}(s) \quad (2.2.19)$$

we can additionally relate the transversal and vectorial components via

$$\Pi^{\mu\nu}(s) = \underbrace{(q^\mu q^\nu - g^{\mu\nu} q^2) \Pi^{(1)}(s) + (q^\mu q^\nu - g^{\mu\nu} q^2) \Pi^{(1)}(s)}_{=(q^\mu q^\nu - g^{\mu\nu} q^2) \Pi^{(1+0)}(s)} + \frac{g^{\mu\nu} s^2}{q^2} \Pi^{(0)}(s), \quad (2.2.20)$$

such that

$$\Pi^{(V,A)}(s) = \Pi^{(1)}(s) + \Pi^{(0)}(s) = \Pi^{(1+0)}(s), \quad (2.2.21)$$

where the vector/axial-vector component of the correlator is now related to the newly defined transversal and longitudinal combination of the correlator.

Having dealt exclusively with the perturbative part of the theory, we have to discuss NP contributions. These arise due to non-negligible long distance-effects. Thus to complete the needed ingredients for the QCDSR we need a final ingredient the OPE, which treats the NP contributions of our theory.

## 2.3. Operator Product Expansion

The OPE was introduced by Wilson in 1969 [89] as an alternative to the in this time commonly used current algebra. The expansion states that products of operators at different space-time points can be rewritten into a sum of composite local operators and their corresponding coefficients:

$$\lim_{x \rightarrow y} A(x)B(y) = \sum_n C_n(x-y) \mathcal{O}_n(x), \quad (2.3.1)$$

where  $C_n(x-y)$  are the so-called *Wilson coefficients* and  $A, B$  and  $\mathcal{O}_n$  are operators.

The OPE lets us separate short distances from long distances. In pure PT, we can only amount for short distances, which are equal to high energies, where the strong coupling  $\alpha_s$  is small. The OPE on the other hand accounts for long-distance effects with higher dimensional operators. Applying the OPE to the two-point function we get a sum over the vacuum expectation values

$$\Pi_{\text{OPE}}(q^2) = -\frac{1}{3q^2} \sum_n \langle \Omega | \mathcal{O}_n(0) | \Omega \rangle \int d^4x e^{iqx} C_n(x). \quad (2.3.2)$$

The form of the composite operators is dictated by gauge and Lorentz symmetry. For the two-point function in eq. 2.3.2 we only have to consider operators  $\mathcal{O}_n$  of dimension

$$d(\mathcal{O}_n) \leq (D-4) + 2N. \quad (2.3.3)$$

The scalar operators up to dimension six are then given by [63]

$$\begin{aligned}
 \text{Dimension 0: } & \mathbb{1} \\
 \text{Dimension 4: } & : m_i \bar{q} q : \\
 & : G_a^{\mu\nu}(x) G_{\mu\nu}^a(x) : \\
 \text{Dimension 6: } & : \bar{q} \Gamma q \bar{q} \Gamma q : \\
 & : \bar{q} \Gamma \frac{\lambda^a}{2} q_\beta(x) \bar{q} \Gamma \frac{\lambda^a}{2} q : \\
 & : m_i \bar{q} \frac{\lambda^a}{2} \sigma_{\mu\nu} q G_a^{\mu\nu} : \\
 & : f_{abc} G_a^{\mu\nu} G_b^{\nu\delta} G_c^{\delta\mu} :,
 \end{aligned} \tag{2.3.4}$$

where  $\Gamma$  stands for one of the possible Dirac matrices (as seen eq. 2.2.4). Note, that the  $D = 2$  operator violates gauge symmetry and is consequently excluded from our list. Within PT only the unit operator would exist, as the higher dimensional operators would appear as normal ordered products of fields and vanish by being sandwiched into the perturbative vacuum. On the contrary, in NP QCD, they appear as *condensates*. Condensates are the vacuum expectation values of non-vanishing, normal ordered, fields by applying the full QCD vacuum, which contribute to all strong processes. For example, the condensates of dimension four are the quark-condensate  $m_i \langle \bar{q} q \rangle$  and the gluon-condensate  $\langle GG \rangle$ .

As long as working with dimensionless functions (e.g. the correlator  $\Pi$  in eq. 2.3.2), the *right-hand side* (RHS) of eq. 2.3.1 has to be dimensionless. As a result, the Wilson coefficients have to cancel the dimension of the operator with their inverse mass dimension. To account for the dimensions we can make the inverse momenta explicit

$$\Pi_{V/A}^{\text{OPE}}(s) = \sum_{D=0,2,4,\dots} \frac{C^{(D)} \langle \Omega | \mathcal{O}^{(D)}(x) | \Omega \rangle}{(-q^2)^{D/2}}, \tag{2.3.5}$$

where we used  $c^{(D)} = C^{(D)} / (-s)^{D/2}$  with  $D$  being the dimension. Thus the OPE should converge with increasing dimension for sufficiently large momenta  $s$ .

### 2.3.1. A practical example

Let us show how the OPE contributions are calculated with a standard example [78, 63]. We will compute the perturbative and quark condensate Wilson

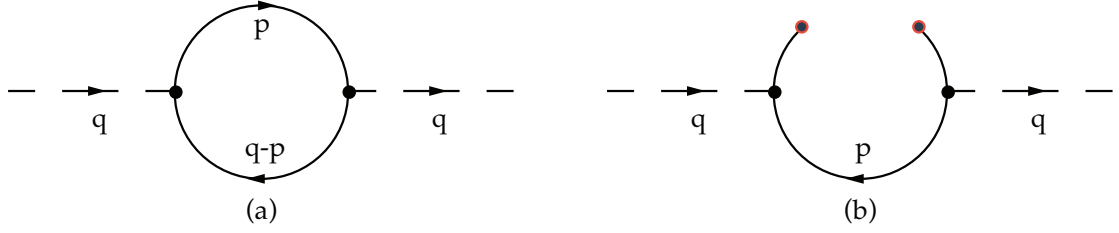


Figure 2.5.: Feynman diagrams of the perturbative (a) and the quark-condensate (b) contribution. The upper part of the right diagram is not Wick contracted and responsible for the condensate.

coefficients for the  $\rho$  meson. To do so we have to evaluate Feynman diagrams using standard PT.

The  $\rho$  meson is a vector meson of isospin one composed of  $u$  and  $d$  quarks. As a result (see. [table 2.2](#)) we can match its quantum numbers with the current

$$J^\mu(x) = \frac{1}{2} \left( : [\bar{u} \gamma^\mu u](x) - [\bar{d} \gamma^\mu d](x) : \right). \quad (2.3.6)$$

Pictorial the dimension zero contribution is given by the quark-antiquark loop Feynman diagram in [fig. 2.5](#). The higher dimension contributions are given by the same Feynman diagram, but with non-contracted fields. These non-contracted fields contain the condensates. Thus not contracting the quark-antiquark field (see. [fig. 2.5 b](#)) will give us access to the Wilson coefficient of the dimension four-quark condensate  $m_i \langle \bar{q} q \rangle$ .

The perturbative part (the Wilson coefficient of dimension zero) can then be taken from the mathematical expression for the scalar correlator

$$\begin{aligned} \Pi(q^2) = & -\frac{i}{4q^2(D-1)} \int d^D x e^{iqx} \langle \Omega | T \{ : \bar{u}(x) \gamma^\mu u(x) - \bar{d}(x) \gamma^\mu d(x) : \\ & \times : \bar{u}(0) \gamma_\mu u(0) - \bar{d}(0) \gamma_\mu d(0) : \} \rangle. \end{aligned} \quad (2.3.7)$$

To extract the dimension zero Wilson coefficient we apply Wick's theorem to contract all of the fields, which represents the lowest order of the perturbative contribution. The calculation is solely using standard PT and we will restrict



ourselves in displaying the result and omitting the calculation<sup>2</sup>

$$\begin{aligned}
 \Pi(q^2) &= \frac{i}{4q^2(D-1)} (\gamma^\mu)_{ij} (\gamma_\mu)_{kl} \int d^D x e^{iqx} \\
 &\times \left[ \overline{u_{j\alpha}(x)} \overline{u_{k\beta}(0)} \cdot \overline{u_{l\beta}(0)} \overline{u_{i\alpha}(x)} + (u \rightarrow d) \right] \\
 &= \frac{3}{8\pi^2} \left[ \frac{5}{3} - \log \left( -\frac{q^2}{v^2} \right) \right].
 \end{aligned} \tag{2.3.8}$$

To calculate the higher dimensional contributions of the OPE we use the same techniques as before. We apply Wick's theorem, but in this case, due to the NP vacuum, we have non-vanishing vacuum expectation value of normal ordered products of fields. Thus some of the fields are left uncontracted, as can be graphically seen in [fig. 2.5](#). For leaving the quark field uncontracted in [eq. 2.3.7](#) we get

$$\begin{aligned}
 \Pi(q^2) &= \frac{i}{4q^2(D-1)} (\gamma^\mu)_{ij} (\gamma_\mu)_{kl} \int d^D x e^{iqx} \left[ \right. \\
 &+ \overline{u_{j\alpha}(x)} \overline{u_{k\beta}(0)} \cdot \langle \Omega | : \overline{u_{i\alpha}(x)} u_{l\beta}(0) : | \Omega \rangle \\
 &\left. + \overline{u_{l\beta}(0)} \overline{u_{i\alpha}(x)} \cdot \langle \Omega | : \overline{u_{k\beta}(0)} u_{j\alpha}(x) : | \Omega \rangle + (u \rightarrow d) \right],
 \end{aligned} \tag{2.3.9}$$

where  $(u \rightarrow d)$  is representing the previous expressions with  $u$  and  $d$  interchanged. Here we can observe the condensates as non-vanishing vacuum values of the normal ordered product of fields:

$$\langle \Omega_{\text{QCD}} | : \overline{q}(x) q(0) : | \Omega_{\text{QCD}} \rangle \neq 0. \tag{2.3.10}$$

We emphasised the QCD vacuum  $\Omega_{\text{QCD}}$ , which is responsible for vacuum expectation values different than zero. E.g. for a vacuum of QED this contributions would vanish by definition. Pictorial the condensates take the form of unconnected propagators, sometimes marked with an  $\times$ , as seen in [fig. 2.5](#).

To make the non-contracted fields local, we can expanded them in  $x$

$$\begin{aligned}
 \langle \Omega | : \overline{q}(x) q(0) : | \Omega \rangle &= \langle \Omega | : \overline{q}(0) q(0) : | \Omega \rangle \\
 &+ \langle \Omega | : [\partial_\mu \overline{q}(0)] q(0) : | \Omega \rangle x^\mu + \dots,
 \end{aligned} \tag{2.3.11}$$

<sup>2</sup>The interested reader can follow [\[63\]](#) for a detailed calculation.

where terms with derivatives lead to higher dimensional operators, which can be seen by applying the equation of motions. We then can focus on the first term and introduce a standard notation for the localised condensate

$$\langle \bar{q} q \rangle \equiv \langle \Omega | : \bar{q}(0) q(0) : | \Omega \rangle. \quad (2.3.12)$$

Finally, the contribution to the  $\rho$  scalar correlator is then given by the following expression

$$\Pi_{(\rho)}(q^2) = \frac{1}{2} \frac{1}{(Q)^2} \left[ m_u \langle \bar{u} u \rangle + m_d \langle \bar{d} d \rangle \right], \quad (2.3.13)$$

where we defined  $Q \equiv -q^2$ . Here we can clearly see that for dimension four we get a factor of  $1/(Q)^2$ , which is responsible for the suppression of the series. The condensates  $\langle \bar{u} u \rangle$  and  $\langle \bar{d} d \rangle$  are numbers, that have to be derived by phenomenological fits or computed from LQCD. Fortunately once found, the value of the condensate can be used for any process.

In summary, we note that the usage of the OPE and its validity is far from obvious. Until today there is no analytic proof of the OPE. Furthermore, we are deriving the OPE from matching the Wilson coefficients to Feynman graph analyses. These Feynman graphs are calculated perturbatively but the coefficients with dimension  $D > 0$  correspond to NP condensates! The condensates by themselves have to be gathered from external, NP methods.

Now that we have a tool to deal with the QCD vacuum and NPT effects we are left with two problems. First, we still do not know how to deal with hadronic states in the quark-gluon picture. This will be tackled by duality. Secondly, we have seen that we can access the two-point function theoretically on the physical sheet except for the positive real axis, due to its analytic properties. Unfortunately, the experimental measurable spectral function is solely be defined on this positive real axis, which is theoretically not accessible. To match the theory with the experiment we will have to apply Cauchy's theorem. In the final section of this chapter, we will combine the two-point function, the OPE, duality and Cauchy's theorem to formulate the QCDSR.

## 2.4. Sum Rules

The QCDSR are a method to connect the *degrees of freedom* (DOF) of QCD, the quarks and gluon fields, to the DOF of the vacuum spectrum of hadrons, thereby allowing for the determination of the strong coupling. To do so we have to treat the in [section 2.2](#) introduced two-point function  $\Pi$  with the help of the OPE

$$\Pi(s) \rightarrow \Pi_{\text{OPE}}(s). \quad (2.4.1)$$

QCDSR furthermore introduce an ad hoc assumption, namely *quark-hadron duality*, stating that the observable hadron picture can be equally described by the QCD quark-gluon picture and that both pictures are equally valid. As the experimentally measured hadronic states are represented in poles and cuts on the positive real axis of the two-point function, which we have encountered in the analytic properties of its spectral decomposition, we will follow the prescription of QCDSR to apply *Cauchy's theorem* and weight functions to take care of perturbative complications close to the positive real axis.

### 2.4.1. The Dispersion Relation

We have already seen the Källén-Lehmann spectral representation in [eq. 2.4.2](#). The general dispersion relation is defined to have an additional polynomial function  $P(s)$

$$\Pi(s) = \int_0^\infty \frac{\rho(s')}{s' - s - i\epsilon} + P(s), \quad (2.4.2)$$

which accounts for the fact, that the two-point function increases for large  $s$ , but the integral on the RHS cannot reproduce this behaviour. For example the vector correlator carries only a constant and the scalar correlator a linear polynomial. The two-point function is, in general, an unphysical quantity, whereas the spectral function  $\rho(s)$  is a physical quantity. As a result, the polynomial accounts for the unphysical scale dependency of the two-point function.

### 2.4.2. Duality

QCD treats quarks and gluon as its fundamental DOF, but due to confinement, we are only ever able to observe hadrons. The mechanism that connects the two worlds is the *quark-hadron duality* (or simply duality), which implies that physical quantities can be described equally good in the hadronic as in the quark-gluon picture. Thus we can connect experimental detected values with theoretically calculated values from the two-point function in the dispersion relation eq. 2.4.2 as

$$\Pi_{\text{th}}(s) = \int_0^\infty \frac{\rho(s')_{\text{exp}}}{s' - s - i\epsilon} + P(s), \quad (2.4.3)$$

where we connected the theoretical correlator  $\Pi_{\text{th}}$  with the experimental measurable spectral function  $\rho_{\text{exp}}$ . We can represent duality as, substituting the two-point function [24]

$$\Pi(s) \rightarrow \Pi_{\text{OPE}}(s). \quad (2.4.4)$$

If this approximation carries no error, we would say that the experimental spectral function is dual to the OPE. On the contrary, if the substitution is not exact we are missing contributions, which are represented by so-called DV.

#### Duality Violations

There exist situations where we cannot make use of duality as an assumption. These situations are referred to as DV and belong to the NP part of the theory. It is often assumed that by applying the OPE to all orders we account for all NP effects, including DV. Unfortunately, this assumption is only partly right. Even if we could compute the OPE to all orders, we would still experience discrepancies to our theoretical results. In general, it is said, that if we have deviations beyond the natural uncertainty of the OPE we call them DV [76]. E.g. if we compute  $\Pi(s)$  to orders of  $\alpha^2$  and  $\frac{1}{Q^4}$ , while we cutoff higher orders ( $\alpha^3$  and  $\frac{1}{Q^6}$ ) we get a natural error because we have not calculated the full series. Values of the hadronic spectral density, out of range of the natural error, are then referred to as DV.

A detailed discussion of duality has been given by the Shifman in [76].

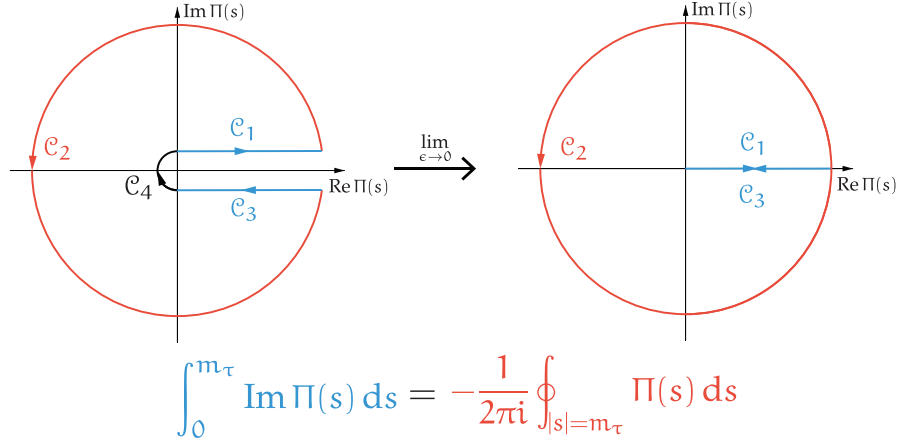


Figure 2.6.: Visualisation of the usage of Cauchy's theorem to transform eq. 2.4.2 into a closed contour integral over a circle of radius  $s_0$ .

### 2.4.3. Finite Energy Sum Rules

To theoretically calculate the two-point function we have to integrate the experimental data  $\rho_{\text{exp}}(s)$  from zero to infinity. No experiment will ever take data for an infinite momentum  $s$ . For  $\tau$  decays we are limited to energies around the  $\tau$  mass of 1.776 GeV. To deal with the upper integration limit several approaches have been made. One of them, the *Borel transform*, is to exponentially suppress higher energy contributions (see [87, 72]). The technique we are focusing on is called *finite energy sum rules* (FESR) and introduces an energy cut-off. We thus integrate the experimental data  $\rho(s)$  only to a certain energy  $s_0$ . Furthermore, we have to theoretically evaluate the integral over the spectral function of the dispersion relation (eq. 2.4.2), which includes singularities caused by the hadronic spectrum. As a result, we have to apply Cauchy's theorem

$$\oint_{\mathcal{C}} f(z) = 0, \quad (2.4.5)$$

which states that any integral over an analytic function  $f(z)$  on a closed contour  $\mathcal{C}$  has to be zero. Thus we can construct a contour to avoid the positive problematic real axis. Pictorial the contour is drawn in fig. 2.6 and mathematically we can express it as

$$\oint \Pi(s) = \int_0^{s_0} \Pi(s + i\epsilon) - \Pi(s - i\epsilon) ds + \int_{0+\alpha(\epsilon)}^{2\pi-\alpha(\epsilon)} \Pi(s_0 e^{i\theta}) d\theta + \int_{3\pi/2}^{\pi/2} \Pi(\epsilon e^{i\theta}) d\theta. \quad (2.4.6)$$

If we make to use of *Schwartz reflection principle*:

$$f(\bar{z}) = \overline{f(z)}, \quad (2.4.7)$$

which can be applied if  $f(z)$  is analytic and maps only to real values on the positive real axis, we can express the integrand of the first integral of eq. 2.4.6 as the imaginary part of the two-point function

$$\Pi(s + i\epsilon) - \Pi(s - i\epsilon) = \Pi(s + i\epsilon) - \Pi^*(s + i\epsilon) = 2i \operatorname{Im} \Pi(s + i\epsilon), \quad (2.4.8)$$

which is by definition equal to the spectral function

$$\rho(s) \equiv \frac{\operatorname{Im} \Pi(s)}{\pi}. \quad (2.4.9)$$

After taking the limit of small  $\epsilon$  we can relate the line integral with the lower limit zero and the upper limit  $s_0$  and the experimental spectral function as integrand to a theoretical accessible circular contour integral of radius  $s_0$

$$\int_0^{s_0} \rho(s) ds = \frac{-1}{2\pi i} \oint_{|s|=s_0} \Pi(s) ds, \quad \text{where we applied } \epsilon \rightarrow 0. \quad (2.4.10)$$

Note that the unphysical contribution of the polynomial in eq. 2.4.2 cancel in the contour integral.

We are free to multiply the upper equation with an analytic function  $\omega(s)$ , which completes the FESR

$$\int_0^{s_0} \omega(s) \rho(s) ds = \frac{-1}{2\pi i} \oint_{|s|=s_0} \omega(s) \Pi_{\text{OPE}}(s) ds \quad (2.4.11)$$

where the *left-hand side* (LHS) can be taken from the experiment and the RHS by the theoretically evaluated correlator  $\Pi_{\text{OPE}}(s)$ . The analytic function  $\omega(s)$  plays the role of a weight. It can be used to further suppress the non-perturbative contributions coming from DV and also enhance or suppress different contributions of the OPE as we will see.

#### 2.4.4. Weighting OPE dimensions

We have seen that the perturbative part of the two-point function carries a discontinuity on the positive real axis. Consequently, we applied Cauchy's

theorem to avoid the non-analytic part of the two-point function. This left us with non-closed contour integral for the perturbative part of the OPE, which will always contribute. On the other hand, the strength of the higher dimension contributions of the OPE can be modified. We can use different weights to control the dimensions of the OPE that contribute. The weights we are using have to be analytic so that we can make use of Cauchy's theorem. Thus they can be represented as polynomials

$$\omega(x) = \sum_i a_i x^i, \quad (2.4.12)$$

every contributing monomial is responsible for a dimension of the OPE. Dimensions that are not represented in the weight polynomial do not contribute at all or are very suppressed as we will demonstrate now.

The residue of a monomial  $x^k$  is only different from zero if its power  $k = -1$ :

$$\oint_C x^k dx = i \int_0^{2\pi} (e^{i\theta})^{k+1} d\theta = \begin{cases} 2\pi i & \text{if } k = -1, \\ 0 & \text{otherwise} \end{cases}. \quad (2.4.13)$$

We will see in discussing the total  $\tau$  decay ratio, that the integrand of the closed-contour integral in eq. 2.4.11 for the different OPE contributions is the weight function divided by a term proportional to  $x^{D/2}$ , where  $D$  is the dimension of the contributing OPE operator. If we regard solely a monomial as weight and neglect all terms of no interest to us we can write

$$\begin{aligned} R'(x)|_{D=0,2,4,\dots} &= \oint_{|x|=1} dx \frac{x^k}{x^{D/2}} C^D \\ &= \oint_{|x|=1} dx x^{k-D/2} C^D, \end{aligned} \quad (2.4.14)$$

where  $C^D$  are the  $D$  dimensional Wilson coefficients. We can make use of eq. 2.4.14 as we neglect the logarithmic corrections of dimension four ope contributions and use a simple ansatz for the higher order OPE dimension, which treats the Wilson coefficients as a constant. Thus combining eq. 2.4.13 with eq. 2.4.14 we see that only dimensions which fulfil

$$k - D/2 = -1 \implies D = 2(k+1) \quad (2.4.15)$$

contribute to the OPE. For example, the polynomial of the kinematic weight

$$\omega_\tau(s) \equiv \left(1 - \frac{s}{m_\tau^2}\right) \left(1 + 2\frac{s}{m_\tau^2}\right) \quad (2.4.16)$$

<b>monomial:</b>	$x^0$	$x^1$	$x^2$	$x^3$	$x^5$	$x^6$	$x^7$
<b>dimension:</b>	$D^{(2)}$	$D^{(4)}$	$D^{(6)}$	$D^{(8)}$	$D^{(10)}$	$D^{(12)}$	$D^{(14)}$

Table 2.3.: List of monomial and their corresponding “active” dimensions in the OPE. Note that the perturbative contributions of the OPE are always present.

, which will appear naturally in the context of the total  $\tau$  decay ratio, is given by

$$(1-x)^2(1+2x) = \underbrace{1}_{D=2} - 3 \underbrace{x^2}_{D=6} + 2 \underbrace{x^3}_{D=8}, \quad (2.4.17)$$

where the underbraced monomials express the active dimensions. A list of monomials and their corresponding dimensions up to dimension 14 can be found in [table 2.3](#). This behaviour enables us to bring out different dimensions of the OPE and suppress contributions of higher order ( $D \geq 10$ ) for which less is known.

For the interested reader, we gathered several introduction texts to the QCDSR, which were of great use to us [[61](#), [72](#), [30](#), [38](#)].



## Tau Decays into Hadrons

The  $\tau$  lepton is an elementary particle with spin 1/2 and a mass of 1.776 86 GeV [82]. It is the only lepton heavy enough to decay into hadrons but also light enough for performing a low-energy QCD analysis. Its inclusive hadronic<sup>1</sup> decay ratio is given by

$$R_\tau = \frac{\Gamma(\tau \rightarrow \nu_\tau + \text{hadrons})}{\Gamma(\tau \rightarrow \nu_\tau e^- \bar{\nu}_e)} \quad (3.0.1)$$

and sensible to the strong coupling, due to its rather large value, at the  $m_\tau^2$  scale, of approximately 0.33. On the other hand  $\alpha_s(m_\tau^2)$  is small enough to apply the OPE. The NP OPE contributions to the decay ratio are suppressed. The dimension two contributions of the OPE are proportional to the quark masses and have only a tiny contribution for light quarks. The dimension four contributions can be suppressed by applying weight functions, that do not have a monomial term  $x$ . E.g. the kinematic weight  $\omega_\tau = (1-x)^2(1+2x) = 1 - 3x^2 + 2x^3$  is not sensitive to OPE corrections of dimension four. The dimension six contributions of the OPE are suppressed by a factor of  $1/s^3$ . They are further suppressed in the  $V+A$  channel, as the vector and axial-vector contributions have opposite signs and partly cancel themselves. Higher dimensional OPE contributions are suppressed by terms of  $1/s^{2n}$  with  $n \geq 4$ . As a result, the perturbative contributions are dominant. They are known up to order  $\mathcal{O}(\alpha_s^4)$  with a total contribution of 20% to  $R_\tau$  [69], which enables us to perform precise calculations of the inclusive  $\tau$  decay ratio. Extracting  $\alpha_s$  at low energies leads

<sup>1</sup>Meaning all decay channels with a hadron in its final state.

to low errors for  $\alpha_s$  at high energies. The strong coupling and their errors run and get smaller with increasing energy. We compare the strong coupling at the Z-boson scale of around 91 GeV. Consequently the strong coupling at  $m_Z^2$  from inclusive tau decays has especially low errors.

Hadronic  $\tau$  decays permit one of the most precise determinations of the strong coupling  $\alpha_s$ . Building on the previously presented QCDSR we will now elaborate the needed theory to extract  $\alpha_s$  from the process of hadronic  $\tau$  decays.

### 3.1. The Inclusive $\tau$ Decay Ratio

The theoretical expression of the inclusive hadronic  $\tau$  decay ratio (eq. 3.0.1) is given by

$$R_\tau(s) = 12\pi \int_0^{m_\tau} \frac{ds}{m_\tau^2} \left(1 - \frac{s}{m_\tau^2}\right) \left[ \left(1 + 2\frac{s}{m_\tau^2}\right) \text{Im } \Pi^{(1)}(s) + \text{Im } \Pi^{(0)}(s) \right], \quad (3.1.1)$$

where we omitted the electroweak correction ( $S_{EW}$ ) and *Cabibbo-Kobayashi-Maskawa* (CKM) matrix element squared ( $|V_{ud}|^2$ ). For brevity the two factors will be implicitly included. Equation 3.1.1 was first derived in [83], using current algebra, a more recent derivation making use of the *optical theorem* can be taken from [75]. Notice that we used the standard Lorentz decomposition into transversal ( $J = 1$ ) and longitudinal ( $J = 0$ ) components of eq. 2.2.14 to display the hadronic decay ratio (eq. 3.1.1).

Applying Cauchy's theorem, as seen in eq. 2.4.11, to the eq. 3.1.1 we can rewrite the line integral into a closed contour integral

$$R_\tau = 6\pi i \oint_{|s|=m_\tau} \frac{ds}{m_\tau^2} \left(1 - \frac{s}{m_\tau^2}\right) \left[ \left(1 + 2\frac{s}{m_\tau^2}\right) \Pi^{(1)}(s) + \Pi^{(0)}(s) \right]. \quad (3.1.2)$$

It is convenient to work with a slightly different combination of transversal and longitudinal components  $\Pi^{(1+0)}$ , which has been defined in eq. 2.2.19 and is free of kinematic singularities. As a result, we can further rewrite the hadronic  $\tau$  decay ratio into

$$R_\tau = 6\pi i \oint_{|s|=m_\tau} \frac{ds}{m_\tau^2} \left(1 - \frac{s}{m_\tau^2}\right)^2 \left[ \left(1 + 2\frac{s}{m_\tau^2}\right) \Pi^{(1+0)}(s) - \left(\frac{2s}{m_\tau^2}\right) \Pi^{(0)}(s) \right]. \quad (3.1.3)$$

In the case of  $\tau$  decays we only have to consider vector and axial-vector contributions of decays into up, down and strange quarks.

With eq. 3.1.3 we have a suitable physical quantity that can be theoretically calculated as well as experimentally measured. By using the QCDSR we apply a closed contour integral of radius  $s_0$ . As a result, we successfully avoid low energies at which the application of PT would be questionable. For example, by choosing a radius with the size of the  $\tau$  mass  $m_\tau \approx 1.78 \text{ MeV}$  the strong coupling has a perturbatively safe value of  $\alpha_s(m_\tau^2) \approx 0.33$  [68]. Obviously, we would benefit even more from a contour integral over a bigger circumference, but  $\tau$  decays are kinematically limited by their mass. Nevertheless, there are promising  $e^+e^-$  annihilation data, which yield inclusive decay ratio values up to 2 GeV [14][54].

### 3.1.1. Renormalisation Group Invariance

We have seen in section 2.2, that the two-point function is not a physical quantity, due to the dispersion relation (eq. 2.4.2) containing an unphysical polynomial. Luckily for the vector correlator, appearing in hadronic  $\tau$  decays, the polynomial is just a constant. Consequently, we can take the derivative with respect to the momentum  $s$  to derive a physical quantity from the two-point function:

$$D(s) \equiv -s \frac{d}{ds} \Pi(s). \quad (3.1.4)$$

$D(s)$  is called the *Adler function* and fulfils, as all physical quantities, the RGE (eq. 2.1.11). The Adler function commonly has separate definitions for the longitudinal plus transversal and the solely longitudinal contributions:

$$D^{(1+0)}(s) \equiv -s \frac{d}{ds} \Pi^{(1+0)}(s), \quad D^{(0)}(s) \equiv \frac{s}{m_\tau^2} \frac{d}{ds} (s \Pi^{(0)}(s)). \quad (3.1.5)$$

The two-point functions in eq. 3.1.3 can now be replaced with the help of partial integration

$$\int_a^b u(x) V(x) dx = [U(x) V(x)]_a^b - \int_a^b U(x) v(x) dx. \quad (3.1.6)$$

We will perform two separate computations for the  $(1+0)$  and  $(0)$  case. Starting by the transversal plus longitudinal contribution we get:

$$\begin{aligned}
 R_\tau^{(1)} &= \frac{6\pi i}{m_\tau^2} \oint_{|s|=m_\tau^2} \underbrace{\left(1 - \frac{s}{m_\tau^2}\right)^2}_{=u(x)} \underbrace{\left(1 + 2\frac{s}{m_\tau^2}\right)}_{=V(x)} \Pi^{(1+0)}(s) \\
 &= \frac{6\pi i}{m_\tau^2} \left\{ \left[ -\frac{m_\tau^2}{2} \left(1 - \frac{s}{m_\tau^2}\right)^3 \left(1 + \frac{s}{m_\tau^2}\right) \Pi^{(1+0)}(s) \right]_{|s|=m_\tau^2} \right. \\
 &\quad \left. + \oint_{|s|=m_\tau^2} \underbrace{-\frac{m_\tau^2}{2} \left(1 - \frac{s}{m_\tau^2}\right)^3}_{=U(x)} \underbrace{\left(1 + \frac{s}{m_\tau^2}\right) \frac{d}{ds} \Pi^{(1+0)}(s)}_{=v(x)} \right\} \\
 &= -3\pi i \oint_{|s|=m_\tau^2} \frac{ds}{s} \left(1 - \frac{s}{m_\tau^2}\right)^3 \left(1 + \frac{s}{m_\tau^2}\right) \frac{d}{ds} D^{(1+0)}(s),
 \end{aligned} \tag{3.1.7}$$

where we fixed the integration constant to  $c = -\frac{m_\tau^2}{2}$  in the second line and left the antiderivatives contained in the squared brackets untouched. If we parametrise the integral appearing in the expression in the squared brackets we can see that it vanishes:

$$\left[ -\frac{m_\tau^2}{2} \left(1 - e^{-i\phi}\right)^3 \left(1 + e^{-i\phi}\right) \Pi^{(L+T)}(m_\tau^2 e^{-i\phi}) \right]_0^{2\pi} = 0, \tag{3.1.8}$$

where  $s \rightarrow m_\tau^2 e^{-i\phi}$  and  $(1 - e^{-i \cdot 0}) = (1 - e^{-i \cdot 2\pi}) = 0$ . Repeating the same calculation for the longitudinal part yields

$$\begin{aligned}
 R_\tau^{(0)} &= \oint_{|s|=m_\tau^2} ds \left(1 - \frac{s}{m_\tau^2}\right)^2 \left(-\frac{2s}{m_\tau^2}\right) \Pi^{(0)}(s) \\
 &= -4\pi i \oint \frac{ds}{s} \left(1 - \frac{s}{m_\tau^2}\right)^3 D^{(0)}(s).
 \end{aligned} \tag{3.1.9}$$

Consequently combining the transversal with the longitudinal contribution results in

$$R_\tau = -\pi i \oint_{|s|=m_\tau^2} \frac{ds}{s} \left(1 - \frac{s}{m_\tau^2}\right)^3 \left[ 3 \left(1 + \frac{s}{m_\tau^2}\right) D^{(1+0)}(s) + 4 D^{(0)}(s) \right]. \tag{3.1.10}$$

It is convenient to define  $x = s/m_\tau^2$  such that we can rewrite the inclusive ratio into

$$R_\tau = -\pi i \oint_{|s|=m_\tau^2} \frac{dx}{x} (1-x)^3 \left[ 3(1+x) D^{(1+0)}(m_\tau^2 x) + 4 D^{(0)}(m_\tau^2 x) \right], \tag{3.1.11}$$

which will be the final expression used to express the inclusive  $\tau$  decay ratio.

## 3.2. Theoretical Computation of $R_\tau$

The previously derived expression for the  $\tau$  decay ratio is at first approximation equal to the number of colours [65]

$$R_\tau \approx N_c. \quad (3.2.1)$$

If we take the perturbative  $\delta_{\text{pt}}$  and non-perturbative  $\delta_{\text{npt}}$  contributions into account we can organise the vector and axial-vector inclusive decay ratio as

$$R_{\tau,V/A}^\omega = \frac{N_c}{2} \left( 1 + \delta_{\text{pt}}^\omega + \delta_{\text{npt}}^\omega \right). \quad (3.2.2)$$

Note that the factor  $1/2$  comes from the fact, that in the chiral limit the vector and axial-vector contributions are equal. The dependence on the chosen weight function  $\omega$  is reflected in the upper indices.

For the kinematic weight (eq. 2.4.16), which appears naturally in the  $\tau$  decay ratio, we have a dominant perturbative contribution of  $\delta_{\text{pt}} \approx 20\%$  to  $R_\tau$  [66] and a minor, but non-negligible, NP contribution of  $\delta_{V+A}^{\text{NP}} \lesssim 1\%$  [51] for the  $V + A$ -channel.

In the following, we want to derive the theoretical expressions needed to calculate both of the corrections to eq. 3.2.2 starting with the perturbative one.

### 3.2.1. The Perturbative Contribution

The perturbative contribution  $\delta_{\text{pt}}$  to the inclusive  $\tau$  decay ratio corresponds to the first term of the OPE. Currently, the perturbative expansion has been calculated to fourth order  $\mathcal{O}(\alpha_s^4)$ . Due to their role as dominant corrections, their uncertainties from unknown higher-order corrections dictate the final error of the determination of the strong coupling [68].

We will treat the correlator in the chiral limit, in which the scalar and pseudo-scalar contributions of the two-point function vanish and the axial and vectorial contributions are equal. As a result, we can focus on the vector correlator

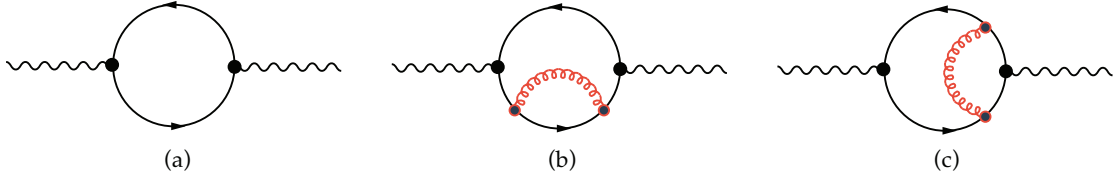


Figure 3.1.: Feynman loop diagrams to calculate the  $c_{n,k}$  coefficients of the expanded correlator  $\Pi_V^{(1+0)}$ . The internal red lines represent gluons. Diagram a) represents the parton model and diagrams b) and c) represent higher order corrections.

$\Pi_V(s)$ , which can be expanded as a sum over different orders of  $\alpha$  [8]:

$$\Pi_V^{(1+0)}(s) = -\frac{N_c}{12\pi^2} \sum_{n=0}^{\infty} a_\mu^n \sum_{k=0}^{n+1} c_{n,k} L^k \quad \text{with} \quad L \equiv \ln \frac{-s}{\mu^2}, \quad (3.2.3)$$

where we defined  $a_\mu \equiv \alpha(\mu)/\pi$ . The coefficient  $c_{n,k}$  up to two-loop order can be obtained by Feynman diagram calculations. With the diagrams of fig. 3.1 we can calculate the one-loop result of the correlator [50]

$$\Pi_V^B(q^2) \Big|^{1\text{-loop}} = \frac{N_c}{12\pi^2} \left( \frac{1}{\hat{\epsilon}} - \log \frac{(-q^2 - i0)}{\mu^2} + \frac{5}{3} + \mathcal{O}(\epsilon) \right), \quad (3.2.4)$$

where  $\Pi_{\mu\nu}^B(q^2)$  is the bare two-point function<sup>2</sup>. This result can then be used to extract the first two coefficients of the correlator expansion given in eq. 3.2.4

$$c_{0,0} = -\frac{5}{3} \quad \text{and} \quad c_{0,1} = 1. \quad (3.2.5)$$

The second loop can also be calculated by diagram techniques resulting in [10]

$$\Pi_V^{(1+0)}(s) \Big|^{2\text{-loop}} = -\frac{N_c}{12\pi^2} a_\mu \log\left(\frac{-s}{\mu^2}\right) + \dots. \quad (3.2.6)$$

From the above equation we can then extract the Adler coefficient  $c_{1,1} = 1$ .

Beginning from three loop diagrams the algebra becomes exhausting and one has to use dedicated algorithms to compute the higher loops. The third loop calculations have been done in the late seventies [28, 37, 27]. The four loop evaluation has been completed a little more than ten years later [42, 81]. The

<sup>2</sup>The term  $1/\hat{\epsilon}$ , which is of order zero in  $\alpha_s$ , is not present in the Adler function or the imaginary part of the correlator.

highest calculated loop, that amounts to  $\alpha_s^4$ , was published in 2008 [5] almost 20 years later.

By fixing the number of colours to  $N_c = 3$ , we can write the missing coefficients up to order four in  $\alpha_s$ :

$$\begin{aligned} c_{2,1} &= \frac{365}{24} - 11\zeta_3 - \left(\frac{11}{12} - \frac{2}{3}\zeta_3\right) N_f \\ c_{3,1} &= \frac{87029}{288} - \frac{1103}{4}\zeta_3 + \frac{275}{6}\zeta_5 \\ &\quad - \left(\frac{7847}{216} - \frac{262}{9}\zeta_3 + \frac{25}{9}\zeta_5\right) N_f + \left(\frac{151}{162} - \frac{19}{27}\zeta_3\right) N_f^2 \\ c_{4,1} &= \frac{78631453}{20736} - \frac{1704247}{432}\zeta_3 + \frac{4185}{8}\zeta_3^2 + \frac{34165}{96}\zeta_5 - \frac{1995}{16}\zeta_7, \end{aligned} \quad (3.2.7)$$

where we used the flavour number  $N_f = 3$  for the last line.

The six loop calculation has until today not been computed, but Beneke and Jamin [8] made an educated guess to estimate the coefficient

$$c_{5,1} \approx 283 \pm 283. \quad (3.2.8)$$

We often see  $c_{5,1}$  applied to estimate the perturbative errors related to missing higher order contributions.

In stating the coefficients  $c_{n,k}$  of the correlator expansion we have restricted ourselves to  $k$  indices equal to one. This is due to the RGE, which relates coefficients with  $k$  different than one to coefficients with  $k$  equal to one ( $c_{n,1}$ ). Consequently, the vector correlator  $\Pi_V^{(1+0)}(s)$  needs to be transformed into a physical quantity, which can be achieved by applying the derivative with respect to  $s$ , yielding the previously defined Adler function (eq. 3.1.5). The correct expression for the correlator expansion in eq. 3.2.4 is then given by

$$D_V^{(1+0)} = -s \frac{d\Pi_V^{(1+0)}(s)}{ds} = \frac{N_c}{12\pi^2} \sum_{n=0}^{\infty} a_\mu^n \sum_{k=1}^{n+1} k c_{n,k} L^{k-1}, \quad (3.2.9)$$

where we used  $dL^k/ds = k \ln(-s/\mu^2)^{k-1} (-1/\mu^2)$ . Applying the RGE (eq. 2.1.11) to the scale-invariant Adler function yields

$$-\mu \frac{d}{d\mu} D_V^{(1+0)} = -\mu \frac{d}{d\mu} \left( \frac{\partial}{\partial L} D_L + \frac{\partial}{\partial a_s} D_{a_s} \right) D_V^{(1+0)} = \left( 2 \frac{\partial}{\partial L} + \beta \frac{\partial}{\partial a_s} \right) D_V^{(1+0)} = 0, \quad (3.2.10)$$

where we made use of the  $\beta$ -function, which is defined in eq. 2.1.12, and of the expression  $dL/d\mu = -2/\mu$ .

The relation between the correlator expansion coefficients can then be taken by calculating the Adler function for a desired order and plugging it into the RGE. For example, the Adler function to the second order in  $\alpha_s$  is expressed as

$$D(s) = \frac{N_c}{12\pi^2} \left[ c_{01} + a_\mu(c_{11} + 2c_{12}L) + a_\mu^2(c_{21} + 2c_{22}L + 3c_{23}L^2) \right]. \quad (3.2.11)$$

Inserting the newly obtained Adler function into eq. 3.2.11 yields

$$4a_\mu c_{12} + 2a_\mu^2(2c_{22} + 6c_{23}L) + \beta_1 a_\mu^2(c_{11} + 2c_{12}L) + \mathcal{O}(a_\mu^3) = 0. \quad (3.2.12)$$

From this equation, we can compare the coefficients order by order in  $\alpha_s$  to constrain the Adler function coefficients. At order  $\alpha_\mu$  only the  $c_{12}$  term is present and has to be zero. For  $\mathcal{O}(a_\mu^2 L)$  solely  $c_{23}$  exists as  $c_{12} = 0$  and has to vanish. Finally for  $\mathcal{O}(a)$  we can relate  $c_{22}$  with  $c_{11}$  resulting in

$$c_{12} = 0, \quad c_{22} = \frac{\beta_1 c_{11}}{4} \quad \text{and} \quad c_{23} = 0. \quad (3.2.13)$$

Implementing the newly obtained Adler coefficients we can write out the Adler function to the first order:

$$D(s) = \frac{N_c}{12\pi^2} \left[ c_{01} + c_{11} a_\mu \left( c_{21} - \frac{1}{2} \beta_1 c_{11} L \right) a_\mu^2 \right] + \mathcal{O}(a_\mu^3). \quad (3.2.14)$$

We have used the RGE to relate Adler function coefficients and thus only need to know the coefficients of type  $c_{n,1}$ . Unfortunately, as we will see in the following section, the RGE gives us two different choices to compute the perturbative contribution to the inclusive  $\tau$  decay ratio.

### Renormalisation Group Summation

By making use of the RGE we have to decide about the order of mathematical operations we perform. As the all order perturbative contribution  $\delta_{pt}$  is independent on the scale  $\mu$  we are confronted with two choices, namely FOPT and CIPT. Each of them yields a different result, which is the main source of error in extracting the strong coupling from  $\tau$  decays.



Working in the chiral limit additionally permits us to neglect the longitudinal contribution  $D^{(0)}$ , in eq. 3.1.11 of the perturbative contribution  $\delta_{\text{pt}}$  of  $R_\tau$  (eq. 3.2.2). Thus inserting the expansion of  $D_V^{(1+0)}$  into the hadronic  $\tau$  decay width eq. 3.1.11 yields

$$\delta_{\text{pt}} = \sum_{n=1}^{\infty} a_\mu^n \sum_{k=1}^n k c_{n,k} \frac{1}{2\pi i} \oint_{|x|=1} \frac{dx}{x} (1-x)^3 (1+x) \log \left( \frac{-m_\tau^2 x}{\mu^2} \right)^{k-1}, \quad (3.2.15)$$

where the contributions from the vector and axial-vector correlator are identical in the massless case.

To continue evaluating the perturbative part we can now either follow the description of FOPT or CIPT.

In FOPT, we fix the renormalisation scale at the  $\tau$  mass ( $\mu^2 = m_\tau^2$ ), which leaves us with the integration over the logarithm, as can be seen in

$$\delta_{\text{FOPT}}^{(0)} = \sum_{n=1}^{\infty} a(m_\tau^2)^n \sum_{k=1}^n k c_{n,k} J_{k-1}, \quad (3.2.16)$$

where the contour integrals  $J_l$  are defined by

$$J_l \equiv \frac{1}{2\pi i} \oint_{|x|=1} \frac{dx}{x} (1-x)^3 (1+x) \log^l(-x). \quad (3.2.17)$$

The integrals  $J_l$  up to order  $\alpha_s^4$  are given by [8]:

$$J_0 = 1, \quad J_1 = -\frac{19}{12}, \quad J_2 = \frac{265}{72} - \frac{1}{3}\pi^2, \quad J_3 = -\frac{3355}{288} + \frac{19}{12}\pi^2. \quad (3.2.18)$$

Using FOPT the strong coupling  $a(\mu)$  is fixed at the  $\tau$  mass scale  $a(m_\tau^2)$  and can be taken out of the closed-contour integral. Thus we solely have to integrate over the logarithms  $\log(x)$ .

Using CIPT, on the contrary, we can sum the logarithms by setting the scale to  $\mu^2 = -m_\tau^2 x$  in eq. 3.2.16, resulting in:

$$\delta_{\text{CI}}^{(0)} = \sum_{n=1}^{\infty} c_{n,1} J_n^a(m_\tau^2), \quad (3.2.19)$$

where the contour integrals  $J_n^a$  are defined by

$$J_n^a(m_\tau^2) \equiv \frac{1}{2\pi i} \oint_{|x|=1} \frac{dx}{x} (1-x)^3 (1+x) a^n(-m_\tau^2 x). \quad (3.2.20)$$

Note that all logarithms vanish, except the ones with index  $k = 1$ :

$$\log(1)^{k-1} = \begin{cases} 1 & \text{if } k = 1, \\ 0 & k \neq 1 \end{cases} \quad (3.2.21)$$

which selects the Adler function coefficients  $c_{n,1}$ . Handling the logarithms left us with the integration of the strong coupling  $\alpha_s(-m_\tau^2 x)$  over the closed-contour  $\oint_{|x|=1}$ , which now depends on the integration variable  $x$ .

In general, we have to decide if we want to perform a contour integration with a constant strong coupling parameter and variable logarithms (FOPT) or “constant logarithms” and a running coupling (CIPT). To emphasise the differences in both approaches we can calculate the perturbative contribution  $\delta^{(0)}$  to  $R_\tau$  for the two different prescriptions yielding [8]

$$\begin{array}{cccccc} \alpha_s^2 & \alpha_s^2 & \alpha_s^3 & \alpha_s^4 & \alpha_s^5 & \\ \delta_{\text{FOPT}}^{(0)} = 0.1082 + 0.0609 + 0.0334 + 0.0174(+0.0088) = 0.2200(0.2288) & (3.2.22) \end{array}$$

$$\delta_{\text{CIPT}}^{(0)} = 0.1479 + 0.0297 + 0.0122 + 0.0086(+0.0038) = 0.1984(0.2021). \quad (3.2.23)$$

The series indicate, that CIPT converges faster and that both series approach a different value. FOPT has larger contributions than CIPT, which leads to a smaller strong coupling if using FOPT. The discrepancy, between FOPT and CIPT, represents currently the biggest theoretical uncertainty for extracting the strong coupling.

As today FOPT or CIPT are equally valid approaches to calculate the perturbative contributions, even though it has been stated by Beneke et al. [8] to favour the former. Within this work, we will further elaborate on the consistency of FOPT and do not state our results in CIPT.

### 3.2.2. The Non-Perturbative OPE Contributions

The perturbative contributions to the sum rule are the dominant one, but NP have to be taken into account. The contributions of the NP part can be quoted as [51]

$$\delta_{V+A,\text{FOPT}}^{\text{NP}} = -0.086(80), \quad (3.2.24)$$

which are small, but not negligible. The NP OPE contributions are commonly categorised by even, increasing dimensions. Contributions of dimension larger than eight are normally neglected, due to the increasing suppression by factors of  $1/s^D$ , where  $D$  stands for the corresponding dimension.

The dimension two contributions are proportional to the quark masses and vanish while working in the chiral limit. Consequently, we will neglect them and start by stating the  $D = 4$  contributions.

### 3.2.3. Dimension Four Corrections

The next apparent OPE contributions are of dimension four. Here we have to take the terms with masses to the fourth power ( $m^4$ ) into account, the quark condensate multiplied by a mass ( $m\langle\bar{q}q\rangle$ ) and the gluon condensate ( $\langle\bar{G}G\rangle$ ). The resulting expression can be taken from the appendix of [67], yielding:

$$D_{ij}^{(1+0)}(s)\Big|_{D=4} = \frac{1}{s^2} \sum_n \Omega^{(1+0)}(s/\mu^2) a^n, \quad (3.2.25)$$

where the  $\Omega^{(1+0)}(s/\mu^2)$  is given by

$$\begin{aligned} \Omega_n^{(1+0)}(s/\mu^2) = & \frac{1}{6} \langle a G G \rangle p_n^{(1+0)}(s/\mu^2) + \sum_k m_k \langle \bar{q}_k q_k \rangle r_n^{(1+0)}(s/\mu^2) \\ & + 2 \langle m_i \bar{q}_i q_i + m_j \bar{q}_j q_j \rangle q_n^{(1+0)}(s/\mu^2) \pm \frac{8}{3} \langle m_j \bar{q}_i q_i + m_i \bar{q}_j q_j \rangle t_n^{(1+0)} \\ & - \frac{3}{\pi^2} (m_i^4 + m_j^4) h_n^{(1+0)}(s/\mu^2) \mp \frac{5}{\pi^2} m_i m_j (m_i^2 + m_j^2) k_n^{(1+0)}(s/\mu^2) \\ & + \frac{3}{\pi^2} m_i^2 m_j^2 g_n^{(1+0)}(s/\mu^2) + \sum_k m_k^4 j_n^{(1+0)}(s/\mu^2) + 2 \sum_{k \neq l} m_k^2 m_l^2 u_n^{(1+0)}(s/\mu^2). \end{aligned} \quad (3.2.26)$$

The perturbative expansion coefficients are known to second order  $\mathcal{O}(a^2)$  for the condensate contributions,

$$\begin{aligned} p_0^{(1+0)} = 0, \quad p_1^{(1+0)} = 1, \quad p_2^{(1+0)} = \frac{7}{6}, \\ r_0^{(1+0)} = 0, \quad r_1^{(1+0)} = 0, \quad r_2^{(1+0)} = -\frac{5}{3} + \frac{8}{3} \zeta_3 - \frac{2}{3} \log(s/\mu^2), \\ q_0^{(1+0)} = 1, \quad q_1^{(1+0)} = -1, \quad q_2^{(1+0)} = -\frac{131}{24} + \frac{9}{4} \log(s/\mu^2), \\ t_0^{(1+0)} = 0, \quad t_1^{(1+0)} = 1, \quad t_2^{(1+0)} = \frac{17}{2} + \frac{9}{2} \log(s/\mu^2). \end{aligned} \quad (3.2.27)$$

while the  $m^4$  terms have been only computed to first order  $\mathcal{O}(a)$

$$\begin{aligned}
 h_0^{(1+0)} &= 1 - 1/2 \log(s/\mu^2), & h_1^{(1+0)} &= \frac{25}{4} - 2\zeta_3 - \frac{25}{6} \log(s/\mu^2) - 2 \log(s/\mu^2)^2, \\
 k_0^{(1+0)} &= 0, & k_1^{(1+0)} &= 1 - \frac{2}{5} \log(s/\mu^2), \\
 g_0^{(1+0)} &= 1, & g_1^{(1+0)} &= \frac{94}{9} - \frac{4}{3} \zeta_3 - 4 \log(s/\mu^2), \\
 j_0^{(1+0)} &= 0, & j_1^{(1+0)} &= 0, \\
 u_0^{(1+0)} &= 0, & u_1^{(1+0)} &= 0.
 \end{aligned} \tag{3.2.28}$$

The gluon and quark condensates depend on the scale  $\mu^2$ , but we can express them in the form of the scale-invariant gluon- and quark-condensate [79], which are combinations of the minimally subtracted operators

$$\begin{aligned}
 \beta_1 \langle aG^2 \rangle_I &\equiv \beta(s) \langle G_{(a)}^{\mu\nu} G_{\mu\nu}^{(a)} \rangle + 4\gamma(a) \sum_{i=u,d} \langle m_i \bar{q}_i q_i \rangle \\
 &\quad - \frac{3}{4\pi^2} \sum_{i,j=u,d} m_i^2 m_j^2 \gamma_0^{ij}(a)
 \end{aligned} \tag{3.2.29}$$

$$\langle m_i \bar{q}_j q_j \rangle_I \equiv \langle m_i \bar{q}_j q_j \rangle + \frac{3m_i m_j^3}{7\pi^2 a} \left\{ 1 - \frac{53}{24} a + \mathcal{O}(a^2) \right\}, \tag{3.2.30}$$

where  $\gamma_0^{ij}(a) = -2 - 8/3a$ . During this work, we will insert the known invariant quark condensates (see table A.1) as constants and state our results for the invariant gluon condensate.

### 3.2.4. Dimension Six and Eight Corrections

Our application of dimension six contributions is founded in [19]. They have previously been calculated beyond leading order by [55]. The operators appearing are the masses to the power six ( $m^6$ ), the four-quark condensates ( $\langle \bar{q} q \bar{q} q \rangle$ ), the three-gluon condensates ( $\langle g^3 G^3 \rangle$ ) and lower dimensional condensates multiplied by the corresponding masses, such that in total the mass dimension of the operators will be six. The largest contributions come from the 4-quark operators. The three-gluon condensate does not contribute at leading order [45] and is neglected. Operators proportional to the light quark masses will also be neglected. The resulting contributions of dimension six operators have been calculated in [55] and lead to many operators, which until today cannot be accurately determined by phenomenology methods. To reduce the

number of operators we can make use of the *vacuum saturation approximation* (vsa) [8, 19, 78]. The vsa is used to express the four-quark condensates as squares of quark-antiquark condensates  $(\langle \bar{q}_i q_i \rangle)^2$ . If we apply the vsa to first order in  $\alpha_s$ , we can write out the dimension six OPE contributions

$$D_{ij,V/A}^{1+0}(s) \Big|_{D=6} = \frac{32\pi^2}{3} a(\mu) \frac{\langle \bar{q}_i q_i(\mu) \rangle \langle \bar{q}_j q_j \rangle}{s^3} - \frac{32}{7} \pi^2 a_\mu \frac{\langle \bar{q}_i q_i \rangle^2 \langle \bar{q}_j q_j \rangle^2}{s^3}. \quad (3.2.31)$$

Unfortunately, the scaling properties of the dimension six contributions are inconsistent with the scaling properties of the 4-quark operators [62, 47] and terms of order  $\alpha_s^2$  are usually ignored. In addition to the scaling problematic, the vsa is known to underestimate the dimension six contribution [56].

In our work we, take the simplest approach possible. We introduce an effective dimension six coefficient  $\rho_{V/A}^{(6)}$  divided by the appropriate power in  $s$

$$D_{ij,V/A}^{(1+0)}(s) \Big|_{D=6} = 3 \frac{\rho_{V/A}^{(6)}}{s^3}. \quad (3.2.32)$$

Here we also neglected the scale dependence of the dimension six operators, which is determined by the anomalous dimension. We have calculated the leading-order anomalous dimension matrices corresponding to the dimension six four-quark operators of flavour non-diagonal, as well as flavour diagonal, mesonic vector and axial-vector currents in [11].

For higher dimensional contributions the situation is not better than the dimension six one. Up to dimension twelve we will keep the simplest approach of introducing a parameter for every OPE dimension leading to

$$\begin{aligned} D_{ij,V/A}^{(1+0)} \Big|_{D=8} &= 4 \frac{\rho_{V/A}^{(8)}}{s^4}, & D_{ij,V/A}^{(1+0)} \Big|_{D=10} &= 5 \frac{\rho_{V/A}^{(10)}}{s^5} \\ \text{and } D_{ij,V/A}^{(1+0)} \Big|_{D=12} &= 6 \frac{\rho_{V/A}^{(12)}}{s^6}. \end{aligned} \quad (3.2.33)$$

The NP contribution of dimension twelve is the highest order that we are going to implement. Higher orders will be neglected. Next, to the NP treatment of the OPE, we have to discuss possible DV.

### 3.3. Duality Violations

As seen in [section 2.4.2](#) we have to assume quark-hadron duality for the QCDSR to work. Unfortunately, duality is always to some extent broken through so-called DV, which are well known [\[25, 26\]](#). Experimental data show an oscillating behaviour that cannot be reproduced by the OPE. Moreover, in the large  $N_c$  limit, it can be shown that DV have an exponential decreasing, sinusoidal appearance [\[24\]](#). Consequently, for the cases with apparent DV, we have to include the corrections coming from DV and adapt [eq. 3.2.2](#), leading to

$$R_{\tau,V/A}^\omega = \frac{N_c}{2} S_{EW} |V_{ud}|^2 \left( 1 + \delta_{pt}^\omega + \delta_{npt}^\omega + \delta_{dv}^\omega \right), \quad (3.3.1)$$

where we extracted  $\delta_{dv}$  from  $\delta_{npt}$ , even though DV are NP. The DV corrections have been modelled with the following ansatz [\[26\]](#)

$$\rho_{V/A}^{DV}(s) = e^{-(\delta_{V/A} + \gamma_{V/A}s)} \sin(\alpha_{V/A} + \beta_{V/A}s), \quad (3.3.2)$$

which contains four parameters for the vector and another four parameters for the axial-vector contribution. Note that for fitting the kinematic weight in the V-channel, which is known to be sensible for DV at lower energies [\[12\]](#), we would have seven parameters instead of only three. By including the model, we append the DV as an additional term in the inclusive  $\tau$  decay ratio

$$R_{\tau,V/A} = -\pi i \oint_{|s|=m_\tau^2} \frac{dx}{x} (1-x)^3 \left[ 3(1+x) D^{(1+0)}(m_\tau^2 x) + 4 D^{(0)}(m_\tau^2 x) \right] + \mathcal{D}_{V/A}(m_\tau^2), \quad (3.3.3)$$

where the DV contributions would be given as

$$\mathcal{D}_\omega(m_\tau^2) = -12\pi^2 \int_{m_\tau^2}^{\infty} \frac{ds}{m_\tau^2} \omega(s) \rho_{V/A}. \quad (3.3.4)$$

#### 3.3.1. Pinched Weights to avoid DVs

The general QCDSR ([eq. 2.4.11](#)) contain a weight function  $\omega$ , which is not only used to suppress higher order dimensions, but also DV. The weights that suppress DV are so-called pinched weights of the form

$$\omega(s) = \left( 1 - \frac{s}{m_\tau^2} \right)^k, \quad (3.3.5)$$

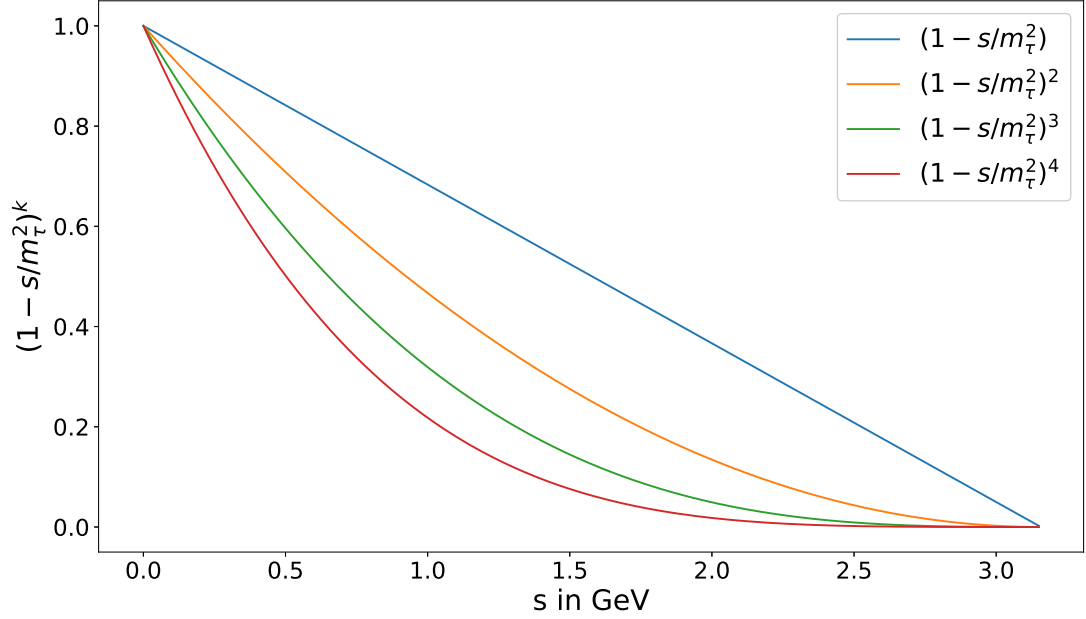


Figure 3.2.: Pinched weights  $(1 - s/m_\tau^2)^k$  for degrees one to four. We can see that weights of higher pinching decrease faster, which comes in handy if we want to suppress  $\text{dv}$ .

where  $k$  is the degree of the pinched weight. The higher the degree of the pinching, the lower the contribution of the critical region close to the real axis (see. [fig. 3.2](#)). Thus for higher pinchings, we are better protected from  $\text{dv}$  effects. For the transversal component of the inclusive  $\tau$  decay ratio ([eq. 3.1.2](#)) a pinching of second degree appears quite naturally as the kinematic weight (see [eq. 2.4.16](#)). In general, it is said that a double pinched weight is sufficient to neglect effects caused by  $\text{dv}$ . In our analysis, we show that double pinched weights indeed sufficiently suppress  $\text{dv}$  and that even single pinched weights lead to acceptable results. Next, to applying pinched weights, we focus on combinations of vector and axial-vector contributions, which as we will see, regarding the ALEPH data have visibly suppressed  $\text{dv}$ .

### 3.4. Borel Summation

The Adler function of [eq. 3.1.5](#) is given by a divergent asymptotic series. We only know the needed Adler function coefficients  $c_{n,m}$  up to fifth order. To get

the best possible sum for such a series we can apply the *Borel summation* (BS). The BS is a long known summation method for divergent series introduced by Émile Borel [18].

Regarding the sum

$$A = \sum_{n=0}^{\infty} a_n \quad (3.4.1)$$

we can introduce the faculty of  $n$ , which can be rewritten in its integral form

$$A = \sum_{n=0}^{\infty} \frac{n!}{n!} a_n = \sum_{n=0}^{\infty} \frac{a_n}{n!} \int_0^{\infty} e^{-t} t^n dt. \quad (3.4.2)$$

Interchanging the integral and the sum is referred to as the *Borel integral*

$$A \equiv \int_0^{\infty} dt e^{-t} \sum_{n=0}^{\infty} \frac{a_n}{n!} t^n, \quad (3.4.3)$$

which contains the *Borel transform*

$$B[A](t) = \sum_{n=0}^{\infty} \frac{a_n}{n!} t^n. \quad (3.4.4)$$

The Borel integral is only valid for Borel transforms with no singularities for real positive  $t$ . In the cases of a valid Borel integral, the BS can now be used to get exact answers of divergent series, by first applying the Borel transform and then integrating over it, with the help of the Borel integral.

In our case, we want to calculate the BS of the Adler function given in eq. 3.1.5 to argue if FOPT or CIPT gives the better approximation to the  $\tau$  decay ratio. For convenience, the Adler function is redefined by

$$\frac{12\pi^2}{N_c} D_V^{1+0}(s) \equiv 1 + \widehat{D}(s) \equiv 1 + \sum_{n=0}^{\infty} r_n \alpha_s(\sqrt{s})^{n+1}. \quad (3.4.5)$$

Following the BS prescription, we apply the Borel transformation to  $\widehat{D}$

$$B[\widehat{D}](t) \equiv \sum_{n=0}^{\infty} r_n \frac{t^n}{n!} \quad \text{with} \quad t \in \mathbb{C}. \quad (3.4.6)$$

As  $t$  is a complex number we can study the Borel transform in the so-called *Borel plane*. The Borel plane for the Adler function is visualised in fig. 3.3. For real  $t$  the Borel transform of the Adler function has poles. Poles of the Borel



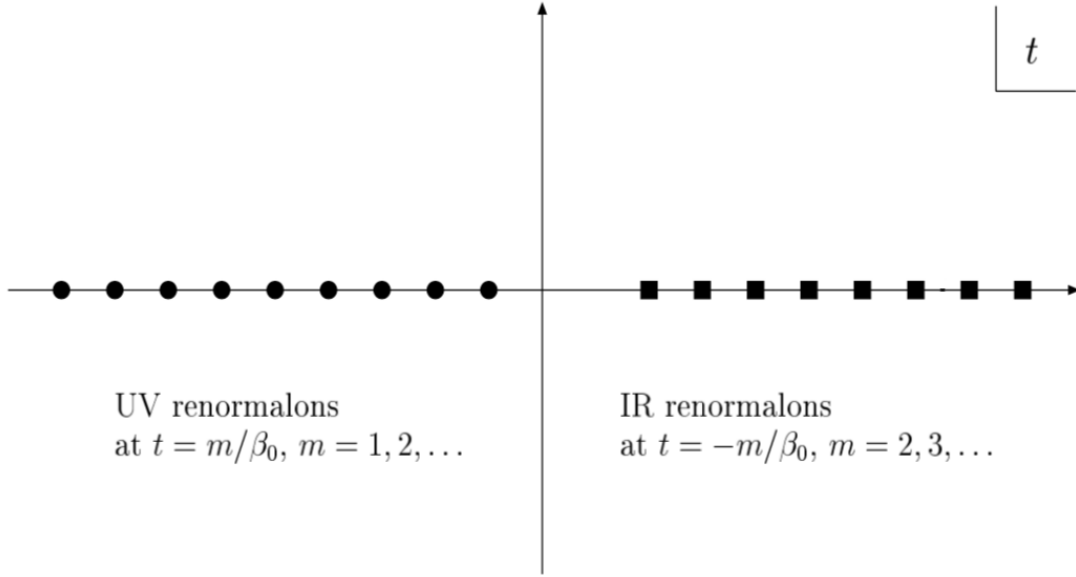


Figure 3.3.: Singularities in the Borel plane of the Adler function, taken from[6].

transform are referred to as renormalons [Beneke1999, 91]. We have to distinguish between *ultraviolet* (UV) and *infrared* (IR) renormalons. UV renormalons are located at  $t = m/\beta_0$  with positive integer  $m = 1, 2, \dots$  and IR renormalons are located at  $t = -m\beta_0$  with positive integer  $m = 2, 3, \dots$ . The Borel integral of the redefined Adler function is given by

$$\hat{D}(\alpha) \equiv \int_0^\infty dt e^{-t/\alpha} B[\hat{D}](t). \quad (3.4.7)$$

It is not well defined, due to poles of the positive real axis. Consequently, to have a valid Borel integral we have to move the contour above or below the singularities.

The ansatz we use to express the Adler function in terms of the  $B$ s was introduced by Beneke et al. [8]. They have built a physical model for the Adler function series

$$B[\hat{D}](u) = B[\hat{D}_1^{\text{UV}}](u) + B[\hat{D}_2^{\text{IR}}](u) + B[\hat{D}_3^{\text{IR}}](u) + d_0^{\text{PO}} + d_1^{\text{PO}}u, \quad (3.4.8)$$

where  $B[\hat{D}_p^{\text{UV/IR}}](u)$  are ansätze for the ultraviolet and infrared appearing renor-

malon poles

$$B[\widehat{D}_p^{\text{IR}}](u) \equiv \frac{d_p^{\text{IR}}}{(p-u)^{1+\bar{\gamma}}} \left[ 1 + \tilde{b}_1(p-u) + \tilde{b}_2(p-u)^2 + \dots \right] \quad (3.4.9)$$

$$B[\widehat{D}_p^{\text{UV}}](u) \equiv \frac{d_p^{\text{UV}}}{(p+u)^{1+\bar{\gamma}}} \left[ 1 + \bar{b}_1(p+u) + \bar{b}_2(p+u)^2 \right], \quad (3.4.10)$$

which have been defined in section five of [8]. As the large order behaviour of the Adler function is governed by a sign-alternating uv renormalon divergence and the lower-orders are not, only the leading uv singularity has been included. Furthermore, the intermediate orders are governed by IR renormalons. Thus the first two ( $m = 2$  and  $m = 3$ ) have been included into the model. The five parameters  $d_1^{\text{UV}}, d_2^{\text{IR}}, d_3^{\text{IR}}, d_0^{\text{PO}}$  and  $d_1^{\text{PO}}$  have then to be matched to the known perturbative expansion of the Adler function. They are found to be [8]

$$\begin{aligned} d_1^{\text{UV}} &= -0.0156, & d_2^{\text{IR}} &= 3.16, & d_3^{\text{IR}} &= -13.5, \\ d_0^{\text{PO}} &= 0.781 & \text{and} & & d_1^{\text{PO}} &= 0.00766. \end{aligned} \quad (3.4.11)$$

We will apply the Borel integral of this model to perform fits as an alternative to FOPT.

### 3.5. Experiment

The  $\tau$  decay data we use to perform our QCD analysis is from the ALEPH experiment. The ALEPH experiment was located at the *large-electron-positron* (LEP) collider at *European Organisation for Nuclear Research* (CERN) in Geneva. LEP started producing particles in 1989 and was replaced in the late 90s by the *large-hadron-collider* (LHC), which makes use of the same tunnel of 27 km circumference. The data produced within the experiment is still maintained by former ALEPH group members led by M. Davier, which have performed regular updates on the data-sets [35, 32, 73]. The last update was motivated by Boito et al. [9], who discovered irregularities in the covariances by comparing data from a Monte Carlo generator with the ALEPH.

The measured spectral functions for the ALEPH data are defined in [33] and are

given for the transverse and longitudinal components separately

$$\begin{aligned}
 \rho_{V/A}^{(1)}(s) &= \frac{m_\tau^2}{12|V_{ud}|^2 S_{EW}} \frac{\mathcal{B}(\tau^- \rightarrow V^-/A^- \nu_\tau)}{\mathcal{B}(\tau^- \rightarrow e^- \bar{\nu}_e \nu_\tau)} \\
 &\quad \times \frac{dN_{V/A}}{N_{V/A} ds} \left[ \left(1 - \frac{s}{m_\tau^2}\right)^2 \left(1 + \frac{2s}{m_\tau^2}\right) \right]^{-1} \\
 \rho_A^{(0)}(s) &= \frac{m_\tau^2}{12|V_{ud}|^2 S_{EW}} \frac{\mathcal{B}(\tau^- \rightarrow \pi^- (K^-) \nu_\tau)}{\mathcal{B}(\tau^- \rightarrow e^- \bar{\nu}_e \nu_\tau)} \times \frac{dN_A}{N_A ds} \left(1 - \frac{s}{m_\tau^2}\right)^{-2}.
 \end{aligned} \tag{3.5.1}$$

The data relies on a separation into vector and axial-vector channels. In the case of the  $\pi$  this can be achieved via counting. The vector channel is characterised by a negative G-parity, whereas the axial-vector channel has positive G-parity. A single  $\pi$  carries negative G-parity, thus an even number of  $\pi$  carries positive G-parity and an odd number of  $\pi$  carry negative G-parity:

$$n \times \pi = \begin{cases} \text{vector} & \text{if } n \text{ is even,} \\ \text{axial-vector} & \text{otherwise.} \end{cases} \tag{3.5.2}$$

The separation into vector and axial-vector channel of mesons including strange quarks, like  $K\bar{K}$  pairs, is more difficult because these are not in general eigenstates of G-parity and contribute to both V and A channels.

The contributions to the spectral function for the vector, axial-vector and v+A channels can be seen in [fig. 3.4](#). The dominant modes in the vector case are decays into two ( $\tau^- \rightarrow \pi^- \pi^0 \nu_\tau$ ) or four ( $\tau^- \rightarrow \pi^- \pi^- \pi^+ \pi^0 \nu_\tau$ ) pions [\[34\]](#). The first of these is produced by an intermediate  $\rho(770)$  meson, which in contrary to the pions carries angular momentum of one and is clearly visible as peak around 770 GeV in [fig. 3.4a](#). The dominant modes in the axial-vector case are decays into one ( $\tau^- \rightarrow \pi^- \nu_\tau$ ) or three ( $\tau^- \rightarrow \pi^- \pi^0 \pi^0 \nu_\tau$  and  $\tau^- \rightarrow \pi^- \pi^- \pi^+ \nu_\tau$ ) pions. Here the three pion final states stem from the  $a_1^-$ -meson, which can be seen as a peak in [fig. 3.4b](#).

We furthermore added the perturbative contribution for a fixed  $\alpha_s(m_\tau) = 0.329$  using FOPT in [fig. 3.4c](#). We can see, that the perturbative contribution (the blue line) is an almost straight line and cannot reproduce the oscillating behaviour, given by the ALEPH data. This is especially the case for the not combined v and A channel and is seen as an indicator for DV. Even including NP, higher

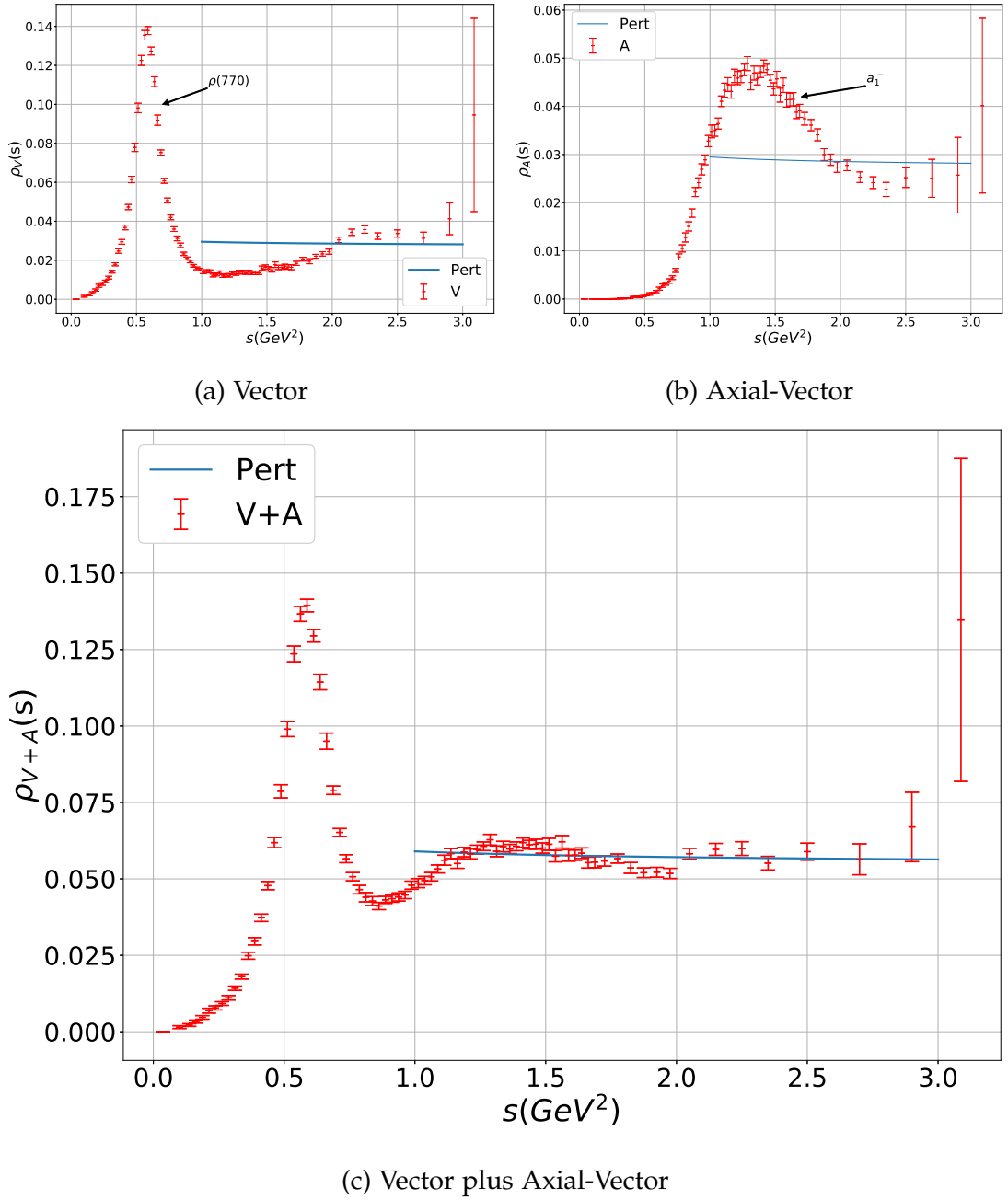


Figure 3.4.: Visualisation of the vector, axial-vector and V+A spectral function given by the ALEPH data [35] in red with errors. We also plotted the FOPT theoretical calculation up to third order in  $\alpha_s$ , for a fixed  $\alpha_s(m_\tau^2) = 0.329$  in blue. Note that the perturbative contributions cannot fully represent the experimental data. They do not reproduce the sinusoidal form.

dimensions of the ope is not reproducing the wavy structure. In the case of  $v+A$  channel, we have a higher agreement between our perturbative graph and the data. In general, we believe that  $dv$  are sufficiently suppressed if we limit ourselves to data from the  $v+A$  channel. We will argue in favour of this statement in the following chapter. This is only the case for energies larger than 1.5 GeV, as the  $\rho$  resonance of the  $v$  channel is impossible to be represented by perturbative tools. For lower energies  $dv$  become too important to be neglected.

### 3.5.1. Total $\tau$ Decay Ratio from Experimental Data

The data has been last revised in 2014 [35] and is publicly available [31]. It consists of the mass squared bin centre ( $sbin$ ), the bin size ( $dsbin$ ), the normalised invariant mass squared distribution ( $sfm2$ ), the total errors ( $derr$ ) and their correlations ( $correrr$ ). To make the data comparable to our theoretical calculations we have to give the normalised invariant mass squared distribution ( $sfm2$ ) in the form of the total decay ratio  $R_\tau$ . The data is given as the normalised invariant mass squared distribution ( $dN_i/ds$ )/ $N_i$  scaled by a factor 100 and further normalised to the corresponding branching ratio  $i \in \{V, A, V+A\}$ . Thus we can connect the branching ratio of the  $i^{\text{th}}$  channel to  $sfm2$  as follows

$$\mathcal{B}_{V/A} \equiv \int_0^{s_\tau} ds \frac{sfm2_{V/A}(s)}{100} \equiv \int_0^{s_\tau} ds \mathcal{B}_{V/A} \left( \frac{dN_{V/A}}{N_{V/A} ds} \right), \quad (3.5.3)$$

where we used  $s_\tau \equiv m_\tau^2$ . The total decay ratio  $R_\tau$  is defined as the ratio  $\tau$  decaying into hadrons and  $\tau$  decaying into electrons. It can be expressed via the corresponding branching ratios, which can be connected to the invariant mass squared distribution  $sfm2$

$$R_{\tau, V/A} = \frac{\mathcal{B}_{V/A}}{\mathcal{B}_e} = \int_0^{s_\tau} ds \frac{sfm2_{V/A}(s)}{100 \mathcal{B}_e}. \quad (3.5.4)$$

Theoretically, the decay ratio is given in eq. 3.0.1. If we neglect the longitudinal contribution  $\text{Im} \Pi^{(0)}(s)$  and remember the definition of the spectral function (eq. 2.4.9) and the kinematic weight (eq. 2.4.16), we can write the decay ratio as

$$R_{\tau, i} = \int_0^{s_\tau} \frac{ds}{s_\tau} \omega_\tau(s) \rho(s) \quad (3.5.5)$$

and thus relate the spectral function to the experimental data

$$\rho(s) = \frac{s_\tau}{12\pi^2 100\mathcal{B}_e} \frac{\text{sfm2}}{\omega_\tau}. \quad (3.5.6)$$

To fit the experimental data we define a so-called *spectral function moment* (or *moment*)

$$I_i^{\text{exp},\omega} \equiv \int_0^{s_0} \frac{ds}{s_0} \omega\left(\frac{s}{s_0}\right) \rho(s), \quad (3.5.7)$$

which will be used in our  $\chi^2$  fits, explained in the upcoming section. The data is given for discrete bins so we have to express the integral of the spectral function moment as a sum over those bins. The final expression we use to fit parameters to the experimental data is then given by

$$I_{\text{exp},V/A}^\omega(s_0) = \frac{s_\tau}{100\mathcal{B}_e s_0} \sum_{i=1}^{N(s_0)} \frac{\omega\left(\frac{s_i}{s_0}\right)}{\omega_\tau\left(\frac{s_i}{s_\tau}\right)} \text{sfm2}_{V/A}(s_i). \quad (3.5.8)$$

## 3.6. The Method of Least Squares

We apply the *method of least squares* (LS) to fit the parameters  $\vec{\alpha}$  from the experimental data. Our  $\chi^2$ -function can be expressed as

$$\chi^2 = \left( I_i^{\text{exp}} - I_i^{\text{th}}(\vec{\alpha}) \right) C_{ij}^{\text{exp}-1} \left( I_j^{\text{exp}} - I_j^{\text{th}}(\vec{\alpha}) \right), \quad (3.6.1)$$

where  $I^{\text{exp}}/I^{\text{th}}$  is a vector of experimental moments/theoretical moments with the same weight, but different energy cutoffs  $s_0$ , labelled by the indices  $i$  and  $j$ .  $C^{\text{exp}}$  is the covariance matrix describing the correlation of the different experimental moments  $C_{ij}^{\text{exp}} = \text{cov}[I_i^{\text{exp}} I_j^{\text{exp}}]$ , which can be computed by the given correlation matrix of the ALEPH data.

We aim to minimise the value of  $\chi^2$ , which will fix the parameter vector  $\vec{\alpha}$ . The properties of the  $\chi^2$ -function are well known and the best fits are characterised through  $\chi^2/\text{dof} \approx 1$ , where the DOF of the fit can be calculated through

$$\text{DOF} = \text{experimental moments} - \text{parameters}. \quad (3.6.2)$$

E.g. if we want to fit  $\alpha_s$  and the dimension four Wilson coefficient  $C_4$  we get  $7 - 2 = 5$  DOF.

The values we obtain for  $\chi^2/\text{dof}$  for stable fits are smaller than one. We explain this behaviour with missing correlations in the ALEPH data. Consequently we will declare  $\chi^2/\text{dof} < 1$  as good, if the  $\chi^2/\text{dof}$  is not close to zero.

For our purposes, we use the numerical minimisation computer program MINUIT, which was originally written in FORTRAN by Fred James in the seventies [46]. Today in its second version the program has been ported to C++ by the ROOT [21] project at CERN.

The parameter vector  $\vec{\alpha}$  includes the strong coupling  $\alpha_s$ , and higher dimensional OPE contributions. We should have at least as many, if not more moments as the parameters count. We are limited to fit a set of only a few parameters, because moments of similar weights are highly correlated.

It is possible to increase the number of moments used by applying multiple weights  $\omega$ . Unfortunately using different weights leads to even higher correlated moments, which cause numerical complications in inverting the covariance matrix in eq. 3.6.1. To handle the high correlations we have to redefine our fit quality.

### 3.6.1. Block Diagonal “Fit-Quality”

For fits including multiple weights, which we do not perform in this work, we can redefine LS [16] to

$$Q^2 = \sum_{\omega} \sum_{s_0^i, s_0^j} \left( I_{\omega}^{\text{exp}}(s_0^i) - I_{\omega}^{\text{th}}(s_0^i, \vec{\alpha}) \right) \tilde{C}_{ij, \omega}^{-1} \left( I_{\omega}^{\text{exp}}(s_0^j) - I_{\omega}^{\text{th}}(s_0^j, \vec{\alpha}) \right), \quad (3.6.3)$$

where the covariance matrix  $\tilde{C}$  is now a diagonal of the experimental covariance matrices  $C_{\omega}^{\text{exp}}$  for each weight

$$\tilde{C} = \begin{pmatrix} C_{\omega=1}^{\text{exp}} & 0 & \dots & 0 \\ 0 & C_{\omega=2}^{\text{exp}} & \ddots & \vdots \\ \vdots & \ddots & \ddots & 0 \\ 0 & \dots & 0 & C_{\omega=n}^{\text{exp}} \end{pmatrix}. \quad (3.6.4)$$

As a result, we are still able to invert the newly defined covariance matrix  $\tilde{C}$ , but minimisation routines like CERN MINUIT are not able to calculate the

proper errors for the parameters we want to extract. We have to perform our own error propagation to obtain meaningful errors for the parameters. The error propagation has been derived in [12, 10] and is given as

$$\langle \delta\alpha_k \alpha_l \rangle = A_{km}^{-1} A_{ln}^{-1} \frac{\partial I_i^{\text{th}}(\vec{\alpha})}{\partial \alpha_m} \frac{\partial I_r^{\text{th}}(\vec{\alpha})}{\partial \alpha_n} \tilde{C}_{ij}^{-1} \tilde{C}_{ij}^{-1} \langle \delta I_k^{\text{exp}} \delta I_l^{\text{exp}} \rangle, \quad (3.6.5)$$

where

$$A_{kl} = \frac{\partial I^{\text{th}}(\vec{\alpha})}{\partial \alpha_k} C_{ij}^{-1} \frac{I_j^{\text{th}}(\vec{\alpha})}{\alpha_l}. \quad (3.6.6)$$



## Measuring the Strong Coupling

Table 4.1.: Timeline

1991	• [19]: Systematic description, including NP corrections to extract $\alpha_s$ from $R_\tau$ .
1992	• [57]: Introducing weights and fit methodology.
1993	• [22] ALEPH measures the strong coupling constant $\alpha_s$ .
1998	• [3] OPAL measures the strong coupling constant $\alpha_s$ .
2005	• [73] ALEPH improves their data.
2011	• [12, 9]: Include DV. Discover inconsistencies in ALEPH data.
2014	• [35] ALEPH updates their data.

The strong coupling has been measured for many years from hadronic  $\tau$  decays. An overview of the recently, but different,  $\alpha_s$  values can be seen in [fig. 4.1](#). Until today QCDSR applied to  $\tau$  decays are based on the methodology developed in the early nineties by Braaten, Pich and Narison [19]. They gathered at this time available perturbative and NP contributions to extract the strong coupling from comparing their theoretical results to the known inclusive hadronic  $\tau$  decay ratio. Pich together with Le Diberder then formulated the fitting strategy of applying multiple moments of different weights to extract  $\alpha_s$  parallel to Wilson coefficients of the OPE [57], which later has

been applied as standard in the ALEPH [22] as well as the OPAL [3] detectors. For the next ten years, the methodology of extracting the strong coupling did not experience any major changes until 2011 when Boito, Cata, Golterman, Jamin, Osborn and Peris [12] applied a duality model to include known DV

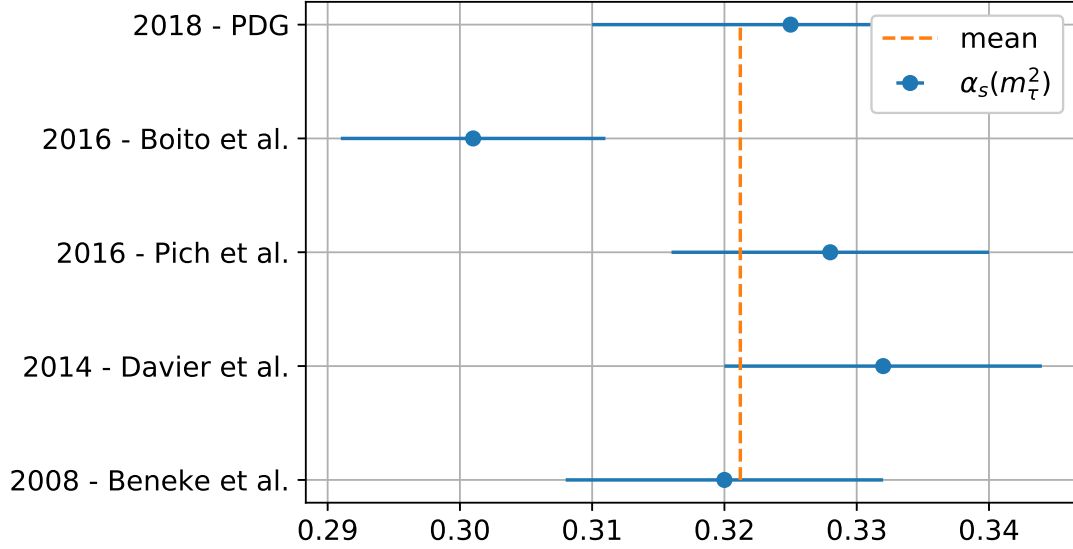


Figure 4.1.: Recent values for  $\alpha_s(m_\tau^2)$  from hadronic  $\tau$  decays. The dashed line represents the mean value of 0.3212. The values are taken from [82, 15, 68, 35, 8], from top to bottom.

effects to the QCD analysis of  $\tau$  decays. The groups around Boito and Pich have different opinions on the importance of the newly introduced duality model [68, 15] and consequently, we want to deliver a third, opinion on the subject, favouring fits without the duality model.

## 4.1. Fit Strategy

In this work we want to extract  $\alpha_s$ , argue about the validity of FOPT and probe the importance of DV. Furthermore, we want to measure higher order OPE contributions.

For performing the fits restrict ourselves to the following approximations

- We used the PT expansion of the Adler function up to fifth order, including the educated guess of  $c_{5,1}$ .
- We ignore the dimension two OPE contributions as they are proportional to the quark masses and we work in the chiral limit.
- We neglect the logarithmic contributions of the dimension four OPE cor-

rections.

- We parametrise contributions of dimension six and higher with a constant divided by the corresponding power in  $s$

$$D_{V/A}^{(1+0)} \Big|_{D=d} \equiv \frac{\rho^{(d)}}{s^{d/2}}. \quad (4.1.1)$$

Our fitting strategy will be in choosing weights of a lower and higher pinching. Lower pinched weights should be affected by  $DV$ , while higher pinched weights should be protected from  $DV$ . As a result in comparing different fits of lower and higher pinched weights, it should be possible to argue about the strength of the  $DV$  that are (or are not) present.

Our hypothesis is that  $DV$  are small enough for fits of the combined  $V+A$  channel in combination with pinched weights. Consequently, we should be able to extract parameters, like the strong coupling  $\alpha_s$  from  $\tau$  decays to high precision without a  $DV$  model.

We will perform our analysis of the  $DV$  in the framework of FOPT for weights without a monomial term  $\chi$ . For weights including a monomial term  $\chi$ , we will apply the BS. To define a fit we have to choose a weight  $\omega$  and a momentum  $s_0$ . The only restriction from choosing a weight is, that, it has to be analytic, leaving us with a variety of choices. For our strategy, we have chosen three categories of weights, each of them containing fits with three or four different  $\omega$ . A table with an overview of all used weights is given in [table 4.2](#). To test the stability of the fitted values and have enough DOF to fit the higher OPE contributions we furthermore fit every weight for various momenta  $s_0$ .

To probe the validity of FOPT we apply the BS for weights without a monomial term  $\chi$ . If FOPT is valid the parameters obtained from both approaches, the Borel model and FOPT, should be similar. CIPT leads to different values compared to FOPT, it should be less valid than FOPT.

## 4.2. Fits

In the following, we will show the results of each of the three previously mentioned fit categories.

	Symbol	Term	Expansion	OPE Contributions
Pinched	$\omega_\tau$	$(1-x)^2(1+2x)$	$1-3x^2+2x^3$	D6, D8
	$\omega_{\text{cube}}$	$(1-x)^3(1+3x)$	$1-6x^2+8x^3-3x^4$	D6, D8, D10
	$\omega_{\text{quartic}}$	$(1-x)^4(1+3x)$	$1-10x^2+20x^3-15x^4+4x^5$	D6, D8, D10, D12
Monomial	$\omega_{M2}$	$1-x^2$	$1-x^2$	D6
	$\omega_{M3}$	$1-x^3$	$1-x^3$	D8
	$\omega_{M4}$	$1-x^4$	$1-x^4$	D10
Pinched +x	$\omega_{1,0}$	$(1-x)$	$1-x$	D4
	$\omega_{2,0}$	$(1-x)^2$	$1-2x+x^2$	D4, D6
	$\omega_{3,0}$	$(1-x)^3$	$1-3x+3x^2-x^3$	D4, D6, D8
	$\omega_{4,0}$	$(1-x)^4$	$1-4x+6x^2-4x^3+x^4$	D4, D6, D8, D10

Table 4.2.: Displaying three categories of fits, each containing three to four weights with their corresponding mathematical expression and the OPE contributions the fitted integral momentum will be sensitive to.

The first category contains the *pinched weights without a monomial term  $x$* . The chosen weights are double ( $\omega_\tau$ ), triple ( $\omega_{\text{cube}}$ ) and quadruple ( $\omega_{\text{quartic}}$ ) pinched and do not contain a monomial term  $x$ . An  $x$  term would make the fits sensitive to the  $D = 4$  OPE contribution, which causes an unreliable perturbative expansion [7]. The higher the pinching, the higher the suppression of  $\text{dv}$ . Consequently, if we obtain stable values for  $\alpha_s$  from the different pinched fits we should expect the  $\text{dv}$  to have no influence on the value of the strong coupling. The different weights imply an increasing number of active OPE contributions  $D_6, D_8, D_{10}$  and  $D_{12}$ , which can be used to probe the stability of higher order OPE contributions and to test for the convergence of the OPE.

The second category contains the *single pinched monomial weights*. In this case, all of the weights are only single pinched and, as in the first category, do not carry a monomial term  $x$ . Consequently, if  $\text{dv}$  affect the fits we should notice different fitting results in comparison to the fits of the first category. Furthermore, the single pinched moments only carry two parameters, the strong coupling and an OPE Wilson coefficient. Thus we can further compare the  $\rho^{(6)}, \rho^{(8)}$  and  $\rho^{(10)}$  Wilson coefficients and argue about the stability of the fits.

The third and last category contains a similar pinching as the first category, but this time contains a monomial term in  $x$ . Consequently, these fits are unreliable in the framework of FOPT and we have to apply the BS. Following the logic of the second and first category, we then can compare the result to analyse the role of DV and compare the OPE contributions.

#### 4.2.1. Pinched Weights without a Monomial term $x$

$$\text{Kinematic Weight: } \omega_\tau(x) \equiv (1-x)^2(1+2x)$$

We previously encountered the kinematic weight in eq. 2.4.16. It is a polynomial weight function, defined as  $\omega_\tau(x) = (1-x)^2(1+2x)$ , double pinched, contains the unity and does not contain a term proportional to  $x$ . Consequently, it is an optimal weight [7]. As a doubled pinched weight it should have good suppression of DV contributions and its polynomial contains terms proportional to  $x^2$  and  $x^3$ , which makes it sensitive to the dimension six and eight OPE contributions. The fits have been performed within the framework of FOPT for different numbers of  $s_0$ . The momentum sets are characterised by its lowest energy  $s_{\min}$ . We fitted values down to 1.5 GeV. Going to lower energies is questionable due to the coupling constant becoming large, which implies a breakdown of PT. Furthermore, it bears the risk to be affected by the  $\rho(770)$  and  $a_1$  peaks in the vector and axial-vector spectral function, which we cannot model within the framework of the OPE. For the three fitting parameters  $\alpha_s$ ,  $\rho^{(6)}$  and  $\rho^{(8)}$  we have given the results in table 4.3 and graphically in fig. 4.2.

We only display the fits for  $s_{\min}$  larger than 2.1 GeV. We note a jump of the  $\chi^2/\text{dof}$  from 0.19 to 1.3 between fits of  $s_{\min} = 2.1$  GeV and  $s_{\min} = 2.2$  GeV. We consequently discard fits with a  $s_{\min} < 2.2$  GeV, as fits with a lower  $s_{\min}$  behave more stable<sup>1</sup>. The values with fewer momenta are preferred by us due to two reasons. First, below energies of 2.2 GeV, we have to face the problematic influence of increasing resonances. Second, we will see, that the values obtained from the lower moment fits are more compatible with our other fit series. We further discarded the fit with four  $s_0$ s momenta, which has

<sup>1</sup>As will be seen by comparing the kinematic weight with the cubic and quartic weight

	$s_{\min}$	$\#s_0s$	$\alpha_s(m_\tau^2)$	$\rho^{(6)}$	$\rho^{(8)}$	$\chi^2/\text{dof}$
BS	2.200	7	0.3274(42)	-0.82(21)	-1.08(40)	0.21
FOPT	2.100	8	0.3256(38)	-0.43(15)	-0.25(28)	1.30
	2.200	7	0.3308(44)	-0.72(20)	-0.85(38)	0.19
	2.300	6	0.3304(52)	-0.69(25)	-0.80(50)	0.25
	2.400	5	0.3339(70)	-0.91(39)	-1.29(83)	0.10
	2.600	4	0.3398(15)	-1.3(1.0)	-2.3(2.5)	0.01

Table 4.3.: Table of our fitting values of  $\alpha_s(m_\tau^2)$ ,  $\rho^{(6)}$  and  $\rho^{(8)}$  for the kinematic weight  $\omega(x) = (1-x)^2(1+2x)$  using FOPT ordered by increasing  $s_{\min}$ . The errors are given in parenthesis after the observed value.

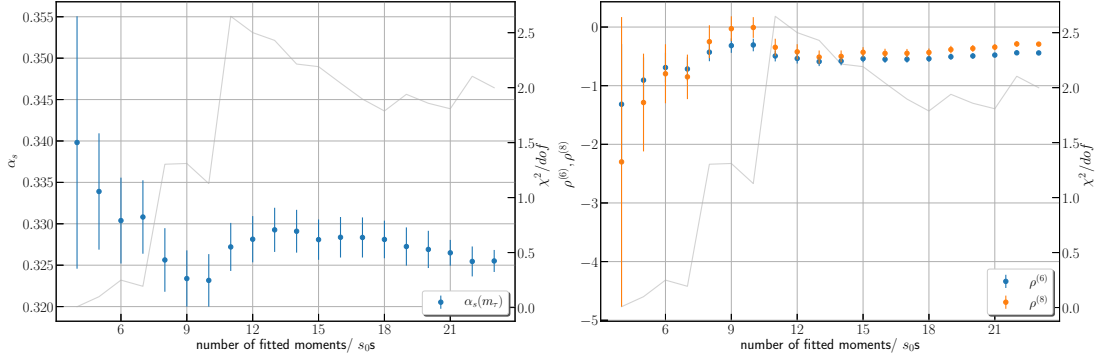


Figure 4.2.: Fitting values of  $\alpha_s(m_\tau^2)$ ,  $\rho^{(6)}$  and  $\rho^{(8)}$  for the kinematic weight  $\omega(x) = (1-x)^2(1+2x)$  using FOPT for different  $s_{\min}$ . The left graph plots  $\alpha_s(m_\tau^2)$  for different numbers of used  $s_0s$ . The right plot contains dimension six and eight contributions to the OPE. Both plots have in grey the  $\chi^2$  per DOF.

very small  $\chi^2/\text{dof} = 0.01$ . Having four  $s_0$ s momenta to fit three parameters, leaves us with too few DOF.

The selected fits with five to eight momenta have a good  $\chi^2$  per DOF. The  $\chi^2/\text{dof}$  of almost all our fits is smaller than one, which to our opinion is caused by missing correlations. Thus we will take  $\chi^2/\text{dof} < 1$  as good, if their value is not too close to zero. The fitted parameters,  $\alpha_s$ ,  $\rho^{(6)}$  and  $\rho^{(8)}$  are in good agreement with each other. The OPE shows good convergence. For later comparisons, we will focus on the fit right below the  $\chi^2/\text{dof}$  threshold. For the kinematic weight we obtain for the strong coupling,  $D = 6$  and  $D = 8$  contributions:

$$\alpha_s(m_\tau^2) = 0.3308(44), \quad \rho^{(6)} = -0.72(20) \quad \text{and} \quad \rho^{(8)} = -0.85(38). \quad (4.2.1)$$

We further tested the stability of dimension six and eight contributions to the OPE within the same fit series but for a fixed value of the strong coupling  $\alpha_s(m_\tau^2) = 0.3179$ . The values for  $\rho^{(6)}$  and  $\rho^{(8)}$  are larger than the values given in our final results from [table 4.3](#). This is explained with a smaller contribution from the strong coupling, which has to be compensated by larger OPE contributions.

Additionally, we applied the BS for the fit below the  $\chi^2$  threshold containing seven  $s_0$ s. Even though we used a different framework than FOPT the results are compatible. This further underlines the good results of the kinematic weight fits and can be seen as an indicator for FOPT being the superior framework as compared to CIPT, which has been argued in [\[8\]](#).

$$\textbf{Cubic Weight: } \omega_{\text{cube}}(x) \equiv (1 - x)^3(1 + 3x)$$

To further consolidate the results from the kinematic weight, we tested a weight of higher pinching, which should suppress DV more than a double pinched weight. If we obtain similar results to our previous fits we could exclude DV effects for the kinematic weight. On the other hand, any differences to the previous fit would indicate present DV for the kinematic weight. Our *cubic* weight will be triple pinched and optimal, as it does not contain a monomial term  $x$ . It is due to its polynomial structure sensitive to the dimensions six, eight and ten contributions of the OPE, which yields one more parameter

$s_{\min}$	$\#s_0s$	$\alpha_s(m_\tau^2)$	$\rho^{(6)}$	$\rho^{(8)}$	$\rho^{(10)}$	$\chi^2/\text{dof}$
2.000	9	0.3228(26)	-0.196(27)	0.075(28)	0.420(56)	1.96
2.100	8	0.3302(40)	-0.52(11)	-0.58(22)	-1.00(45)	0.43
2.200	7	0.3312(43)	-0.56(12)	-0.68(23)	-1.23(50)	0.55
2.300	6	0.336(11)	-0.78(47)	-1.17(98)	-2.38(22)	0.29
2.400	5	0.3330(96)	-0.63(47)	-0.82(10)	-1.51(26)	0.48

Table 4.4.: Table of our fitting values of  $\alpha_s(m_\tau^2)$ ,  $\rho^{(6)}$ ,  $\rho^{(8)}$  and  $\rho^{(10)}$  for the cubic weight  $\omega(x) = (1-x)^3(1+3x)$  using FOPT ordered by increasing  $s_{\min}$ . The errors are given in parenthesis after the observed value.

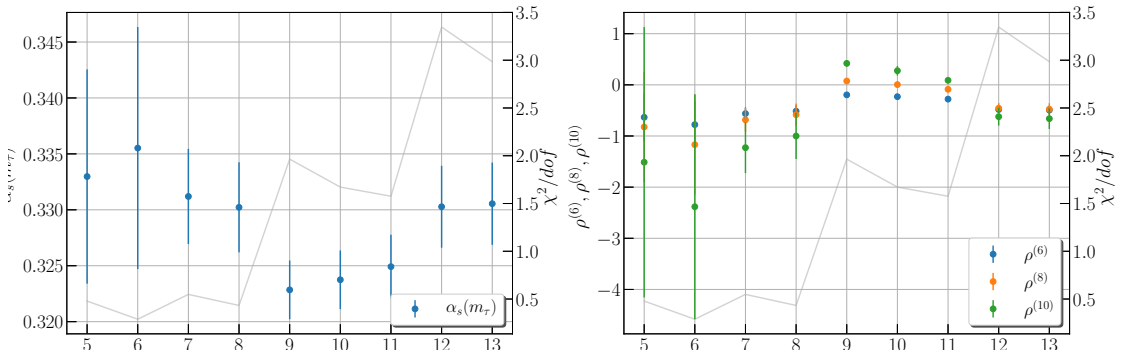


Figure 4.3.: Graphic representation of the fitting values of  $\alpha_s(m_\tau^2)$  in the left and  $\rho^{(6)}$ ,  $\rho^{(8)}$  and  $\rho^{(10)}$  in the right plot for the cubic weight  $\omega(x) = (1-x)^3(1+3x)$ . The fits have been performed in the FOPT scheme and the data points are given with error bars and are ordered by increasing  $s_{\min}$ . The grey line displays the  $\chi^2$  function.

to fit than with the kinematic weight  $\omega_\tau$ . The fitting results can be seen in [table 4.4](#) and graphically in [fig. 4.3](#).

We performed fits for  $s_0 \leq 1.5 \text{ GeV}$ , but could only reach convergence for fits with energies larger or equal than  $1.8 \text{ GeV}$ . As before the  $\chi^2$  jumps at  $s_0 = 2.1 \text{ GeV}$  to values per dof of almost 2. Consequently, we exclude these fits and focused on fits from five to eight  $s_0s$  momenta.

The selected fits have a good  $\chi^2/\text{dof}$  and the fitted parameters,  $\alpha_s$ ,  $\rho^{(6)}$ ,  $\rho^{(8)}$  and  $\rho^{(10)}$  are in agreement with each other, except for the fit with six momenta. The fit with a  $s_{\min} = 2.3 \text{ GeV}$  has the lowest  $\chi^2 = 0.29$ . It furthermore has an



abnormally low error and different OPE values, which could indicate problems with the fit. The fit right below the  $\chi^2/\text{dof}$  threshold yields

$$\begin{aligned} \alpha_s(m_\tau^2) = 0.3302(40), \quad \rho^{(6)} = -0.52(11), \quad \rho^{(8)} = -0.58(22) \\ \text{and} \quad \rho^{(10)} = -1.00(45) \end{aligned} \quad (4.2.2)$$

for the strong coupling,  $D = 6$  and  $D = 8$  contributions. We furthermore found that the OPE is converging, but not as fast as for the kinematic weight. The value of  $|\delta^{(8)}|$  is only half as large as  $|\delta^{(6)}|$ . The values of the lower momentum count are in high agreement with the ones obtained from the kinematic weight. The conclusions we take from the *cubic weight* are, that the kinematic weight, with its double pinching, should sufficiently suppress any contributions from DVs. If DV would have an effect on the kinematic weight, we should have seen an improvement of the fits with the *cubic weight*, due to its triple pinching, which is not the case.

**Quartic Weight:**  $\omega(x) \equiv (1-x)^4(1+4x)$

The last fits of the pinched weights without a monomial term in  $x$  uses the *quartic weight* defined as  $\omega(x) \equiv (1-x)^4(1+4x)$ . It contains five fitting parameters ( $\alpha_s, \rho^{(6)}, \rho^{(8)}, \rho^{(10)}, \rho^{(12)}$ ) and did only converge for  $s_{\min} = 2 \text{ GeV}$  (nine  $s_0$ s momenta). The results for the quartic weight with a  $\chi^2$  per DOF of 0.67 are given by:

$$\begin{aligned} \alpha_s(m_\tau^2) = 0.3290(11), \quad \rho^{(6)} = -0.3030(46), \quad \rho^{(8)} = -0.1874(28), \\ \rho^{(10)} = 0.3678(45) \quad \text{and} \quad \rho_{(12)} = -0.4071(77). \end{aligned} \quad (4.2.3)$$

Due to the problematic of the fitting routing, which is caused by too many OPE contributions fitted simultaneously, we discard the fitting results for the quartic weight.

#### 4.2.2. Single Pinched Monomial Weights

To further argue in favour of our hypothesis we want to probe some weights with a single pinching. If DV play a role then we should note deviating results to fits with higher pinchings. The advantage of these weights is that they only

$s_{\min}$	$\#s_0s$	$\alpha_s(m_\tau^2)$	$\rho^{(6)}$	$\chi^2/\text{dof}$
2.100	8	0.3179(47)	-0.42(17)	1.62
2.200	7	0.3248(52)	-0.77(22)	0.38
2.300	6	0.3260(60)	-0.85(28)	0.43

Table 4.5.: Table of our fitting values of  $\alpha_s(m_\tau^2)$ , and  $\rho^{(6)}$  for the single pinched double power monomial weight  $\omega_{M2}(x) = 1 - x^2$  using FORT ordered by increasing  $s_{\min}$ . The errors are given in parenthesis after the observed value.

let one OPE dimension contribute, thus leaving us with only two parameters per fit.

**Second Power Monomial:**  $\omega_{M2}(x) \equiv 1 - x^2$

The first weight is defined as  $\omega_{M2}(x) \equiv 1 - x^2$ . We only have to fit two parameters, the strong coupling  $\alpha_s$  and the dimension six OPE contributions. The results can be seen in [table 4.5](#). For this fit, we only obtained two fits without converging problems for a  $s_{\min} \leq 2.2$  GeV. Like in the  $\omega_\tau$  and  $\omega_{\text{cubic}}$  we obtain stable fits for  $s_{\min} \leq 2.2$  GeV, but the  $\chi^2/\text{dof}$  jumps to values of  $\chi^2/\text{dof} > 1.6$  for smaller  $s_{\min}$ . The values obtained for fitting six and seven  $s_0s$  moments are in good agreement with each other and furthermore carry a good  $\chi^2$  per dof. The best fit, chosen to be closest to the  $\chi^2/\text{dof}$  threshold, then yields the following parameter values

$$\alpha_s(m_\tau^2) = 0.3248(52) \quad \text{and} \quad \rho^{(6)} = -0.77(22). \quad (4.2.4)$$

We note that the strong coupling obtained from the single pinched weight is similar to one of the previous fits ( $\approx 3.33$ ) which indicates, that even single pinched weights have sufficiently suppressed dv.

**Third Power Monomial:**  $\omega_{M3}(x) \equiv 1 - x^3$

The second weight is defined as  $\omega_{M3}(x) \equiv 1 - x^3$  and contains a single third power monomial. Consequently, it is sensitive to dimension eight contribu-

$s_{\min}$	$\#s_0s$	$\alpha_s(m_\tau^2)$	$\rho^{(8)}$	$\chi^2/\text{dof}$
2.100	8	0.3147(44)	-0.27(29)	1.71
2.200	7	0.3214(49)	-1.01(39)	0.41
2.300	6	0.3227(57)	-1.18(54)	0.46
2.400	5	0.3257(67)	-1.58(74)	0.39
2.600	4	0.325(10)	-1.54(1.53)	0.58
2.800	3	0.326(21)	-1.69(4.03)	1.17

Table 4.6.: Table of our fitting values of  $\alpha_s(m_\tau^2)$ , and  $\rho^{(8)}$  for the single pinched third power monomial weight  $\omega_{M3}(x) = 1 - x^3$  using FOPT ordered by increasing  $s_{\min}$ . The errors are given in parenthesis after the observed value.

tions of the OPE. Our fitting results can be taken from [table 4.6](#). We note a good  $\chi^2/\text{dof}$  except for the last row. The last row, at  $s_{\min} = 2.8 \text{ GeV}$  has only one dof and consequently high errors. The fit closest to the  $\chi^2/\text{dof}$  threshold then yields the following parameter values

$$\alpha_s(m_\tau^2) = 0.3214(49) \quad \text{and} \quad \rho^{(8)} = -1.01(39). \quad (4.2.5)$$

**Fourth Power Monomial:**  $\omega_{M4}(x) \equiv 1 - x^4$

We already analysed the cubic and quartic weights, which depend on the dimension ten OPE contributions, in [section 4.2.1](#) and [section 4.2.1](#). Regarding the weight  $\omega_{M4} \equiv 1 - x^4$ , we can study the dimension ten OPE contribution. The results of the fits are given in [table 4.7](#). The fitting behaviour is very similar to the third power monomial ([table 4.6](#)) and we will directly cite the fits closest to the  $\chi^2/\text{dof}$  threshold:

$$\alpha_s(m_\tau^2) = 0.3203(48) \quad \text{and} \quad \rho^{(10)} = -1.64(77). \quad (4.2.6)$$

The values for the strong coupling are a little bit lower than the ones obtained by the kinematic and cubic weight fits. Furthermore, the error on the tenth dimension contribution of the OPE is large. Even with only one fitting parameter, we cannot take conclusions for the dimension ten OPE contribution. All in all

$s_{\min}$	$\#s_0s$	$\alpha_s(m_\tau^2)$	$\rho^{(10)}$	$\chi^2/\text{dof}$
2.100	8	0.3136(43)	-0.07(54)	1.75
2.200	7	0.3203(48)	-1.64(77)	0.42
2.300	6	0.3216(56)	-2.01(1.13)	0.47
2.400	5	0.3247(66)	-2.98(1.62)	0.39
2.600	4	0.324(10)	-2.86(3.69)	0.58
2.800	3	0.325(20)	-3.43(10.74)	1.17

Table 4.7.: Table of our fitting values of  $\alpha_s(m_\tau^2)$  and  $\rho^{(10)}$  for the single pinched fourth power monomial weight  $\omega_{M4}(x) = 1 - x^4$  using FOPT ordered by increasing  $s_{\min}$ . The errors are given in parenthesis after the observed value.

the usage of the single pinched fourth power monomial weight is questionable and does not deliver any additional insights.

### 4.2.3. Pinched Weights with a Monomial Term $x$

Next, to the previously mentioned *optimal weights* from Beneke et al. [7], which are weights without a monomial term in  $x$ , there exists another type of *optimal' weights*<sup>2</sup> introduced by Pich [57]

$$\omega_{(n,m)}(x) = (1-x)^n \sum_{k=0}^m (k+1)x^k. \quad (4.2.7)$$

Combinations of these optimal moments have been widely used by the ALEPH collaboration to perform QCD analysis on the LEP data. To keep our study as simple as possible we will only use weights without the sum and set  $m = 0$ . The resulting weights  $\omega_{n,0}$  are  $n$ -pinched but do not contain higher dimensional OPE contributions. The moments fitted in this section include the for FOPT problematic proportional term in  $x$ . Thus we will perform additional fits using the BS.

<sup>2</sup>Pich has a different definition of “optimal” moments than Beneke, Boito and Jamin. To differentiate the two definitions we marked Pich’s optimal’ moments with an apostrophe.

	$s_{\min}$	$\#s_0s$	$\alpha_s(m_\tau^2)$	$\langle aGG \rangle_I$	$\chi^2/\text{dof}$
BS	2.100	8	0.3176(47)	-0.0134(48)	1.62
	2.200	7	0.3246(52)	-0.2262(59)	0.38
	2.300	6	0.3260(60)	-0.2453(73)	0.43
FOPT	2.100	8	0.357(12)	-0.072(23)	0.95
	2.200	7	0.3593(97)	-0.079(19)	0.2
	2.300	6	0.3589(99)	-0.078(20)	0.24

Table 4.8.: Table of our fitting values of  $\alpha_s(m_\tau^2)$  and  $\langle aGG \rangle_I$  for the single pinched optimal weight  $\omega_{1,0}(x) = (1 - x)$  using the FOPT and BS ordered by increasing  $s_{\min}$ . The errors are given in parenthesis after the observed value.

$$\omega_{1,0} \equiv (1 - x)$$

The first weight is single pinched with only two fitting parameters:  $\alpha_s$  and  $\langle aGG \rangle_I$ . The results for BS and FOPT fits have been displayed in [table 4.8](#). We note that the  $\alpha_s$  values of the two frameworks differ, which is due to the problematic of the monomial term  $x$ , of the weight function. The BS produces similar values for the parameters as the previous fits. The values obtained from the FOPT framework differ from the previous fits. In general, we trust the results of the BS more than those of the FOPT for weights containing a monomial term  $x$ . This is further underlined while regarding the higher  $\chi^2/\text{dof}$  values of the FOPT fits. Moreover, the values of the BS fits agree, within the different used  $s_0s$  moments for this particular weight, whereas the fits of the FOPT yield inconsistent values. Regarding explicitly the fits from the BS we note that the fits have good  $\chi^2/\text{dof}$  values, although they jump from 0.2 to 0.95 between the first two fitted moments. Note that we had to fit the invariant gluon condensate for the first time. In the literature  $\langle aGG \rangle_I$  should be around 2.1, but here we obtain a smaller, negative value, which could be connected to problems in the fit.

	$s_{\min}$	$\#s_0s$	$\alpha_s(m_\tau^2)$	$\langle aGG \rangle_I$	$\rho^{(6)}$	$\chi^2/\text{dof}$
BS	2.100	8	0.3207(48)	-0.0170(50)	-0.45(17)	1.90
	2.200	7	0.3270(54)	-0.0254(61)	-0.77(21)	0.74
	2.300	6	0.3253(63)	-0.0232(75)	-0.69(27)	0.9
FOPT	2.100	8	0.3331(54)	-0.0108(45)	0.361(76)	1.9
	2.200	7	0.3401(57)	-0.0185(52)	0.220(88)	0.73
	2.300	6	0.3383(68)	-0.0165(67)	0.26(12)	0.89

Table 4.9.: Table of our fitting values of  $\alpha_s(m_\tau^2)$ ,  $\langle aGG \rangle_I$  and  $\rho^{(6)}$  for the double pinched optimal weight  $\omega_{2,0}(x) = (1-x)^2$  using the BS or FOPT ordered by increasing  $s_{\min}$ . The errors are given in parenthesis after the observed value.

$$\omega_{2,0} \equiv (1-x)^2$$

The next weight is double pinched. Additional to the strong coupling and the invariant gluon-condensate we also had to fit the dimension six OPE contribution. Our fits can be seen in [table 4.9](#). If we compare the BS with the FOPT fits we note, next to the before mentioned incompatibilities, a sign difference for the  $D = 6$  contributions. From now we will skip the FOPT discussion for weights containing a monomial term  $x$  term, and trust in the BS fits. In comparison to the previous fit with the single pinched weight we have higher  $\chi^2/\text{dof}$  values, a lower  $\alpha_s$  value and a  $\langle aGG \rangle_I$  numeric value similar to the value from the literature around 0.21, but with opposite sign. We observe a high agreement between the double pinched and single pinched weight containing a monomial term  $x$  by applying the BS, which further stresses the even for single pinched weights DV are sufficiently suppressed.

$$\omega_{3,0} \equiv (1-x)^3 \text{ and } \omega_{4,0} \equiv (1-x)^4$$

The fits with a triple and quadruple pinched weight do not give any further insights. We give the results in [table 4.10](#) and [table 4.11](#). Both of the weights include similar values to the double pinched weights, which affirms the validity of the fits and the sufficiently suppressed DV. The quadruple pinched

	$s_{\min}$	$\#s_0s$	$\alpha_s(m_\tau^2)$	$\langle aGG \rangle_I$	$\rho^{(6)}$	$\rho^{(8)}$	$\chi^2/\text{dof}$
BS	2.000	9	0.3169(20)	-0.0123(34)	-0.29(12)	-0.05(24)	2.0
	2.100	8	0.3239(40)	-0.0212(42)	-0.63(15)	-0.74(29)	0.46
	2.200	7	0.3251(17)	-0.02283(56)	-0.689(12)	-0.879(33)	0.56
FOPT	2.000	9	0.33985(81)	-0.01124(43)	0.002(10)	-0.242(26)	1.59
	2.100	8	0.3480(47)	-0.0201(36)	-0.264(89)	-1.03(28)	0.31
	2.200	7	0.3483(23)	-0.0204(41)	-0.27(15)	-1.05(40)	0.41

Table 4.10.: Table of our fitting values of  $\alpha_s(m_\tau^2)$ ,  $\langle aGG \rangle_I$ ,  $\rho^{(6)}$  and  $\rho^{(8)}$  for the optimal weight  $\omega_{3,0}(x) = (1-x)^3$  using the BS or FOPT ordered by increasing  $s_{\min}$ . The errors are given in parenthesis after the observed value.

weight contains five fitting parameters and as a result has notable convergence problems.

### 4.3. Comparison

To create an overview of our previous results we have gathered the most compatible rows by hand. The fits have been selected by regarding the  $\chi^2/\text{dof}$  threshold. For every weight, which has not been excluded by being problematic, we have chosen a fit closest, but below the  $\chi^2/\text{dof}$  threshold. They are shown in [table 4.12](#), which is composed of two parts. The upper four rows are fits using FOPT and the lower two rows are fits using BS. For the weights with a monomial term  $x$  we only included fits, which make use of the BS. Fits applying the FOPT result in deviating parameter values in comparison with fit results from weights without a monomial term  $x$ . This behaviour has already been illustrated in [\[7\]](#) and is further supported by this work. Consequently, for fits including weights without a monomial term  $x$ , we can apply FOPT, but for fits including weights with a monomial term in  $x$  the BS is needed.

The fits of the comparison [table 4.12](#) are in great agreement with each other. The strong coupling as the OPE contributions up to dimension eight are com-

	$s_{\min}$	$\#s_0s$	$\alpha_s(m_\tau^2)$	aGGInv	$\rho^{(6)}$	$\rho^{(8)}$	$\rho^{(10)}$	$\chi^2/\text{dof}$
BS	1.950	10	0.31711(67)	-0.012432(24)	-0.30013(73)	-0.06785(16)	0.26104(50)	1.09
	2.000	9	0.3206(24)	-0.0167(14)	-0.455(38)	-0.373(67)	-0.36(14)	0.83
	2.100	8	0.3248(21)	-0.02230(47)	-0.6724(63)	-0.834(14)	-1.352(28)	0.23
FOPT	1.950	10	0.3416(14)	-0.01306(83)	-0.050(22)	-0.390(59)	-0.50(19)	1.71
	2.100	8	0.3480(25)	-0.0201(27)	-0.264(91)	-1.02(23)	-339.00(20)	0.41

Table 4.11.: Table of our fitting values of  $\alpha_s(m_\tau^2)$ ,  $\langle \text{aGG} \rangle_I$ ,  $\rho^{(6)}$ ,  $\rho^{(8)}$  and  $\rho^{(10)}$  for the optimal weight  $\omega_{4,0}(x) = (1-x)^4$  using the BS or FOPT ordered by increasing  $s_{\min}$ . The errors are given in parenthesis after the observed value.

	weight	$s_{\min}$	$\alpha_s(m_\tau^2)$	$\langle \text{aGG} \rangle_I$	$\rho^{(6)}$	$\rho^{(8)}$	$\rho^{(10)}$	$\chi^2/\text{dof}$
FOPT	$\omega_\tau$	2.2	0.3308(44)	-	-0.72(20)	-0.85(38)	-	0.19
	$\omega_{\text{cube}}$	2.1	0.3302(40)	-	-0.52(11)	-0.58(22)	-1.00(45)	0.43
	$\omega_{M2}$	2.2	0.3248(52)	-	-0.77(22)	-	-	0.38
	$\omega_{M3}$	2.2	0.3214(49)	-	-	-1.01(39)	-	0.41
BS	$\omega_{1,0}$	2.2	0.3246(52)	-0.2262(59)	-	-	-	0.38
	$\omega_{2,0}$	2.2	0.3270(54)	-0.0254(61)	-0.77(21)	-	-	0.74
	$\omega_{3,0}$	2.1	0.3239(40)	-0.0212(42)	-0.63(15)	-0.74(29)	-	0.46

Table 4.12.: Table of the best fits. The fits have been selected as being closest to the previously discussed  $\chi^2/\text{dof}$  jump. Each weight includes the strong coupling  $\alpha_s(m_\tau^2)$  as a fitting variable. The first four fits have been performed using FOPT and the last two have been performed using BS. They are visually distinguished in the table by a horizontal line.



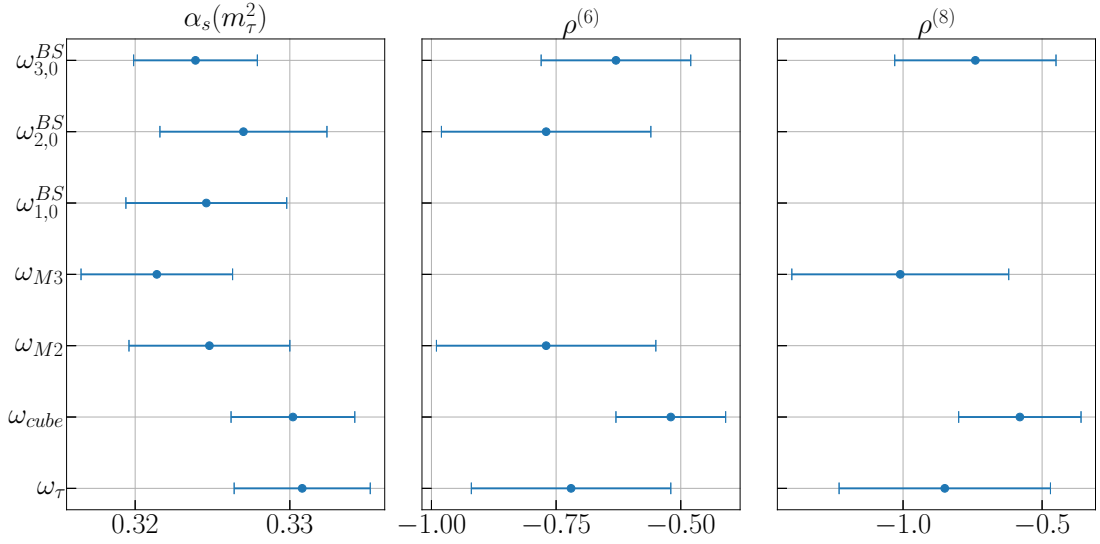


Figure 4.4.: Visual comparison of the fitted parameters  $\alpha_s(m_\tau^2)$ ,  $\rho^{(6)}$  and  $\rho^{(8)}$  for the results of table 4.12. The values of the different fits and models values are very comparable to each other. For the weights including a monomial term in  $x$  display the results obtained from the BS as can be seen from the upper index of  $\omega_{n,0}^{BS}$ .

patible within small error ranges. To underline their agreement we have visualised the different values and errors in fig. 4.4. The fits furthermore all have a good  $\chi^2/\text{dof}$ .

The high agreement between all fits shows that no DV have to be taken into account while implementing fits in the v+A channel and the corresponding framework, FORT or BS depending if the weight does not or does include a monomial term in  $x$ , for at least single pinched weights. At least single and not double pinched, because the weights  $\omega_{M2}$  and  $\omega_{M3}$  are only single pinched, but still in high agreement with the other higher pinched weights! We consequently do not see any need to include DV terms in an analysis of  $\alpha_s$  from  $\tau$  decay data.

	$c_{5,1} = 0$	$c_{5,1} = 283$	$c_{5,1} = 566$	$\Delta$
$\alpha_s(m_\tau^2)$	0.3333	0.3308	0.3285	0.0025
$\rho^{(6)}$	-0.74	-0.72	-0.69	0.03
$\rho^{(8)}$	-0.87	-0.85	0.82	0.03

Table 4.13.: Values of  $\alpha_s$ ,  $\rho^{(6)}$  and  $\rho^{(8)}$  for varying  $c_{5,1}$  and the corresponding, symmetric error  $\Delta$  for each parameter to the central value of  $c_{5,1} = 283$ .

## 4.4. Final Results

Here we will state our final results for the strong coupling and the dimensions six and eight OPE contributions. We have decided to average over all values of the selected fits seen in [table 4.12](#), but focus on the error given by the FOPT fit of the kinematic weight. We did not want to use the value for the strong coupling of the kinematic weight solely, because it is representing a rather large value in comparison to the other selected fits. We further did not want to average over the errors of all compared fits, as we do not know their correlations. Averaging over all errors would most probably lead to an underestimated error.

### 4.4.1. Theoretical Error

The values have a statistical error given by the fitting routine MINUIT and a theoretical error. The main contribution from the theoretical error comes from the fifth Adler function coefficient  $c_{5,1}$ , which has not been calculated yet. Though estimated in [\[8\]](#) with a value of  $c_{5,1} = 283$  we will assume a relative error of 100% to its value. Consequently, we performed two additional fits with  $c_{5,1} = 0$  and  $c_{5,1} = 566$  and via comparison extracted the error to the central value of the corresponding parameter. We have further decided instead of stating the resulting asymmetric errors the larger value of the upper and lower error as a symmetric error. The results of the additional fits with varying the fifth Adler function coefficient can be seen in [table 4.13](#). The symmetrical theoretical errors are then given by 0.0025, 0.03 and 0.03 for  $\alpha_s$ ,  $\rho^{(6)}$  and  $\rho^{(8)}$  correspondingly.

### 4.4.2. Parameter Values

We will average over the values of [table 4.12](#) leading to

$$\alpha_s(m_\tau^2) = 0.3261 \pm (0.0044)_{\text{MINUIT}} \pm (0.0025)_{c_{5,1}} = 0.3261 \pm 0.0051 \quad (4.4.1)$$

for the strong coupling at the  $\tau^2$  scale. The dimension six and eight OPE contributions are very stable in the fits we compared. Consequently we will state their averaged numerical values

$$\rho^{(6)} = -0.68 \pm (0.2)_{\text{MINUIT}} \pm (0.03)_{c_{5,1}} = -0.68 \pm 0.20 \quad (4.4.2)$$

$$\rho^{(8)} = -0.80 \pm (0.38)_{\text{MINUIT}} \pm (0.03)_{c_{5,1}} = -0.80 \pm 0.38. \quad (4.4.3)$$

Note that the  $\rho^{(6)}$  values from the cubic weight are slightly different. The cubic weight includes contributions from a fourth fitting parameter, which need to be compensated by the other parameters.

The value of higher dimension OPE parameters are still compatible but have a higher variation than the previous two parameters. Beginning from the  $D = 10$  contributions we do not have enough good fits to evaluate their contribution. Consequently, we do not state a single value for OPE parameters of dimension eight and higher.



## Conclusions

We have performed a QCD analysis on hadronic  $\tau$  decays to determine a value of  $\alpha_s$  at the  $m_\tau^2$  scale without including  $DV$ . We have excluded  $DV$  to contrast the previous analysis of Boito et al. [12, 13, 16], which stated the necessity of incorporating a model describing  $DV$ . To argue, we employed a new set of analytic weights to probe the suppression of  $DV$ .

We compared seven selected fits of different weights with single, double and triple pinching. All fits gave similar values for the strong coupling and dimension six and eight OPE contributions. The conclusion we take is that  $DV$  are sufficiently suppressed in the framework of FOPT in the  $V+A$  channel, even for single pinched weights. To extract precise values of the strong coupling from hadronic  $\tau$  decay data no additional model is needed.

For the kinematic weight and the weights carrying a monomial term  $x$ , we performed fits using both, the BS and the FOPT approach. The fitted parameters of both frameworks show great compatibility. The fact that both frameworks yield similar results argues in favour of FOPT, as CIPT would give different values for the fitting parameters. Consequently, we discourage the usage of CIPT and favour the usage FOPT and further underline the opinion of Beneke et al. [8] in the debate of FOPT vs CIPT.

The final value for the strong coupling we obtained at the  $m_\tau^2$  scale is given by

$$\alpha_s(m_\tau^2) = 0.3261(50). \quad (5.0.1)$$

Running this value to the  $m_Z$  scale yields

$$\alpha_s(m_Z^2) = 0.11940(60), \quad (5.0.2)$$

which is comparable to the world average value of  $\alpha_s(M_Z^2) = 0.1181(11)$  taken from the [82]. For dimension six and eight OPE contributions we extracted values of

$$\rho^{(6)} = -0.68 \pm 0.20 \quad (5.0.3)$$

$$\rho^{(8)} = -0.80 \pm 0.38. \quad (5.0.4)$$

## Constants

In [table A.1](#) we collect all used constants that we have used in performing our fits.

Quantity	Value	Reference
$V_{ud}$	$0.9742 \pm 0.00021$	<a href="#">[82]</a>
$S_{EW}$	$1.0198 \pm 0.0006$	<a href="#">[60]</a>
$B_e$	$17.818 \pm 0.023$	<a href="#">[32]</a>
$m_\tau$	$1.776\,86(12000) \text{ MeV}$	<a href="#">[82]</a>
$\langle aGG \rangle_I$	$0.012 \text{ GeV}^2$	<a href="#">[77]</a>
$\langle \bar{q}_{u/d} q_{u/d} \rangle(m_\tau)$	$-272(15) \text{ MeV}$	<a href="#">[49]</a>
$\bar{s}s/\langle \bar{q}q \rangle$	$0.8 \pm 0.3$	<a href="#">[49]</a>

Table A.1.: Numerical values of used constants in our fitting routine.





## Coefficients

### B.1. $\beta$ function

There are several conventions for defining the  $\beta$  coefficients, depending on a minus sign and/or a factor of two (if one substitutes  $\mu \rightarrow \mu^2$ ) in the  $\beta$ -function [2.1.12](#). We follow the convention from Pascual and Tarrach (except for the minus sign) and have taken the values from [\[10\]](#)

$$\beta_1 = \frac{1}{6}(11N_c - 2N_f), \tag{B.1.1}$$

$$\beta_2 = \frac{1}{12}(17N_c^2 - 5N_cN_f - 3C_fN_f), \tag{B.1.2}$$

$$\beta_3 = \frac{1}{32} \left( \frac{2857}{54}N_c^3 - \frac{1415}{54}N_c^2N_f + \frac{79}{54}N_cN_f^2 - \frac{205}{18}N_cC_fN_f + \frac{11}{9}C_fN_f^2 + C_f^2N_f \right), \tag{B.1.3}$$

$$\beta_4 = \frac{140599}{2304} + \frac{445}{16}\zeta_3, \tag{B.1.4}$$

where we used  $N_f = 3$  and  $N_c = 3$  for  $\beta_4$ .

## B.2. Anomalous mass dimension

$$\gamma_1 = \frac{3}{2}C_f, \quad (\text{B.2.1})$$

$$\gamma_2 = \frac{C_f}{48}(97N_c + 9C_f - 10N_f), \quad (\text{B.2.2})$$

$$\gamma_3 = \frac{C_f}{32} \left[ \frac{11413}{108}N_c^2 - \frac{129}{4}N_cC_f - \left( \frac{278}{27} + 24\zeta_3 \right) N_cN_f + \frac{129}{2}C_f^2 - (23 - 24\zeta_3)C_fN_f - \frac{35}{27}N_f^2 \right], \quad (\text{B.2.3})$$

$$\gamma_4 = \frac{2977517}{20736} - \frac{9295}{216}\zeta_3 + \frac{135}{8}\zeta_4 - \frac{125}{6}\zeta_5, \quad (\text{B.2.4})$$

where  $N_c$  is the number of colours,  $N_f$  the number of flavours and  $C_f = (N_c^2 - 1)/2N_c$ . We fixed furthermore fixed  $N_f = 3$  and  $N_c = 3$  for  $\gamma_4$ .

## B.3. Adler function

The the derivative of the two-point function can be expressed as the Adler function, which can be written in terms of the Adler function coefficients

$$D_V^{(1+0)} = \frac{N_c}{12\pi^2} \sum_{n=0}^{\infty} a_\mu^n \sum_{k=1}^{n+1} k c_{n,k} L^{k-1}. \quad (\text{B.3.1})$$

The coefficients are partly dependent on each other via the RGE

$$-\mu \frac{d}{d\mu} D_V^{(1+0)} = \left( 2 \frac{\partial}{\partial L} + \beta \frac{\partial}{\partial a_s} \right) D_V^{(1+0)} = 0, \quad (\text{B.3.2})$$

which implies, that for every order, there exists only one coefficient we have to know to describe the Adler function. For completeness we will mention the necessary coefficients up to order  $n = 5$  here once again

$$\begin{aligned} c_{1,1} &= 1 \\ c_{2,1} &= \frac{365}{24} - 11\zeta_3 - \left( \frac{11}{12} - \frac{2}{3}\zeta_3 \right) N_f \\ c_{3,1} &= \frac{87029}{288} - \frac{1103}{4}\zeta_3 + \frac{275}{6}\zeta_5 \\ &\quad - \left( \frac{7847}{216} - \frac{262}{9}\zeta_3 + \frac{25}{9}\zeta_5 \right) N_f + \left( \frac{151}{162} - \frac{19}{27}\zeta_3 \right) N_f^2 \\ c_{4,1} &= \frac{78631453}{20736} - \frac{1704247}{432}\zeta_3 + \frac{4185}{8}\zeta_3^2 + \frac{34165}{96}\zeta_5 - \frac{1995}{16}\zeta_7. \end{aligned} \quad (\text{B.3.3})$$

## APPENDIX B. COEFFICIENTS

The rest of the coefficients are given by

$$\begin{aligned}
c_{2,2} &= -\frac{1}{4}\beta_1 c_{1,1} \\
c_{3,2} &= (-\beta_2 c_{1,1} - 2\beta_1 c_{2,1}), \quad c_{3,3} = \frac{1}{12}\beta_1^2 c_{1,1} \\
c_{4,2} &= \frac{1}{4}(-\beta_3 c_{1,1} - 2\beta_2 c_{2,1} - 3\beta_1 c_{3,1}), \\
c_{4,3} &= \frac{1}{24}(6c_{2,1}\beta_1^2 + 5\beta_2\beta_1 c_{1,1}), \quad c_{4,4} = -\frac{1}{32}\beta_1^3 c_{1,1} \\
c_{5,2} &= \frac{1}{4}(-\beta_4 c_{1,1} - 2\beta_3 c_{2,1} - 3\beta_2 c_{3,1} - 4\beta_1 c_{4,1}), \\
c_{5,3} &= \frac{1}{24}(12c_{3,1}\beta_1^2 + 6\beta_1\beta_3 c_{1,1} + 14\beta_2\beta_1 c_{2,1} + 3\beta_2^2 c_{1,1}), \\
c_{5,4} &= \frac{1}{96}(-12\beta_1^3 c_{2,1} - 13\beta_2\beta_1^2 c_{1,1}), \quad c_{5,5} = \frac{1}{80}\beta_1^4 c_{1,1}
\end{aligned} \tag{B.3.4}$$

and all related to the previous stated Adler function coefficients  $c_{n,1}$ .



# List of Abbreviations

A	axial-vector
BS	Borel summation
CERN	European Organisation for Nuclear Research
CKM	Cabibbo-Kobayashi-Maskawa
DOF	degrees of freedom
FESR	finite energy sum rules
FESR	finite energy sum rules
FLAG	Flavour Lattice Averaging Group
GR	general relativity
IR	infrared
LEP	large-electron-positron
LHC	large-hadron-collider
LHS	left-hand side
LS	method of least squares
MS	minimal subtraction scheme
NP	non-perturbative

## LIST OF ABBREVIATIONS

P-V Pauli-Villars

PQCD perturbative QCD

PT perturbation theory

P pseudo-scalar

QFT quantum field theory

RGE renormalisation group equation

RGE renormalisation group equation

RHS right-hand side

SM Standard Model

S scalar

UV ultraviolet

VSA vacuum saturation approach

V vector

CHPT Chiral Perturbation Theory

LQCD Lattice Quantum Chromodynamics

QCDSR Quantum Chromodynamics Sum Rules

# Bibliography

- [1] Gerard 't Hooft. “Dimensional regularization and the renormalization group”. In: *Nucl. Phys.* B61 (1973), pp. 455–468. DOI: [10.1016/0550-3213\(73\)90376-3](https://doi.org/10.1016/0550-3213(73)90376-3).
- [2] Gerard 't Hooft and M. J. G. Veltman. “Regularization and Renormalization of Gauge Fields”. In: *Nucl. Phys.* B44 (1972), pp. 189–213. DOI: [10.1016/0550-3213\(72\)90279-9](https://doi.org/10.1016/0550-3213(72)90279-9).
- [3] K. Ackerstaff et al. “Measurement of the strong coupling constant  $\alpha_s$  and the vector and axial vector spectral functions in hadronic tau decays”. In: *Eur. Phys. J.* C7 (1999), pp. 571–593. DOI: [10.1007/s100520050430](https://doi.org/10.1007/s100520050430), [10.1007/s100529901061](https://doi.org/10.1007/s100529901061). arXiv: [hep-ex/9808019](https://arxiv.org/abs/hep-ex/9808019) [hep-ex].
- [4] S. Aoki et al. “FLAG Review 2019”. In: (2019). arXiv: [1902.08191](https://arxiv.org/abs/1902.08191) [hep-lat].
- [5] P. A. Baikov, K. G. Chetyrkin, and Johann H. Kuhn. “Order  $\alpha_s^4$ (s) QCD Corrections to Z and tau Decays”. In: *Phys. Rev. Lett.* 101 (2008), p. 012002. DOI: [10.1103/PhysRevLett.101.012002](https://doi.org/10.1103/PhysRevLett.101.012002). arXiv: [0801.1821](https://arxiv.org/abs/0801.1821) [hep-ph].
- [6] M. Beneke. “Renormalons”. In: *Phys. Rept.* 317 (1999), pp. 1–142. DOI: [10.1016/S0370-1573\(98\)00130-6](https://doi.org/10.1016/S0370-1573(98)00130-6). arXiv: [hep-ph/9807443](https://arxiv.org/abs/hep-ph/9807443) [hep-ph].
- [7] Martin Beneke, Diogo Boito, and Matthias Jamin. “Perturbative expansion of tau hadronic spectral function moments and  $\alpha_s$  extractions”. In: *JHEP* 01 (2013), p. 125. DOI: [10.1007/JHEP01\(2013\)125](https://doi.org/10.1007/JHEP01(2013)125). arXiv: [1210.8038](https://arxiv.org/abs/1210.8038) [hep-ph].

- [8] Martin Beneke and Matthias Jamin. “ $\alpha(s)$  and the tau hadronic width: fixed-order, contour-improved and higher-order perturbation theory”. In: *JHEP* 09 (2008), p. 044. DOI: [10.1088/1126-6708/2008/09/044](https://doi.org/10.1088/1126-6708/2008/09/044). arXiv: [0806.3156](https://arxiv.org/abs/0806.3156) [hep-ph].
- [9] D. R. Boito et al. “Duality violations in tau hadronic spectral moments”. In: *Nucl. Phys. Proc. Suppl.* 218 (2011), pp. 104–109. DOI: [10.1016/j.nuclphysbps.2011.06.018](https://doi.org/10.1016/j.nuclphysbps.2011.06.018). arXiv: [1011.4426](https://arxiv.org/abs/1011.4426) [hep-ph].
- [10] Diogo Boito. “QCD phenomenology with  $\tau$  and charm decays”. PhD thesis. Universitat Autònoma de Barcelona, Sept. 2011.
- [11] Diogo Boito, Dirk Hornung, and Matthias Jamin. “Anomalous dimensions of four-quark operators and renormalon structure of mesonic two-point correlators”. In: *JHEP* 12 (2015), p. 090. DOI: [10.1007/JHEP12\(2015\)090](https://doi.org/10.1007/JHEP12(2015)090). arXiv: [1510.03812](https://arxiv.org/abs/1510.03812) [hep-ph].
- [12] Diogo Boito et al. “A new determination of  $\alpha_s$  from hadronic  $\tau$  decays”. In: *Phys. Rev. D* 84 (2011), p. 113006. DOI: [10.1103/PhysRevD.84.113006](https://doi.org/10.1103/PhysRevD.84.113006). arXiv: [1110.1127](https://arxiv.org/abs/1110.1127) [hep-ph].
- [13] Diogo Boito et al. “An Updated determination of  $\alpha_s$  from  $\tau$  decays”. In: *Phys. Rev. D* 85 (2012), p. 093015. DOI: [10.1103/PhysRevD.85.093015](https://doi.org/10.1103/PhysRevD.85.093015). arXiv: [1203.3146](https://arxiv.org/abs/1203.3146) [hep-ph].
- [14] Diogo Boito et al. “Strong coupling from  $e^+e^- \rightarrow$  hadrons below charm”. In: *Phys. Rev. D* 98.7 (2018), p. 074030. DOI: [10.1103/PhysRevD.98.074030](https://doi.org/10.1103/PhysRevD.98.074030). arXiv: [1805.08176](https://arxiv.org/abs/1805.08176) [hep-ph].
- [15] Diogo Boito et al. “Strong coupling from hadronic  $\tau$  decays: A critical appraisal”. In: *Phys. Rev. D* 95.3 (2017), p. 034024. DOI: [10.1103/PhysRevD.95.034024](https://doi.org/10.1103/PhysRevD.95.034024). arXiv: [1611.03457](https://arxiv.org/abs/1611.03457) [hep-ph].
- [16] Diogo Boito et al. “Strong coupling from the revised ALEPH data for hadronic  $\tau$  decays”. In: *Phys. Rev. D* 91.3 (2015), p. 034003. DOI: [10.1103/PhysRevD.91.034003](https://doi.org/10.1103/PhysRevD.91.034003). arXiv: [1410.3528](https://arxiv.org/abs/1410.3528) [hep-ph].
- [17] C. G. Bollini and J. J. Giambiagi. “Dimensional Renormalization: The Number of Dimensions as a Regularizing Parameter”. In: *Nuovo Cim. B* 12 (1972), pp. 20–26. DOI: [10.1007/BF02895558](https://doi.org/10.1007/BF02895558).



## BIBLIOGRAPHY

- [18] Émile Borel. “Mémoire sur les séries divergentes”. fr. In: *Annales scientifiques de l’École Normale Supérieure* 3e série, 16 (1899), pp. 9–131. DOI: [10.24033/asens.463](https://doi.org/10.24033/asens.463). URL: [http://www.numdam.org/item/ASENS\\_1899\\_3\\_16\\_\\_9\\_0](http://www.numdam.org/item/ASENS_1899_3_16__9_0).
- [19] E. Braaten, Stephan Narison, and A. Pich. “QCD analysis of the tau hadronic width”. In: *Nucl. Phys.* B373 (1992), pp. 581–612. DOI: [10.1016/0550-3213\(92\)90267-F](https://doi.org/10.1016/0550-3213(92)90267-F).
- [20] David J. Broadhurst. “Chiral Symmetry Breaking and Perturbative QCD”. In: *Phys. Lett.* 101B (1981), pp. 423–426. DOI: [10.1016/0370-2693\(81\)90167-2](https://doi.org/10.1016/0370-2693(81)90167-2).
- [21] R. Brun and F. Rademakers. “ROOT: An object oriented data analysis framework”. In: *Nucl. Instrum. Meth.* A389 (1997), pp. 81–86. DOI: [10.1016/S0168-9002\(97\)00048-X](https://doi.org/10.1016/S0168-9002(97)00048-X).
- [22] D. Buskulic et al. “Measurement of the strong coupling constant using tau decays”. In: *Phys. Lett.* B307 (1993), pp. 209–220. DOI: [10.1016/0370-2693\(93\)90212-Z](https://doi.org/10.1016/0370-2693(93)90212-Z).
- [23] Irinel Caprini and Jan Fischer. “alpha(s) from tau decays: Contour-improved versus fixed-order summation in a new QCD perturbation expansion”. In: *Eur. Phys. J.* C64 (2009), pp. 35–45. DOI: [10.1140/epjc/s10052-009-1142-8](https://doi.org/10.1140/epjc/s10052-009-1142-8). arXiv: [0906.5211 \[hep-ph\]](https://arxiv.org/abs/0906.5211).
- [24] O. Cata, M. Golterman, and S. Peris. “Duality violations and spectral sum rules”. In: *JHEP* 08 (2005), p. 076. DOI: [10.1088/1126-6708/2005/08/076](https://doi.org/10.1088/1126-6708/2005/08/076). arXiv: [hep-ph/0506004 \[hep-ph\]](https://arxiv.org/abs/hep-ph/0506004).
- [25] Oscar Cata, Maarten Golterman, and Santi Peris. “Unraveling duality violations in hadronic tau decays”. In: *Phys. Rev.* D77 (2008), p. 093006. DOI: [10.1103/PhysRevD.77.093006](https://doi.org/10.1103/PhysRevD.77.093006). arXiv: [0803.0246 \[hep-ph\]](https://arxiv.org/abs/0803.0246).
- [26] Oscar Cata, Maarten Golterman, and Santiago Peris. “Possible duality violations in tau decay and their impact on the determination of alpha(s)”. In: *Phys. Rev.* D79 (2009), p. 053002. DOI: [10.1103/PhysRevD.79.053002](https://doi.org/10.1103/PhysRevD.79.053002). arXiv: [0812.2285 \[hep-ph\]](https://arxiv.org/abs/0812.2285).

- [27] William Celmaster and Richard J. Gonsalves. “An Analytic Calculation of Higher Order Quantum Chromodynamic Corrections in  $e^+ e^-$  Annihilation”. In: *Phys. Rev. Lett.* 44 (1980), p. 560. DOI: [10.1103/PhysRevLett.44.560](https://doi.org/10.1103/PhysRevLett.44.560).
- [28] K. G. Chetyrkin, A. L. Kataev, and F. V. Tkachov. “Higher Order Corrections to  $\Sigma$ -t ( $e^+ e^- \rightarrow$  Hadrons) in Quantum Chromodynamics”. In: *Phys. Lett.* 85B (1979), pp. 277–279. DOI: [10.1016/0370-2693\(79\)90596-3](https://doi.org/10.1016/0370-2693(79)90596-3).
- [29] K. G. Chetyrkin, Johann H. Kuhn, and M. Steinhauser. “RunDec: A Mathematica package for running and decoupling of the strong coupling and quark masses”. In: *Comput. Phys. Commun.* 133 (2000), pp. 43–65. DOI: [10.1016/S0010-4655\(00\)00155-7](https://doi.org/10.1016/S0010-4655(00)00155-7). arXiv: [hep-ph/0004189](https://arxiv.org/abs/hep-ph/0004189) [hep-ph].
- [30] Pietro Colangelo and Alexander Khodjamirian. “QCD sum rules, a modern perspective”. In: (2000), pp. 1495–1576. DOI: [10.1142/9789812810458\\_0033](https://doi.org/10.1142/9789812810458_0033). arXiv: [hep-ph/0010175](https://arxiv.org/abs/hep-ph/0010175) [hep-ph].
- [31] The Aleph Collaboration. *Invariant mass squared distributions from ALEPH*. 2005. URL: <http://aleph.web.lal.in2p3.fr/tau/specfun13.html> (visited on 06/09/2019).
- [32] M. Davier et al. “The Determination of  $\alpha(s)$  from Tau Decays Revisited”. In: *Eur. Phys. J. C* 56 (2008), pp. 305–322. DOI: [10.1140/epjc/s10052-008-0666-7](https://doi.org/10.1140/epjc/s10052-008-0666-7). arXiv: [0803.0979](https://arxiv.org/abs/0803.0979) [hep-ph].
- [33] Michel Davier, Andreas Hocker, and Zhiqing Zhang. “ALEPH Tau Spectral Functions and QCD”. In: *Nucl. Phys. Proc. Suppl.* 169 (2007). [,22(2007)], pp. 22–35. DOI: [10.1016/j.nuclphysbps.2007.02.109](https://doi.org/10.1016/j.nuclphysbps.2007.02.109). arXiv: [hep-ph/0701170](https://arxiv.org/abs/hep-ph/0701170) [hep-ph].
- [34] Michel Davier, Andreas Hocker, and Zhiqing Zhang. “The physics of hadronic tau decays”. In: *Rev. Mod. Phys.* 78 (4 Oct. 2006), pp. 1043–1109. DOI: [10.1103/RevModPhys.78.1043](https://doi.org/10.1103/RevModPhys.78.1043). URL: <https://link.aps.org/doi/10.1103/RevModPhys.78.1043>.
- [35] Michel Davier et al. “Update of the ALEPH non-strange spectral functions from hadronic  $\tau$  decays”. In: *Eur. Phys. J. C* 74.3 (2014), p. 2803. DOI: [10.1140/epjc/s10052-014-2803-9](https://doi.org/10.1140/epjc/s10052-014-2803-9). arXiv: [1312.1501](https://arxiv.org/abs/1312.1501) [hep-ex].

- [36] Alexandre Deur, Stanley J. Brodsky, and Guy F. de Teramond. “The QCD Running Coupling”. In: *Prog. Part. Nucl. Phys.* 90 (2016), pp. 1–74. DOI: [10.1016/j.pnpnp.2016.04.003](https://doi.org/10.1016/j.pnpnp.2016.04.003). arXiv: [1604.08082](https://arxiv.org/abs/1604.08082) [hep-ph].
- [37] Michael Dine and J. R. Sapirstein. “Higher Order QCD Corrections in  $e^+ e^-$  Annihilation”. In: *Phys. Rev. Lett.* 43 (1979), p. 668. DOI: [10.1103/PhysRevLett.43.668](https://doi.org/10.1103/PhysRevLett.43.668).
- [38] C. A. Dominguez. “Introduction to QCD sum rules”. In: *Mod. Phys. Lett. A* 28 (2013), p. 1360002. DOI: [10.1142/S021773231360002X](https://doi.org/10.1142/S021773231360002X). arXiv: [1305.7047](https://arxiv.org/abs/1305.7047) [hep-ph].
- [39] L. D. Faddeev and V. N. Popov. “Feynman Diagrams for the Yang-Mills Field”. In: *Phys. Lett. B* 25 (1967). [325(1967)], pp. 29–30. DOI: [10.1016/0370-2693\(67\)90067-6](https://doi.org/10.1016/0370-2693(67)90067-6).
- [40] H. Fritzsch, Murray Gell-Mann, and H. Leutwyler. “Advantages of the Color Octet Gluon Picture”. In: *Phys. Lett.* 47B (1973), pp. 365–368. DOI: [10.1016/0370-2693\(73\)90625-4](https://doi.org/10.1016/0370-2693(73)90625-4).
- [41] M. Gell-Mann. “Quarks”. In: *Acta Phys. Austriaca Suppl.* 9 (1972). [5(2015)], pp. 733–761. DOI: [10.1142/9789814618113\\_0002](https://doi.org/10.1142/9789814618113_0002), [10.1007/978-3-7091-4034-5\\_20](https://doi.org/10.1007/978-3-7091-4034-5_20).
- [42] S. G. Gorishnii, A. L. Kataev, and S. A. Larin. “The  $O(\alpha_s^3)$ -corrections to  $\sigma_{\text{tot}}(e^+e^- \rightarrow \text{hadrons})$  and  $\Gamma(\tau^- \rightarrow \nu_\tau + \text{hadrons})$  in QCD”. In: *Phys. Lett. B* 259 (1991), pp. 144–150. DOI: [10.1016/0370-2693\(91\)90149-K](https://doi.org/10.1016/0370-2693(91)90149-K).
- [43] D. J. Gross and Frank Wilczek. “Asymptotically Free Gauge Theories - I”. In: *Phys. Rev. D* 8 (1973), pp. 3633–3652. DOI: [10.1103/PhysRevD.8.3633](https://doi.org/10.1103/PhysRevD.8.3633).
- [44] Florian Herren and Matthias Steinhauser. “Version 3 of RunDec and CRunDec”. In: *Comput. Phys. Commun.* 224 (2018), pp. 333–345. DOI: [10.1016/j.cpc.2017.11.014](https://doi.org/10.1016/j.cpc.2017.11.014). arXiv: [1703.03751](https://arxiv.org/abs/1703.03751) [hep-ph].
- [45] W. Hubschmid and S. Mallik. “OPERATOR EXPANSION AT SHORT DISTANCE IN QCD”. In: *Nucl. Phys. B* 207 (1982), pp. 29–42. DOI: [10.1016/0550-3213\(82\)90134-1](https://doi.org/10.1016/0550-3213(82)90134-1).

- [46] F. James and M. Roos. “Minuit: A System for Function Minimization and Analysis of the Parameter Errors and Correlations”. In: *Comput. Phys. Commun.* 10 (1975), pp. 343–367. DOI: [10.1016/0010-4655\(75\)90039-9](https://doi.org/10.1016/0010-4655(75)90039-9).
- [47] M. Jamin and M. Kremer. “Anomalous Dimensions of Spin o Four Quark Operators Without Derivatives”. In: *Nucl. Phys. B* 277 (1986), pp. 349–358. DOI: [10.1016/0550-3213\(86\)90446-3](https://doi.org/10.1016/0550-3213(86)90446-3).
- [48] Matthias Jamin. “Contour-improved versus fixed-order perturbation theory in hadronic tau decays”. In: *JHEP* 09 (2005), p. 058. DOI: [10.1088/1126-6708/2005/09/058](https://doi.org/10.1088/1126-6708/2005/09/058). arXiv: [hep-ph/0509001](https://arxiv.org/abs/hep-ph/0509001) [[hep-ph](#)].
- [49] Matthias Jamin. “Flavor symmetry breaking of the quark condensate and chiral corrections to the Gell-Mann-Oakes-Renner relation”. In: *Phys. Lett. B* 538 (2002), pp. 71–76. DOI: [10.1016/S0370-2693\(02\)01951-2](https://doi.org/10.1016/S0370-2693(02)01951-2). arXiv: [hep-ph/0201174](https://arxiv.org/abs/hep-ph/0201174) [[hep-ph](#)].
- [50] Matthias Jamin. *QCD and Renormalisation Group Methods*. Lecture presented at Herbstschule für Hochenergiephysik Maria Laach. Sept. 2006.
- [51] Matthias Jamin. “Strong coupling from tau lepton decays”. In: *Mod. Phys. Lett. A* 28 (2013), p. 1360006. DOI: [10.1142/S0217732313600067](https://doi.org/10.1142/S0217732313600067).
- [52] Matthias Jamin and Manfred Munz. “Current correlators to all orders in the quark masses”. In: *Z. Phys. C* 60 (1993), pp. 569–578. DOI: [10.1007/BF01560056](https://doi.org/10.1007/BF01560056). arXiv: [hep-ph/9208201](https://arxiv.org/abs/hep-ph/9208201) [[hep-ph](#)].
- [53] Gunnar Kallen. “On the definition of the Renormalization Constants in Quantum Electrodynamics”. In: *Helv. Phys. Acta* 25 (417). [509(1952)]. DOI: [10.1007/978-3-319-00627-7\\_90](https://doi.org/10.1007/978-3-319-00627-7_90).
- [54] Alexander Keshavarzi, Daisuke Nomura, and Thomas Teubner. “ $\mu\text{on } g - 2$  and  $\alpha(M_Z^2)$ : a new data-based analysis”. In: *Phys. Rev. D* 97.11 (2018), p. 114025. DOI: [10.1103/PhysRevD.97.114025](https://doi.org/10.1103/PhysRevD.97.114025). arXiv: [1802.02995](https://arxiv.org/abs/1802.02995) [[hep-ph](#)].
- [55] L. V. Lanin, V. P. Spiridonov, and K. G. Chetyrkin. “Contribution of Four Quark Condensates to Sum Rules for  $\rho$  and  $A_1$  Mesons. (In Russian)”. In: *Yad. Fiz.* 44 (1986), pp. 1372–1374.

## BIBLIOGRAPHY

- [56] G. Launer, Stephan Narison, and R. Tarrach. “Nonperturbative QCD Vacuum From  $e^+e^- \rightarrow I = 1$  Hadron Data”. In: *Z. Phys. C* 26 (1984), pp. 433–439. DOI: [10.1007/BF01452571](https://doi.org/10.1007/BF01452571).
- [57] F. Le Diberder and A. Pich. “Testing QCD with tau decays”. In: *Phys. Lett. B* 289 (1992), pp. 165–175. DOI: [10.1016/0370-2693\(92\)91380-R](https://doi.org/10.1016/0370-2693(92)91380-R).
- [58] F. Le Diberder and A. Pich. “The perturbative QCD prediction to  $R(\tau)$  revisited”. In: *Phys. Lett. B* 286 (1992), pp. 147–152. DOI: [10.1016/0370-2693\(92\)90172-Z](https://doi.org/10.1016/0370-2693(92)90172-Z).
- [59] H. Lehmann. “On the Properties of propagation functions and renormalization constants of quantized fields”. In: *Nuovo Cim.* 11 (1954), pp. 342–357. DOI: [10.1007/BF02783624](https://doi.org/10.1007/BF02783624).
- [60] W. J. Marciano and A. Sirlin. “Electroweak Radiative Corrections to tau Decay”. In: *Phys. Rev. Lett.* 61 (1988), pp. 1815–1818. DOI: [10.1103/PhysRevLett.61.1815](https://doi.org/10.1103/PhysRevLett.61.1815).
- [61] Stephan Narison. “QCD spectral sum rules”. In: *World Sci. Lect. Notes Phys.* 26 (1989), pp. 1–527.
- [62] Stephan Narison and R. Tarrach. “Higher Dimensional Renormalization Group Invariant Vacuum Condensates in Quantum Chromodynamics”. In: *Phys. Lett.* 125B (1983), pp. 217–222. DOI: [10.1016/0370-2693\(83\)91271-6](https://doi.org/10.1016/0370-2693(83)91271-6).
- [63] R. Tarrach P. Pascual. *QCD: Renormalization for the Practitioner*. Springer-Verlag, 1984.
- [64] W. Pauli and F. Villars. “On the Invariant Regularization in Relativistic Quantum Theory”. In: *Rev. Mod. Phys.* 21 (3 July 1949), pp. 434–444. DOI: [10.1103/RevModPhys.21.434](https://doi.org/10.1103/RevModPhys.21.434). URL: <https://link.aps.org/doi/10.1103/RevModPhys.21.434>.
- [65] Michael E. Peskin and Daniel V. Schroeder. *An Introduction to quantum field theory*. Reading, USA: Addison-Wesley, 1995. URL: <http://www.slac.stanford.edu/~mpeskin/QFT.html>.

- [66] Antonio Pich. “Precision Tau Physics”. In: *Prog. Part. Nucl. Phys.* 75 (2014), pp. 41–85. DOI: [10.1016/j.pnpnp.2013.11.002](https://doi.org/10.1016/j.pnpnp.2013.11.002). arXiv: [1310.7922](https://arxiv.org/abs/1310.7922) [hep-ph].
- [67] Antonio Pich and Joaquim Prades. “Strange quark mass determination from Cabibbo suppressed tau decays”. In: *JHEP* 10 (1999), p. 004. DOI: [10.1088/1126-6708/1999/10/004](https://doi.org/10.1088/1126-6708/1999/10/004). arXiv: [hep-ph/9909244](https://arxiv.org/abs/hep-ph/9909244) [hep-ph].
- [68] Antonio Pich and Antonio Rodríguez-Sánchez. “Determination of the QCD coupling from ALEPH  $\tau$  decay data”. In: *Phys. Rev. D* 94 (3 Aug. 2016), p. 034027. DOI: [10.1103/PhysRevD.94.034027](https://doi.org/10.1103/PhysRevD.94.034027). URL: <https://link.aps.org/doi/10.1103/PhysRevD.94.034027>.
- [69] Antonio Pich and Antonio Rodríguez-Sánchez. “Updated determination of  $\alpha_s(m_\tau^2)$  from tau decays”. In: *Mod. Phys. Lett. A* 31.30 (2016), p. 1630032. DOI: [10.1142/S0217732316300329](https://doi.org/10.1142/S0217732316300329). arXiv: [1606.07764](https://arxiv.org/abs/1606.07764) [hep-ph].
- [70] A. A. Pivovarov. “Renormalization group analysis of the tau lepton decay within QCD”. In: *Z. Phys. C* 53 (1992). [*Yad. Fiz.* 54,1114(1991)], pp. 461–464. DOI: [10.1007/BF01625906](https://doi.org/10.1007/BF01625906). arXiv: [hep-ph/0302003](https://arxiv.org/abs/hep-ph/0302003) [hep-ph].
- [71] H. David Politzer. “Reliable Perturbative Results for Strong Interactions?” In: *Phys. Rev. Lett.* 30 (1973). [274(1973)], pp. 1346–1349. DOI: [10.1103/PhysRevLett.30.1346](https://doi.org/10.1103/PhysRevLett.30.1346).
- [72] Eduardo de Rafael. “An Introduction to sum rules in QCD: Course”. In: *Probing the standard model of particle interactions. Proceedings, Summer School in Theoretical Physics, NATO Advanced Study Institute, 68th session, Les Houches, France, July 28-September 5, 1997. Pt. 1, 2.* 1997, pp. 1171–1218. arXiv: [hep-ph/9802448](https://arxiv.org/abs/hep-ph/9802448) [hep-ph].
- [73] S. Schael et al. “Branching ratios and spectral functions of tau decays: Final ALEPH measurements and physics implications”. In: *Phys. Rept.* 421 (2005), pp. 191–284. DOI: [10.1016/j.physrep.2005.06.007](https://doi.org/10.1016/j.physrep.2005.06.007). arXiv: [hep-ex/0506072](https://arxiv.org/abs/hep-ex/0506072) [hep-ex].
- [74] Barbara Schmidt and Matthias Steinhauser. “CRunDec: a C++ package for running and decoupling of the strong coupling and quark masses”. In: *Comput. Phys. Commun.* 183 (2012), pp. 1845–1848. DOI: [10.1016/j.cpc.2012.03.023](https://doi.org/10.1016/j.cpc.2012.03.023). arXiv: [1201.6149](https://arxiv.org/abs/1201.6149) [hep-ph].

- [75] Felix Schwab. “Strange Quark Mass Determination From Sum Rules For Hadronic  $\tau$ -Decays”. German. MA thesis. somewhere, 2002.
- [76] Mikhail A. Shifman. “Quark hadron duality”. In: *At the frontier of particle physics. Handbook of QCD. Vol. 1-3*. [3,1447(2000)]. World Scientific. Singapore: World Scientific, 2001, pp. 1447–1494. DOI: [10.1142/9789812810458\\_0032](https://doi.org/10.1142/9789812810458_0032). arXiv: [hep-ph/0009131](https://arxiv.org/abs/hep-ph/0009131) [hep-ph]. URL: <http://jhep.sissa.it/archive/prhep/preproceeding/hf8/013>.
- [77] Mikhail A. Shifman, A. I. Vainshtein, and Valentin I. Zakharov. “QCD and Resonance Physics: Applications”. In: *Nucl. Phys. B*147 (1979), pp. 448–518. DOI: [10.1016/0550-3213\(79\)90023-3](https://doi.org/10.1016/0550-3213(79)90023-3).
- [78] Mikhail A. Shifman, A. I. Vainshtein, and Valentin I. Zakharov. “QCD and Resonance Physics. Theoretical Foundations”. In: *Nucl. Phys. B*147 (1979), pp. 385–447. DOI: [10.1016/0550-3213\(79\)90022-1](https://doi.org/10.1016/0550-3213(79)90022-1).
- [79] V. P. Spiridonov and K. G. Chetyrkin. “Nonleading mass corrections and renormalization of the operators  $m \bar{\psi} \psi$  and  $g^2(\mu)$ ”. In: *Sov. J. Nucl. Phys.* 47 (1988). [*Yad. Fiz.*47,818(1988)], pp. 522–527.
- [80] David M. Straub. *rundec-python*. <https://github.com/DavidMStraub/rundec-python>. 2016.
- [81] Levan R. Surguladze and Mark A. Samuel. “Total hadronic cross-section in  $e^+ e^-$  annihilation at the four loop level of perturbative QCD”. In: *Phys. Rev. Lett.* 66 (1991). [Erratum: *Phys. Rev. Lett.*66,2416(1991)], pp. 560–563.
- [82] M. Tanabashi et al. “Review of Particle Physics”. In: *Phys. Rev. D*98.3 (2018), p. 030001. DOI: [10.1103/PhysRevD.98.030001](https://doi.org/10.1103/PhysRevD.98.030001).
- [83] Yung-Su Tsai. “Decay Correlations of Heavy Leptons in  $e^+ + e^- \rightarrow l^+ + l^-$ ”. In: *Phys. Rev. D* 4 (9 Nov. 1971), pp. 2821–2837. DOI: [10.1103/PhysRevD.4.2821](https://doi.org/10.1103/PhysRevD.4.2821). URL: <https://link.aps.org/doi/10.1103/PhysRevD.4.2821>.
- [84] Steven Weinberg. “New approach to the renormalization group”. In: *Phys. Rev. D*8 (1973), pp. 3497–3509. DOI: [10.1103/PhysRevD.8.3497](https://doi.org/10.1103/PhysRevD.8.3497).



## BIBLIOGRAPHY

- [85] Steven Weinberg. “Nonabelian Gauge Theories of the Strong Interactions”. In: *Phys. Rev. Lett.* 31 (1973), pp. 494–497. DOI: [10.1103/PhysRevLett.31.494](https://doi.org/10.1103/PhysRevLett.31.494).
- [86] Steven Weinberg. “Phenomenological Lagrangians”. In: *Physica A* 96.1-2 (1979), pp. 327–340. DOI: [10.1016/0378-4371\(79\)90223-1](https://doi.org/10.1016/0378-4371(79)90223-1).
- [87] Steven Weinberg. *The quantum theory of fields. Vol. 2: Modern applications*. Cambridge University Press, 2013.
- [88] Kenneth G. Wilson. “Confinement of quarks”. In: *Phys. Rev. D* 10 (8 Oct. 1974), pp. 2445–2459. DOI: [10.1103/PhysRevD.10.2445](https://doi.org/10.1103/PhysRevD.10.2445). URL: <https://link.aps.org/doi/10.1103/PhysRevD.10.2445>.
- [89] Kenneth G. Wilson. “Nonlagrangian models of current algebra”. In: *Phys. Rev.* 179 (1969), pp. 1499–1512. DOI: [10.1103/PhysRev.179.1499](https://doi.org/10.1103/PhysRev.179.1499).
- [90] Francisco J. Yndurain. *The Theory of Quark and Gluon Interactions. Theoretical and Mathematical Physics*. Berlin, Germany: Springer, 2006. DOI: [10.1007/3-540-33210-3](https://doi.org/10.1007/3-540-33210-3).
- [91] *The whys of subnuclear physics. proceedings of the 1977 international school of subnuclear physics, held in Erice, trapani, sicily, June 23 - August 10, 1977*. 1979.
- [92] Roman Zwicky. “A brief Introduction to Dispersion Relations and Analyticity”. In: *Proceedings, Quantum Field Theory at the Limits: from Strong Fields to Heavy Quarks (HQ 2016): Dubna, Russia, July 18-30, 2016*. 2017, pp. 93–120. DOI: [10.3204/DESY-PROC-2016-04/Zwicky](https://doi.org/10.3204/DESY-PROC-2016-04/Zwicky). arXiv: [1610.06090](https://arxiv.org/abs/1610.06090) [hep-ph].